Pressure Ulcer Prevention System

A Major Qualifying Project submitted to the faculty of Worcester Polytechnic Institute in partial fulfillment of the requirements for the Degree of Bachelor of Science

March 23, 2017

Syed Ali Hussain

Hyunsoo Kim

Victoria Loehle

Professor John McNeill, Advisor, Dpt. of Electrical and Computer Engineering, WPI

Professor Shamsur Mazumder, Co-Advisor, Dpt. of Electrical and Computer Engineering, WPI

Professor Yitzhak Mendelson, Advisor, Dpt. of Biomedical Engineering, WPI

Professor Walter Towner, Advisor, Foisie School of Business, WPI

Professor Helen Vassallo, Co-Advisor, School of Business, WPI

Dr. Raymond Dunn, Co-Advisor, UMASS

Dr. Kelli Hickle, Co-Advisor, Umass

Contents

List of Figures

List of Tables

Abstract

Pressure ulcers (also known as decubitus ulcers and as bedsores) have been considered preventable nearly as long as they have been considered problematic, yet they continue to harm millions of hospital patients every year in medical care facilities across the globe. In the United States alone, hospital-acquired pressure ulcers cause thousands of deaths and cost billions of dollars per year (Agency for Healthcare Research and Quality, 2016). Existing pressure ulcer prevention systems are expensive and have not been designed to monitor localized pressure on specific at-risk areas on patients.

The Electrical and Computer Engineering Department and the Biomedical Engineering Department at Worcester Polytechnic Institute (WPI) and the Division of Plastic and Reconstructive Surgery at the University of Massachusetts Medical School (UMMS) have, therefore, been working together to develop a more effective and more affordable system to monitor localized pressure and microclimate conditions over at-risk areas on patients and to warn caretakers when and where tissue damage might occur before pressure ulcers develop.

The objective of the Pressure Ulcer Prevention Major Qualifying Project was to contribute towards these efforts by converting an existing wired system into a wireless system, with sensor patches able to detect (at a minimum) localized pressure and temperature, to store and transmit data from at least three separate at-risk areas on a patient to a single computer, and to operate untethered for at least seven consecutive days. The methods used to design and assess the system included:

- Research into pressure ulcers, past prototypes, and competing products
- Axiomatic design, with which the problem was defined in terms of constraints and functional requirements, with the top-level functional requirement of the system decomposed into design parameters
- Value analysis, with which individual components were compared based on ability to achieve functional requirements and meet constraints, and the best were selected
- Functional verification of individual components, in addition to calibration when needed
- Functional verification of full system
- Financial analysis, in which net present value calculations were used to estimate savings to medical care facilities, and return-on-investment calculations were used to predict how many would be sold before initial research and development costs were earned back

The project resulted in two prototype circuits: one designed for use on humans and implemented in preliminary form with rigid printed circuit boards (PCBs), one designed for use on rats during an upcoming experiment at UMMS and implemented with flexible PCBs. The design considerations for the flexible PCB system were the subject of a paper accepted to the 2017 IEEE International Symposium on Circuits and Systems (McNeill et al. 2017). Both systems were able to effectively monitor localized pressure, temperature, and relative humidity and to wirelessly communicate these measurements

for storage and later processing by researchers. The outcome shows how axiomatic design can benefit a project team, especially in early stages, and how inadequate problem definition can be detrimental to an engineering design, especially in later stages. The financial analysis confirms the value of the system to the market, suggesting hospitals and other medical care facilities will benefit through its use in the future.

Authorship

Section	Author(s)
Abstract	Victoria Loehle
Introduction	Victoria Loehle and Amanda Agdeppa
Literature Review	All
Project Strategy	Victoria Loehle
Alternative Designs	All
Design Verification	All
Final Design and Validation	All
Financial Analysis	Victoria Loehle
Conclusions and Recommendations	All
Appendices	All

Acknowledgements

This project is based upon work supported by a grant from the UMMS/WPI Collaborative Seed Funding Initiative.

To our MQP advisors in Atwater Kent, Professor John McNeill and Professor Shamsur Mazumder, who never accepted good enough and always challenged us to improve, learn, and surpass their expectations;

To our MQP advisor in Washburn, Professor Walter Towner Jr., who introduced us to axiomatic design, guided us through design decomposition in Acclaro, and challenged us to include a financial analysis;

To our MQP advisor in Gateway Park, Professor Yitzhak Mendelson, whose knowledge and experience have been invaluable resources to us since our project commenced;

To our advisors at UMMS, Dr. Raymond Dunn and Dr. Kelli Hickle, who have supported this project since its inception, and Heather Tessier, who has provided support for recent animal model experiments;

To our graduate-student assistant, Devdip Sen, who was always around and willing to help us out and who learned as much from us as we learned from him;

To our BME project partners, Rachel Ooyama-Searls, Brittney Pachucki, and Benjamin Parent, who were always open to our ideas and who designed an awesome adhesive for our sensor patch;

To Professor Hellen Vassallo, Lisa Wall, Matthew Crivello, Professor Christopher Brown, and everyone else who has advised us, assisted our team, and benefitted our project;

Thank you all for inspiring us to excel and enabling us to contribute to such an incredible project.

Executive Summary

Pressure ulcers, also known as bedsores and as decubitus ulcers, are an international nightmare, plaguing both patients and caretakers in medical care facilities located everywhere from Canada to Brazil, the United States to the Netherlands, India to Australia (Ackroyd-Stolarz, 2014; Inoue & Matsude, 2016; Srivastava et al., 2016). Treatment and prevention efforts cost up to $11 billion per annum in the United States and up to 2.1 billion per annum in the United Kingdom (Ackroyd-Stolarz, 2014; Moore et al., 2012). In hospitals across the United States, hospital-acquired pressure ulcers affect an additional 1 million patients each year, causing an estimated 72 deaths per 1,000 discharges due to related complications and infections (Agency for Healthcare Research and Quality, 2016). Pressure ulcers cause patients immense pain and discomfort, especially in extreme cases where skin damage is severe enough to expose muscle and bone. Such wounds take years to heal and can cost more than $20,000 each in treatment (Leaf Healthcare, Inc., 2016), though sums as high as $130,000 have been reported in stage 4 cases (Brew et al., 2010). Even less severe wounds take months to heal and can cost up to $2,000 each in treatment (Leaf Healthcare, Inc., 2016). No longer covered by Centers for Medicare and Medicaid Services, these exorbitant costs can be devastating to patients and to medical care facilities.

The electrical and computer engineering department and the biomedical engineering department at Worcester Polytechnic Institute and the division of plastic and reconstructive surgery at the University of Massachusetts Medical School have, therefore, been working together on an innovation in pressure ulcer prevention technology since 2010. The objective of the ongoing project is to create a more effective and more affordable means to prevent pressure ulcers. The system discussed here comprises multiple sensor patches and one base station: The sensor patches are meant to adhere to the skin in at-risk areas on the patient, monitor localized pressure, temperature, and relative humidity, and transmit data wirelessly. The base station is meant to receive and process these data, eventually with an algorithm that will determine a probability of ulceration in each at-risk area and issue an alert to caretakers when a threshold value has been exceeded.

The initial project proposal of the Pressure Ulcer Prevention Major Qualifying Project (PUP MQP) team was completed between August 2016 and October 2016. After learning about pressure ulcers, defining customer needs and design constraints, reviewing past accomplishments, and assessing prior art, the PUP MQP team used the axiomatic design method to design the system to meet its constraints and achieve its functional requirements. The design decomposition was then used to determine which components to include, and the value analysis technique (Bitar & Mazumder, personal communication, 2016) was used to assess various options. Factors such as cost, size, power requirement, accuracy, and availability were considered, as comparisons were made between various adhesives, encasings, pressure sensors, temperature sensors, relative humidity sensors, microcontrollers, antennas, and power sources. Based on these analyses, the best adhesive was the OPSITE Film; the best pressure sensor was the Interlink FSR-402 Short (which ended up being replaced in January 2017 with the Tangio TPE-502 shunt mode force sensing resistor); the best digital relative humidity and temperature sensor was the Texas Instruments HDC1010, while the best analog relative humidity and temperature sensor was the Sensirion SHT3X-ARP; the best microcontroller package was the CC2650MODA

module; and the best power source was the GMB CP042345 non-rechargeable lithium polymer battery.

These components were used to implement several sensor patch designs, which were tested under controlled conditions to assess how well each one measured pressure, temperature, and relative humidity compared to standards. Wireless communications were established between up to three patches and one base station, and power consumption on each patch was determined under continuous transmission conditions. Between October 2016 and December 2016, the team designed the printed circuit board (PCB) with which initial component verification and functional testing would be conducted. Once the components selected in October were better understood, the system design was reevaluated, and unnecessary parts were eliminated. The remaining components were incorporated into the first rigid PCB design. Then the pressure sensor was tested, and communication between the initial base station (a smartphone with an Android operating system) and the microcontroller was established. Next the second rigid PCB design was completed. These new patches included both digital and analog relative humidity and temperature sensors, so code used to process signals from the analog pressure sensor could be reused to process signals from the analog relative humidity and temperature sensor.

Between January 2017 and March 2017, the analog relative humidity and temperature sensor was tested; the Interlink sensor was replaced, and the Tangio sensor was tested; the power consumption was analyzed; and the final base station (a laptop with a Linux operating system) was programmed to receive data from multiple sensors via three different microcontrollers on three different boards. Late in January, the team was presented with the opportunity to design sensor patches for experiments on rats, which are expected to commence at UMMS in May 2017. The team thus designed its final sensor patch according to the design constraints associated with the experiments. These patches have been implemented on flexible PCBs and will be tested in March. Additionally, the design principles and the test results for the components on the flexible PCB were the basis of a paper accepted to the 2017 IEEE International Symposium on Circuits and Systems (McNeill et al., 2017) in Baltimore, MD, to be presented in May 2017.

1 Introduction

1.1 Objective

The purpose of the chapter is to explain the aims of the ongoing pressure ulcer prevention system project and to introduce the purpose of the PUP MQP.

1.2 Pressure Ulcer Prevention System Project

The electrical and computer engineering department and the biomedical engineering department at Worcester Polytechnic Institute (WPI) has been working with the division of plastic and reconstructive surgery at the University of Massachusetts Medical School (UMMS) on an innovation in pressure ulcer prevention technology since 2010. They aim to develop a more effective and less expensive means to monitor localized pressure and microclimate conditions over at-risk areas on patients and to warn caretakers when and where tissue damage might occur before pressure ulcers develop. Four specific project goals have been proposed (McNeill, personal communication, 2016):

1. Develop autonomous sensor patch.
2. Investigate appropriate substrate adn adhesive.
3. Develop software and hardware required to support multi-patch network.
4. Create algorithm to determine tissue status and to issue warnings when appropriate.

Though many pressure ulcer prevention products have entered the market in recent years, and though some products (e.g. wireless patient monitoring system by Leaf Healthcare) have met with success, none have combined all twelve characteristics listed below into one system (McNeill, personal communication, 2016):

1. Directly measures external contact pressure on skin
2. Localizes measurement of contact pressure to at-risk area
3. Does not require caregiver interpretation
4. Allows caregiver to input patient-specific information
5. Adjusts alert threshold based on patient-specific factors
6. Enables remote communication via website or software application
7. Wireless
8. Self-powered
9. Disposable
10. Preventive
11. Affordable
12. Applicable in home care setting and with wheelchair bound patients

The most recent prototype of the proposed system included a wired sensor patch that monitored localized pressure and temperature (Crivello et al., 2016b). Past prototypes and accomplishments, in addition to competing products, are described in detail in Chapter 2.

1.3 PUP MQP

The primary objective of the PUP MQP was to develop a wireless system prototype, using the design of the most recent wired patch as a springboard. The team was initially challenged to produce a system consisting of at least three autonomous sensor patches and one base station. Each sensor patch was expected to include at least a pressure sensor, a temperature sensor, a control unit (e.g. microcontroller), a wireless transmitter, a power source, and a mechanism to adhere to skin. Additionally, each patch was required to operate for seven consecutive days without detaching from skin and was expected to be low cost, simple to use, and disposable. The base station was expected to receive, process, and display data from multiple patches. The team was also challenged to estimate the value of the system to the market.

The initial goal of the PUP MQP team was to develop a reproducible, working, wireless pressure ulcer prevention system prototype, in which at least three autonomous sensor patches were able to transmit data to one computer. Each patch was to monitor pressure, temperature, and relative humidity, and relevant data was to be displayed on a graphic user interface. The sensor patches were also to be integrated with the adhesive and tested in a busy wireless communications environment.

Late in January 2017, the team was tasked to design, implement, and test the sensor patches that would be used during the upcoming May 2017 experiment on live rats. The team adjusted the project goal accordingly and intends to deliver a reproducible, working, wireless prototype, including rat-sized sensor patches implemented on flexible PCBs.

The PUP MQP comprised four phases, as outlined in Figure 1. Between August 2016 and October 2016, Phase 1 and Phase 2 were completed, and Phase 3 was initiated. Phase 3 was completed between October 2016 and January 2017. Phase 4 was initiated in February 2017 and will be completed in March 2017.

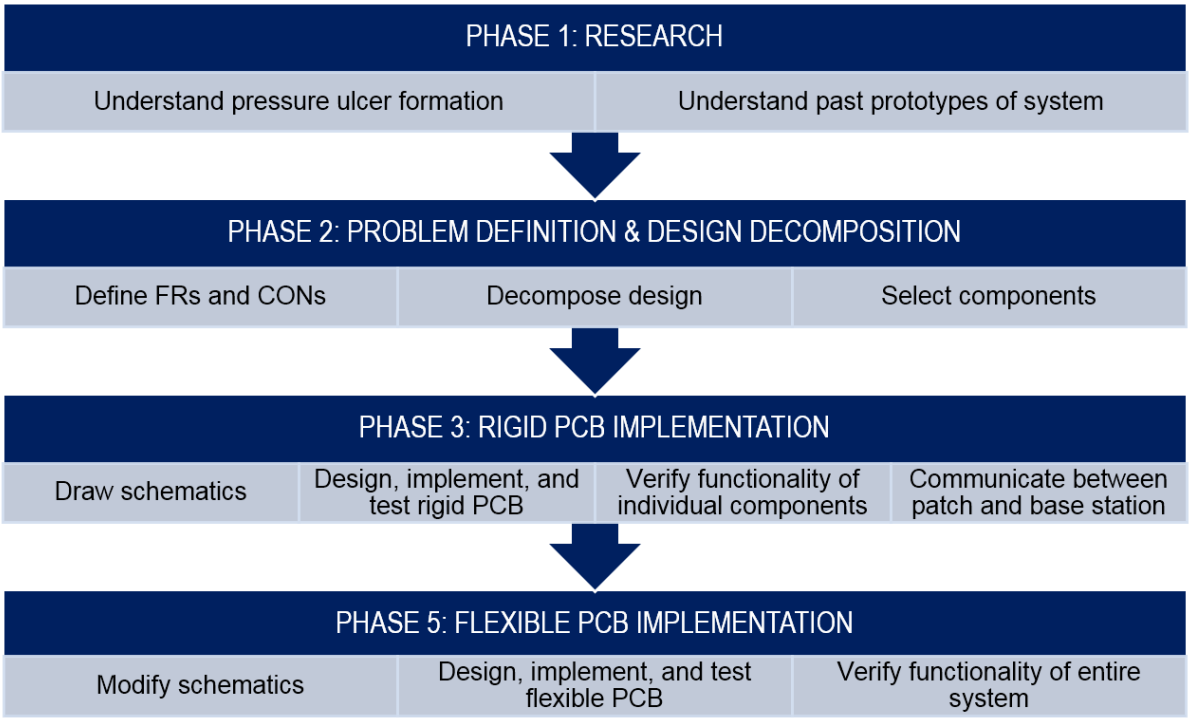

Figure 1: Project Flow Chart

2 Literature Review

2.1 Objective

The objective of the chapter is to introduce pressure ulcers, to discuss merits and shortcomings of existing and developing prevention mechanisms, and to describe the previous prototypes of the proposed pressure ulcer prevention system.

2.2 Pressure Ulcer Problem

Pressure ulcers, also known as bedsores and as decubitus ulcers, are an international nightmare, plaguing both patients and caretakers in medical care facilities located everywhere from Canada to Brazil, The United States to the Netherlands, India to Australia (Ackroyd-Stolarz, 2014; Inoue & Matsude, 2016; Srivastava et al., 2016). Efforts not only to treat them, but also to prevent them, cost up to $11 billion per annum in the United States and up to 2.1 billion per annum in the United Kingdom (Ackroyd-Stolarz, 2014; Moore et al., 2012). In hospitals across the United States, hospital-acquired pressure ulcers affect an additional 1 million patients each year, causing an estimated 72 deaths per 1,000 discharges due to related complications and infections (Agency for Healthcare Research and Quality, 2016). Pressure ulcers cause patients immense pain and discomfort, especially in extreme cases where skin damage is severe enough to expose muscle and bone. Such wounds take years to heal and can cost more than $20,000 each in treatment (Leaf Healthcare, Inc., 2016), though sums as high as $130,000 have been reported in stage 4 cases (Brew et al., 2010). Even less severe wounds take months to heal and can cost up to $2,000 each in treatment (Leaf Healthcare, Inc., 2016). No longer covered by Centers for Medicare and Medicaid Services, these exorbitant costs are devastating to patients and to medical care facilities. With the aging population in the United States and abroad, gaining access to effective, affordable, and easy-to-use pressure ulcer prevention systems will be imperative to providing high quality healthcare in future.

2.2.1 Pressure Ulcer Formation

Published research on pressure ulcer formation places the brunt of the blame on four main factors: pressure, shear, friction, and microclimate (International Review, 2010). Pressure is defined as force per unit area. When the same force is exerted over different areas, a smaller area will experience a higher pressure. When a force is applied over an area of skin for a prolonged period of time without relief, blood supply can be reduced or altogether cut off, preventing oxygen and nutrients from reaching the skin in the area under pressure, resulting in ischemia, maceration, and necrosis of the skin in the area.

Internal shear stress arises when external contact pressure on skin is unevenly distributed and when friction between skin and textiles or support surfaces is present. Internal shear stress is greatest near bony prominences, where the bone displaces the adipose tissue by loading it to the point of deformation, as depicted in Figure 2.

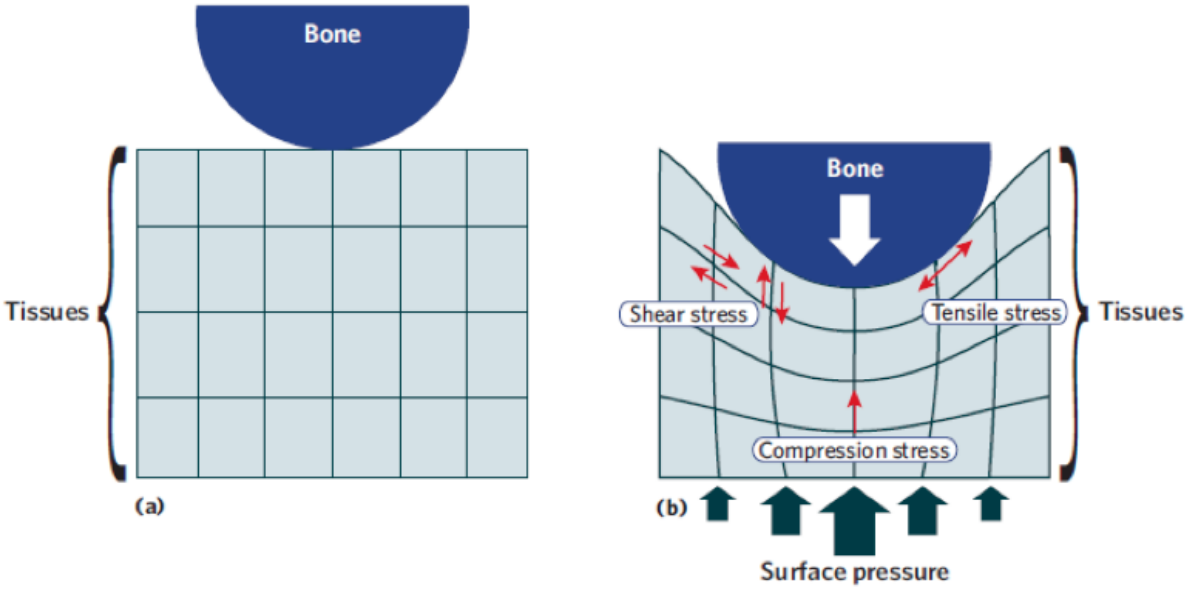

Figure 2: Internal Shear Forces (International Review, 2010)

The displacement of the adipose tissue in the hypodermis effectively displaces the tissue in the dermal layer and the epidermal layer, which are depicted in Figure 3. When these skin tissues are thus displaced, capillaries get pinched, and the blood supply to the area is greatly reduced.

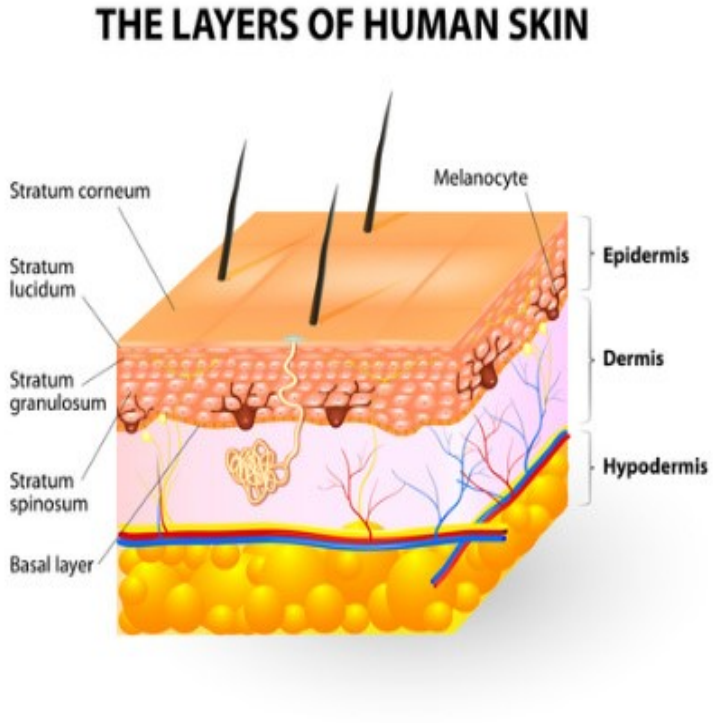

Figure 3: Layers of Skin http://www.skin-remedies.com/skin.html

Microclimate is largely determined by local temperature, humidity, and moisture levels (International Review, 2010). The study done with pigs by Kokate et al. (1995)

identified a positive correlation between temperature and skin damage: Under the same pressure over the same duration, the area at the higher temperature experienced the more severe tissue damage. The researchers applied metals discs to the dorsal side of the animals, maintaining 100 mmHg pressure on all discs for 5 hours, and keeping each disc at specific temperature. These temperatures ranged from 25°C to 45°C. No tissue damage was discerned at 25°C, while some deep tissue damage resulted at 35°C. Both cutaneous and subdermal tissue damage (i.e. necrosis of skin and damage to muscle) resulted at temperatures above 35°C.

Humidity and moisture impact both skin health and skin strength: Excessively high moisture levels often result in weaker skin over time, since moisture can weaken the crosslinks between the collagen in the dermis and soften the stratum corneum (International Review, 2010). Wet skin also has a higher coefficient of friction than dry skin (International Review, 2010). Thus excess moisture quickens the rate of skin maceration, which in turn increases the risk of pressure ulcer development. Moreover, if the dermal layer becomes exposed, then the materials and surfaces surrounding the wound site (e.g. clothing or bed sheets) can irritate the skin and further exacerbate the wound. Excessively dry skin, characterized by relative humidity below 40%, is also very weak due to its reduced tensile strength, flexibility, and junctional integrity between the dermis and the epidermis (International Review, 2010).

The combined effects of the pressure, shear, friction, temperature, and moisture levels in a localized area contribute to pressure ulcer formation.

2.2.2 At Risk Areas

As previously mentioned, pressure ulcers most often form in close proximity to bony prominences, since localized pressures as low as 30 mmHg can obstruct capillary blood flow there, and since internal shear forces near bony prominences are very high. Thus areas in close proximity to bony prominences are most susceptible to pressure ulcers.

Figure 4 displays which particular areas are at highest risk, depending on the position of the patient. If the patient is lying in the left lateral recumbent position (top left in Figure 4), the bony prominences are the ankles, knees, left hip, left shoulder, and left side of the head.

When the patient is in the supine position (bottom left in Figure 4), the at-risk areas change. Instead, the heel, sacrum, elbow, scapula, the back of the ear, and the back of the head are most susceptible to developing a pressure ulcer.

Lastly, when a patient is in the Fowlers position (right side in Figure 4), the at risk areas change once again. The areas that are now affected are the bottom of the feet, behind the knees, the ischial tuberosity, the sacrum, the coccyx, and the scapula.

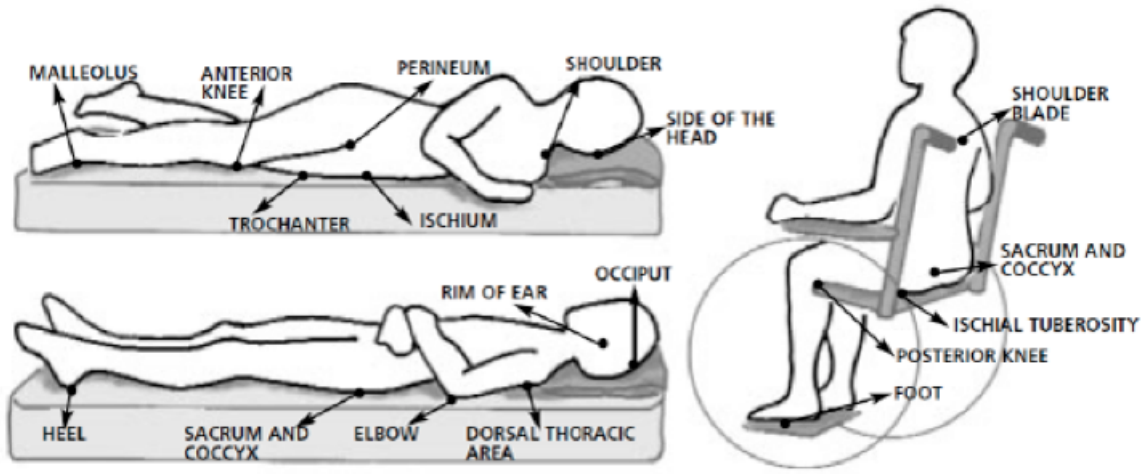

Figure 4: Common At-Risk Areas (Pressure Ulcer and Skin Care, n.d.)

2.2.3 Pressure Ulcer Stages

There are four stages in the progression of pressure ulcer formation as well as two additional stages that are not associated with the progression of ulcer formation.

The first stage (Figure 5), also known as non-blanchable erythema, is the least severe of the stages. At this stage, the skin of the area under pressure appears red, and the normal color of the skin does not return even after pressure has been alleviated. The temperature of the area under pressure also differs from the temperature of the surrounding tissue and can appear to be either cooler or warmer (National Pressure Ulcer Advisory Panel et al., 2014). Once detected, stage 1 ulcers cost patients and hospitals approximately $2,000 each in treatment (Leaf Healthcare, Inc., 2016).

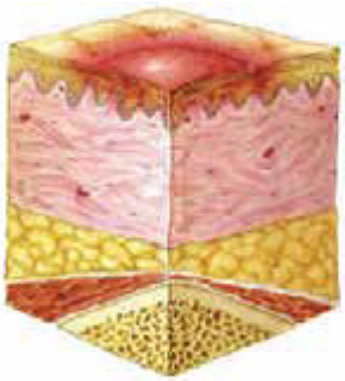

Figure 5: Stage 1 Pressure Ulcer (National PRessure Ulcer Advisory Panel et al., 2014)

The second stage (Figure 6) is defined by partial skin loss. In this stage, the ulcer looks like a dry or shiny open wound without slough or bruising, or like a serum-filled blister (National Pressure Ulcer Advisory Panel et al., 2014).

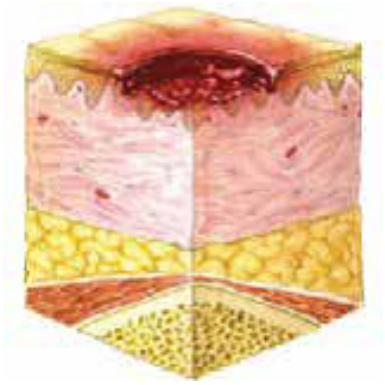

Figure 6: Stage 2 Pressure Ulcer (National PRessure Ulcer Advisory Panel et al., 2014)

The third stage (Figure 7) is defined by full thickness skin loss. The epidermal and dermal layer are lost along with parts of the hypodermal layer, and subcutaneous fat is exposed. Tunneling and undermining of the wound may also be present. The depth of the wound varies throughout the body, depending on location. For example, the depth of a stage 3 pressure ulcer in the cranial area is shallower than the depth of a stage 3 pressure ulcer in the sacrum because the volume of the adipose tissue present in the cranial area is much less than in the sacrum (National Pressure Ulcer Advisory Panel et al., 2014).

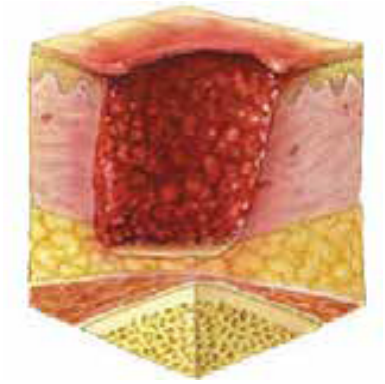

Figure 7: Stage 3 Pressure Ulcer (National PRessure Ulcer Advisory Panel et al., 2014)

In stage 4 pressure ulcers (Figure 8), the tissue of the localized area is completely lost. Muscle, tendon, and bone are completely exposed to the external environment. Tunneling and undermining of the wound are also present along with slough or eschar (National Pressure Ulcer Advisory Panel et al., 2014). Slough is also known as fibrous tissue or pus, and eschar is most commonly known as scabbing, a result of dead skin that appears to be black or dark in color. Stage 4 ulcers cost more than $20,000 each in treatment (Leaf Healthcare, Inc., 2016), though sums as high as $130,000 per stage 4 ulcer patient have been reported (Brew et al., 2010).

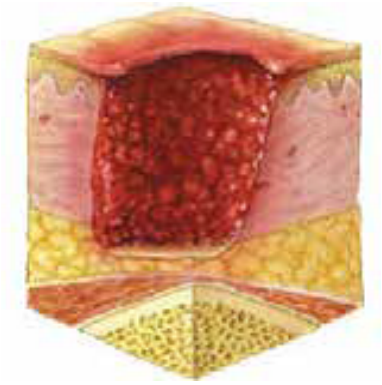

Figure 8: Stage 4 Pressure Ulcer (National PRessure Ulcer Advisory Panel et al., 2014)

There are also unstageable pressure ulcers and pressure ulcers that have caused suspected deep tissue injury. In unstageable pressure ulcers, full thickness loss in the skin has occurred. However, healthcare providers cannot determine the depth of the pressure ulcer to classify the stage since the wound is distorted by slough or eschar. Pressure ulcers that have caused suspected deep tissue injury appear to have discoloration around the affected area. The discoloration is due to blood from the dermal layer filling the epidermal layer of the skin or blister (National Pressure Ulcer Advisory Panel et al., 2014).

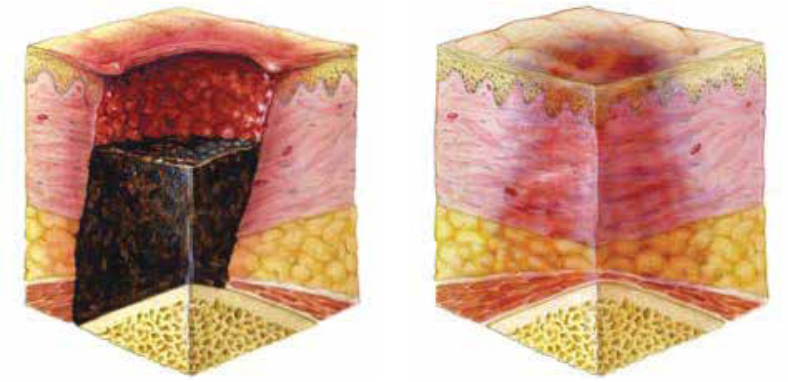

Figure 9: Unstageable Ulcer (L) and Suspected Deep Tissue Injury (R) (National Pressure Ulcer Advisory Panel et al., 2014)

All pressure ulcers are considered preventable; in particular, stage 3, stage 4, and unstageable pressure ulcers are classified as never events (Patient Safety Network, 2016). In the United States, stage 3 and stage 4 pressure ulcers affect about 15 hospital patients per 10,000 hospital discharges (Averill et al., 2016). Though they are least prevalent, they are most expensive, and they are not covered by the Centers for Medicare and Medicaid Services, which stopped paying for never events in 2008 (Patient Safety Network, 2016).

2.2.4 Pressure Ulcer Management

Existing procedures for preventing pressure ulcers are used for all patients regardless of age, weight, nutrition, and other factors that can directly affect the rate at which a pressure ulcer develops for an individual. Caretakers aim to minimize external shear forces and friction experienced by maintaining a delicate balance of moisture at the risk areas (National Guideline Clearinghouse, 2012). While excess moisture does lead to

quicker rates of maceration, friction at areas with dry skin can also result in irritation. Therefore, caretakers are encouraged to use oils or lotions to prevent a harsh contact environment between the skin and fabric. Moreover, if the patient requires assistance in moving, caretakers must lift the patient rather than drag them as that would result in excess friction.

The condition of the skin at high risk areas should also be kept at optimum standards (National Guideline Clearinghouse, 2012). The skin should be kept clean and free of any urinary or fecal matter in order to prevent infection if the skin breaks. When cleaning the skin, caretakers must be mindful not to excessively rub the skin as it can lead to further maceration. It is also recommended that the bedding is breathable and that wound dressings be changed frequently and periodically.

Lastly, pressure and offloading should be minimized as much as possible. Patients are encouraged to use support surfaces, such as special mattresses or additional padding that distribute the localized pressure (National Guideline Clearinghouse, 2012). Sitting patients that have a head elevation greater than 30°are encouraged to move every 15 minutes and are required to be repositioned every hour. On the other hand, patients that are confined to a bed are encouraged to use pillows as buffers between the bed and the contact points, particularly contact points that are high risk areas. These patients must be repositioned at a minimum of every two hours.

2.3 Prior Art

The pressure ulcer prevention systems that are currently on the market have many limitations and constraints that this project aims to eliminate. Devices such as smart beds or mats sense pressure; however, these measurements are made relative to the bed instead of the patient. Smart beds also confine the patient and are not usable outside a hospital setting. Moreover, many of these systems are expensive. A low cost, power efficient pressure ulcer prevention system would provide patients freedom of mobility while still enabling them to receive quality care by doctors who can wirelessly monitor their status.

2.3.1 Existing Devices

There is currently a well-liked and commonly-used wireless pressure ulcer prevention system on the market. However, the device does not sense pressure, temperature, or relative humidity. The Leaf Patient Monitoring System detects and tracks patient movement over time to help doctors follow the traditional 2-hour turning protocol (Leaf Healthcare, Inc., 2014). The system consists of a disposable patch equipped with an accelerometer, wireless communications capabilities, and software that is compatible with a computer or smart device, which is used to receive and interpret the data. The patch is attached to the patients chest and monitors movements. The system requires caretakers to program how often each patient needs to be turned, and the system alerts the caregivers when patients have not been turned according to their specific turning regimens.

While the wireless capabilities of the system distinguish this product from its competitors, there are limitations that make it less desirable. Although moving does help to mitigate the effects of pressure on bony prominences, the extent to which the effects of pressure are reduced is different for each patient. Measuring only patient movement and not direct pressure overlooks a number of variables such as the weight of the patient

and the magnitude of the pressure experienced at the localized area.

Monitor Alert Protect is also an existing product on the market that detects pressure (Wellsense, n.d.). The pressure sensing mat instantaneously measures pressure and transmits the data to a monitor, where it displays a visual image of pressure levels in real time. This system helps medical care professionals position the patient based on visual monitoring of pressure and thus prevents pressure ulcers.

Despite its high resolution pressure mapping and real-time imaging, it has certain constraints. In order to monitor the pressure, the caretaker has to visit the patient to view the visual display and cannot monitor it remotely. Moreover, the measured contact pressure is localized to a coordinate system on the bearing surface as opposed to on the patient. As the patient moves, the location at which high levels of pressure are experienced may continue to affect the same area of the body. However, because the measurements are taken with respect to the bed, the system may show that the pressure has been reduced, since the patient is now in a different location on the beds surface. Thus the time profile of contact pressure on at-risk locations on the body is difficult to track, which would result in inaccuracies if these pressure maps were used to assess the probability of the patient developing a pressure ulcer.

2.3.2 Developing Devices

Other pressure ulcer prevention systems are being developed by researchers in industry and academia throughout the globe. Enokibori et. al (2013) are working in Japan to improve an e-textile-based bed-size pressure sensor meant to prevent pressure ulcers. Their e-textile sensor is comprised of conductive fibers. Each intersection point between two interwoven conductive fibers forms a 1 cm x 1 cm sensing point, at which applied pressure causes a measurable change in capacitance. The system is low-cost, thin, soft, and flexible, and it does not interfere with pressure-balancing mattresses that are currently used in hospitals. However, the system provides very rough depictions of body shape. Exact locations of maximum pressure on the patient are thus difficult to predict. The system was being tested in nursing homes when the 2013 conference paper was published, so the product is likely to hit the market within the next few years.

2.4 Previous Accomplishments

For almost seven years, MQP teams at WPI have been attempting to develop a system that monitors pressure and microclimate near areas in which pressure ulcers are known to develop and that alerts caregivers when conditions are ideal for ulceration to occur.

Two pressure ulcer prevention device prototypes were developed by MQP teams between August 2010 and April 2012:

The first, a standalone computer-based system completed in April 2011, comprised a sensor patch, a data acquisition unit, and a graphic user interface. The sensor patch was designed to attach directly to the skin over the heel and was made to measure pressure and moisture using a Tekscan A401 force sensor and a Honeywell HIH4000 relative humidity sensor, respectively. Wires were used to connect the sensor patch to the data acquisition unit, as shown in Figure 5 (Gutierrez, Jones, & Morianos, 2011).

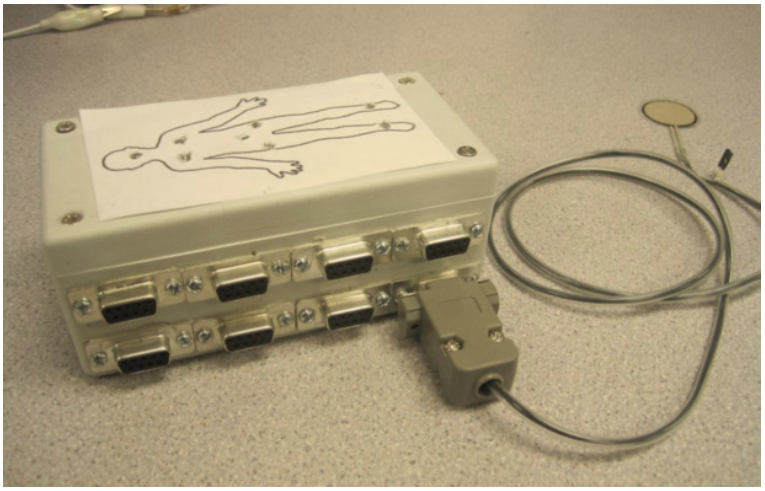

Figure 10: Prototype Completed in April 2011 (Gutierrez, Jones, & Morianos, 2011)

LabVIEW was used to implement an algorithm in which measured pressure and moisture values were compared to predetermined threshold values, and elapsed time was tracked. The program set off a visual alert on the graphic user interface whenever pressure needed to be relieved or moisture levels needed to be adjusted. The prototype was tested on the team members to verify its design, and it later received positive feedback from medical doctors at UMMS.

The MQP succeeded in achieving its goals; however, the team offered several suggestions for improvement:

1. Conduct additional testing with a wider demographic.
2. Make the system wireless.
3. Design the alert system to be compliant with FDA regulations and hospital standards.
4. Make the sensing area larger
5. Make the patches disposable, inexpensive, and sterile.
6. Use a more versatile program than LabVIEW and make the user interface customizable.

The second prototype, a wireless system completed in April 2012, comprised multiple sensor patches, a microcontroller with wireless transmission capabilities, a wireless receiver with UART transmission capabilities, a data acquisition system, and a graphic user interface. The sensor patch was designed to attach directly to the skin over areas susceptible to pressure ulcers, including the heels and the shoulder blades, and to measure pressure, moisture, and temperature using several Interlink FSR406 force sensing resistors, a Honeywell 5030 relative humidity sensor, and a MAX6612 temperature sensor integrated circuit, respectively. The sensor outputs were sampled, converted into digital signals, and transmitted with a TI-CC430 microcontroller on the sensor patch. The data was received with a second identical microcontroller, which was housed in a small box, as shown in Figure 11, and was interfaced to the data acquisition system through a UART USB connection (Hause, Truhanovitch, & Williams, 2012).

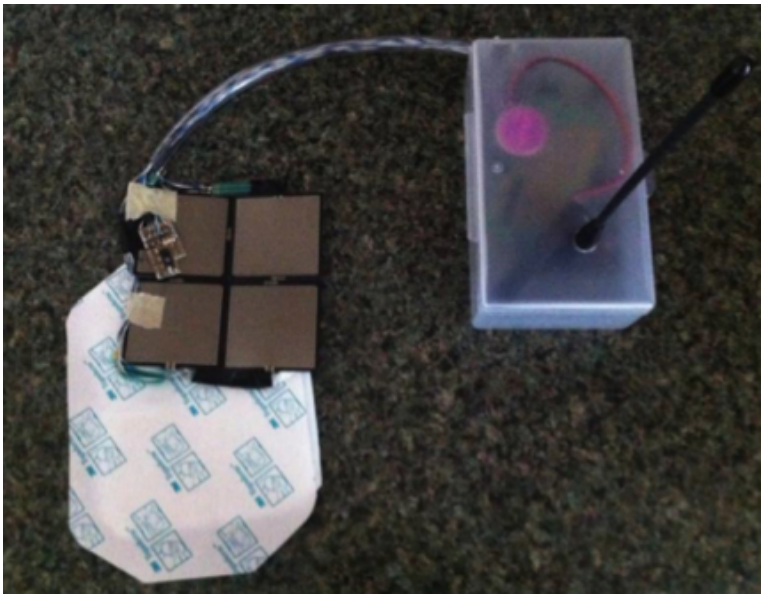

Figure 11: Prototype Completed in April 2012 (Hause, Truhanovitch, &Williams, 2012)

LabVIEW was used as in 2011 to implement an algorithm in which sensor readings were combined with additional patient information, including age, weight, systemic blood pressure, nutrition, and mobility level. The program set off an audible alert through the graphic user interface whenever at least one test condition was met:

1. Pressure readings exceeded 35 mmHg for an extended period.
2. Relative humidity readings increased to a range between 40% and 50%.
3. Temperature readings had increased by 1.2°C within 24 hours.

The prototype was tested on the team members as in 2011, and it later received constructive feedback from a clinician at UMMS. The MQP also succeeded in achieving its goals, but the team suggested making additional improvements to the prototype:

1. Conduct testing with a wider demographic, including patients susceptible to pressure ulcers.
2. Design the alert system to be compliant with FDA regulations and hospital standards.
3. Make the patch smaller and disposable.
4. Use a more versatile program than LabVIEW, and make the user interface simple and resilient to user error.
5. Make the program compatible with inputs form multiple patches on multiple patients.
6. Make the wireless communication compatible with a mesh network, and test it in a clinical setting.

In more recent years, a wired sensor patch on a flexible substrate has been developed by researchers at WPI. Initial tests have been conducted on pigs undergoing a surgical procedure (Crivello et. al, 2016b). The sensor patch, shown in Figure 7, was designed to measure pressure and temperature, using an Interlink FSR402 Short force sensing resistor and a muRata NCP15XH103 resistive temperature detector (Crivello et. al, 2016a; Crivello et. al, 2016b; McNeill, personal communication, 2016).

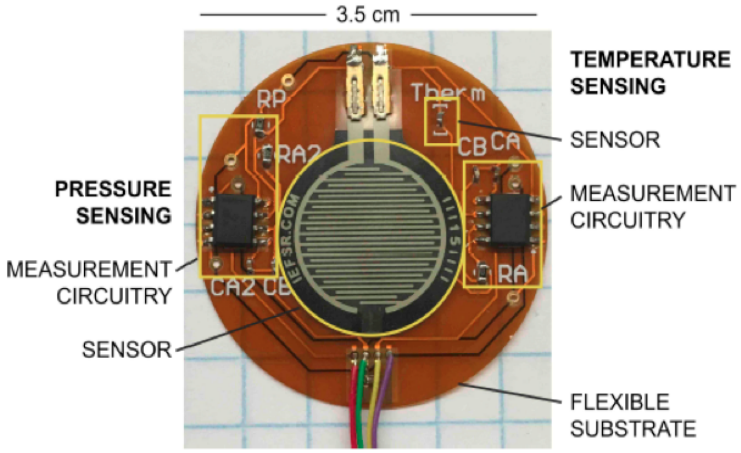

Figure 12: Wired Prototype from Research Published in 2016

The researchers have mentioned several important improvements needed in the existing prototype before the complete system can be brought to market (McNeill, personal communication, 2016):

1. Make the system wireless.
2. Make the sensor patch less than 1mm in thickness.
3. Consider alternative force/pressure sensors.
4. Use a temperature sensor with 0.1°C accuracy.
5. Consider adding sensors to measure moisture and shear force.
6. Encase the electronics to prevent exposure to water and bodily fluids.

3 Project Strategy

3.1 Objective

The purpose of the chapter is to provide an overview of axiomatic design, including fundamental concepts and important benefits, and to show how axiomatic design was used during the development of the pressure ulcer prevention system. The software package, Acclaro (version 5.4), was used to develop the design decomposition, analyze the design matrix, and identify where the functional requirements and the design parameters were coupled.

3.2 Rationale

Though the business school and the engineering departments at WPI share the same campus and, sometimes, the same students, they do not often share the same design methodologies. The business school stresses efficiency, effectiveness, and value: Its professors champion axiomatic design, in which the best designs are the ones with the most independence between functions and the least information content. It requires designers to decompose complex problems into functional requirements and design parameters based on customer needs and design constraints. When used well, axiomatic design enables designers to create better products in less time with less money than other design methodologies, since greater functional independence results in fewer non-productive iterations, and lower information content is related to higher probability of success. Business professors also teach students to evaluate products from the perspective of the customer. Students learn to estimate net value over time and are encouraged to not pursue projects in which potential costs outweigh potential benefits.

Professors in the manufacturing engineering department and the mechanical engineering department also teach axiomatic design. Professors in the electrical and computer engineering department, however, teach the five-step design process defined in Engineering by Design by Gerard Voland (2004). That process neither considers dependencies between functional requirements nor quantifies information content, and its analysis and evaluation step allows for non-productive iterations. Thus projects in the electrical and computer engineering department should benefit from using axiomatic design instead. The PUP MQP, in particular, should be able to use the top functional requirement of the pressure ulcer prevention system to narrow the scope of the project, to establish achievable goals, and to succeed in achieving them before the deadline of the project.

3.3 Axiomatic Design Fundamentals

In lieu of the five-step approach to design originally championed by Gerard Voland (2004) and currently practiced in the ECE Department at WPI, the axiomatic design method was used. Axiomatic design is a very effective and very efficient approach to engineering design based on two axioms, in addition to structures and processes with which to apply them. It is used to objectively evaluate various designs and to calculate how probable each one is to succeed in fulfilling its functional requirements (Towner, 2013e).

3.3.1 Origin

Axiomatic design was brought into existence at MIT by Professor Nam Suh between 1976 and 1990 (Towner, 2013e). Stated in his keynote speech at ICAD 2013, his aim was to generalize what we know about design, and to teach students, and to practice it (as sited in Towner, 2013e). In other words, he intended to develop axioms of design. Drawing from personal experience, in addition to examples in industry and in academia, he and his research team determined twelve commonalities between successful projects; through additional research, these initial hypothetical axioms were ultimately reduced to two comprehensive axioms of design (Towner, 2013e).

3.3.2 Concepts

The two axioms of the axiomatic design approach state the best design is one in which (Suh, 1990):

1. The independence of the functional elements is maximized.

2. The information content is minimized.

Application of these axioms requires a structure, and creation of a structure requires a process (Brown, 2013b). The structure is comprised of horizontal decomposition and vertical decomposition. Horizontal decomposition divides a design into four domains (Towner, 2013b, slide 26):

1. Customer
   The customer domain considers what adds value and encompasses the customer needs (CNs).

2. Functional
   The functional domain accounts for what it does and encompasses the functional requirements (FRs).

3. Physical
   The physical domain examines look and feel and encompasses the design parameters (DPs).

4. Process
   The process domain analyzes how it is made and encompasses the process variables (PVs).

Constraints (CONs) are also considered in each domain.

Vertical decomposition breaks a design down into two parallel hierarchies: one corresponding to functional requirements, and one corresponding to design parameters.

The process is comprised of zigzagging decomposition and physical integration. Zigzagging decomposition is used to map back and forth between the functional domain and the physical domain while moving from higher and more abstract levels to lower and more specific ones in both hierarchies (Brown, 2013b; Towner, 2013b, slide 24, 26; Towner, 2013c, slide 4; Towner, 2013e, slide 14, 17-18). The axioms, the structures, and the processes are summarized in Table 1.

Table 1: Elements and Components of Axiomatic Design (Towner, 2013b; Towner, 2013e; Brown, 2013b; Brown, 2013c, Brown, 2013d; Brown, 2013e)

Elements	Compnents	Subcomponents	
Axioms	Maximize independence	Uncoupled FR-DP design matrix (ideal) Decoupled FR-DP design matrix (next best option)	
	Minimize information	Uncoupled FR-DP design matrix (ideal) Decoupled FR-DP design matrix (next best option)	
Structures	Horizontal decomposition	Customer domain	CNs
		Functional domain	FRs
		Physical domain	DPs
		Process domain	PVs
		Constrains	CONs
	Vertical decomposition	FR hierarchy	DP hierarchy
		FR0 $\rightarrow FR1, FR2,$	DP0 $\rightarrow DP1, DP2,$
Processes	Zigzagging decomposition	FR0 $\rightarrow DP0$	DP0 $\rightarrow FR1, FR2,$
		FR1 $\rightarrow DP1$ FR2 $\rightarrow DP2$	DP1 $\rightarrow FR1.1, FR1.2,$ DP2 $\rightarrow FR2.1, FR2.2,$
	Physical integration	DPs $\rightarrow DPs$	DPs $\rightarrow PVs$

The functional requirements are the foundation of the design. They define its objectives, from the individual component level to the integrated system level, and serve as a means to document the intent associated with each design parameter in the DP hierarchy. The top level functional requirement (FR0) is the most important FR to get right, since it determines the overarching theme of the design. In his manufacturing engineering classes at Worcester Polytechnic Institute, Professor Walter Towner stresses, Formulating good FRs takes time and adds value because a design can be no better than its FRs (Towner, 2013c, slide 10-11).

In order to obey the axioms, the functional requirements must meet three requirements (Towner, 2013c, slide 14):

1. Collectively exhaustive (CE)
    - In a CE design, all necessary functions are included.
2. Mutually exclusive (ME)
    - In a ME design, no two functions overlap; i.e. all functions are unique.
3. Minimum number (min)
    - In a min design, only necessary functions are included; if a single additional function were eliminated, then FR0 could not be achieved.

The vertical decomposition is CEMEmin when the child FRs sum up to equal the parent FR at each level in the FR hierarchy (Towner, 2013c, slide 14).

Successful implementation of axiomatic design involves applying the axioms in accordance with the structures and the processes outlined above.

3.3.3 Benefits

Axiomatic design is expected to make a product or a process better, faster, [and] cheaper (Towner, 2013b, slide 5; Brown, 2013b):

Strict adherence to the independence axiom yields an uncoupled design in which each function can be performed, modified, or altogether eliminated without interfering with any other function. Such a design is easy to customize and to improve over time, since changes to one function can be made through changes to its respective design parameter only. When as few components as possible are impacted by a design change, non-productive iterations can be avoided (Towner, 2013b, slide 5; Brown, 2013b), and modifications can be implemented in less time at lower cost.

Similarly, adherence to the information axiom yields a simple design with a high probability of achieving success. Information can be associated with factors such as tolerances and costs (Towner, 2013e, slide 64 and 66). Thus minimum information corresponds to maximum overlap between not only what a design must achieve and what a parameter can provide, but also what the designer is willing to pay and what the system must charge to be profitable (Towner, 2013e, slide 66). When a design is made to do no more than what must be done, i.e. when requirement creep is avoided and optimal performance is sought, it can be implemented with more success in less time at lower cost.

Other beneficial outcomes of using axiomatic design include detailed documentation of design intent and objective means to measure progress and quality throughout a project (Towner, 2013b, slide 5; Brown, 2013b).

3.4 Problem Definition

3.4.1 Customers and Needs

Most wearable biomedical devices, those with clinical applications in particular, must be made to serve multiple customer segments; the pressure ulcer prevention system is no exception. Patients and caretakers, including physicians, nurses, and assistants, are the intended end users of the system, so their needs must be considered first and foremost. Hospitals, nursing homes, and certain other patient care facilities are the expected buyers of the system once it enters the market. Thus federal and state regulations imposed upon these facilities, in addition to industry and individual standards, must be incorporated as constraints. Medical device manufacturers are the expected buyers of the system prototype, so demands associated with mass production must also be contemplated.

These perspectives were all taken into consideration when Pantelopoulos and Bourbakis (2008) conducted a survey on wearable health monitors and developed a comprehensive list of customer requirements associated with each market segment. Each requirement was assigned a ranking based on its importance to each customer. Of the features tested in the survey, those most valued by these customers were:

- Applicability and usefulness in real-life
- Testing in real cases with sufficient results in which performance is verified
- Reliability in all conditions

More so than physicians and manufacturers, patients also valued:

- Wearability
- Appropriate placement
- Aesthetic appeal
- Operational lifetime
- Real-time results
- Ease of use
- Decision support

Manufacturers were also concerned with features related to data encryption and security and with computational and storage requirements. More so than either patients or physicians, manufacturers cared about cost.

In general, all devices used in clinical settings must be safe and sanitary, and all wearables should be comfortable. Most features listed above are applicable to the entire pressure ulcer prevention system, including its wearable and its non-wearable components. The system is expected to comply with hospital standards and government regulations, those pertaining to wearable medical devices in particular. The wearable components are expected to be long-lasting (i.e. active 24/7 and operational for at least 7 consecutive days), disposable, unobtrusive, lightweight, thin (i.e. no more than 1 millimeter in height), and flexible enough to lie flat against bony prominences. The wearable components are also required to be wireless.

3.4.2 Top Level Functional Requirement

The top level functional requirement (FR0) used in both the first and the final pressure ulcer prevention system decomposition was to prevent pressure ulcer formation by warning patients and caregivers of impending damage to tissues in at-risk areas on patients.

3.4.3 Non-Functional Requirements and Constraints

The non-functional requirements of the pressure ulcer prevention system include being inexpensive and easy to use. The system is expected to comply with hospital standards and government regulations, those pertaining to wearable medical devices in particular. The sensor patch must be safe, wearable, self-powered, wireless, low-cost, and disposable. It should also be waterproof enough to withstand exposure to bodily fluids and flexible enough to lie flat against bony prominences.

Comfort, small size, and low weight go hand-in-hand with wearability. Thus the target size for the sensor patch is the same size as the average ECG electrode (McNeill, personal communication, 2017). The target thickness for the electronic components and the printed circuit board comprising the sensor patch is 1 mm.

Each sensor patch must operate for 7 consecutive days. Pressure readings should be accurate to about +/- 1 mmHg between threshold pressures 15 mmHg and 50 mmHg; less accurate readings would be acceptable at higher and lower pressures. Temperature readings must be accurate to about 0.1C. Relative humidity readings should be accurate to about 5% RH. With all sensors, part-to-part variability and long-term drift must be

as low as possible. The analog-to-digital converter in the microcontroller must have fine resolution and low error. With all components, voltage and current requirements should be as low as possible. Patches used during the research phase of the project may include more sensors than the ultimate marketable product.

3.5 Design Decomposition

FR-DP decomposition was performed in Acclaro. The final decomposition of the pressure ulcer prevention system is shown in Table 2. The sensor patches are the design parameters used to meet FR2.1.1, FR2.1.2, and FR2.1.3. The base station, which comprises the signal processing algorithms, the probability-of-ulceration algorithm, and the graphic user interface, is used to meet the rest of FR2 and the whole of FR3.

Table 2: Complete FR-DP Decomposition

Number	Functional Requirements	Number	DP Description
FR0	Prevent pressure ulcer formation by warning patients and caregivers of impending damage to tissues in at-risk areas on patients	DP0	System to prevent pressure ulcer formation by warning patients and caregivers of impending damage to tissues in at-risk areas on patients
FR1	Identify at-risk areas on patients	DP1	Method to identify at-risk areas on patients
FR1.1	Understand pressure ulcer formation (when, where, why, and how it happens)	DP1.1	Education on pressure ulcer formation
FR1.2	Predict where pressure ulcer formation might occur on each patient	DP1.2	Method to predict where pressure ulcer formation might occur on each patient
FR1.2.1	Identify how patient might be positioned (e.g. lying on back, sitting in wheelchair)	DP1.2.1	Method to identify how long patient might be in each position
FR1.2.2	Identify how long patient might be in each position	DP1.2.2	Method to identify how long patient might be in each position
FR2	Determine whether damage to tissues in at-risk areas is imminent	DP2	System to determine whether damage to tissues in at-risk areas is imminent
FR2.1	Monitor influential factors in each at-risk area	DP2.1	Method to monitor influential factors in each at-risk area
FR2.1.1	Measure pressure on each at-risk area over time	DP2.1.1	System to measure pressure on each at-risk area over time (i.e. sensor patch)
FR2.1.1.1	Attach system to at-risk area (adhere for 7 days)	DP2.1.1.1	Mechanism to attach system to at-risk area (i.e. adhesive)
FR2.1.1.2	Provide power to system	DP2.1.1.2	Mechanism to provide power to system (i.e. batter)
FR2.1.1.3	Record pressure over time	DP2.1.1.3	System to record pressure over time
FR2.1.1.3.1	Measure pressure	DP2.1.1.3.1	Pressure sensor
FR2.1.1.3.2	Measure time	DP2.1.1.3.2	Component with clock
FR2.1.1.3.3	Save measurements	DP2.1.1.3.3	Component with memory and connection to both pressure sensor and clock (i.e. MCU)
FR1.2	Measure moisture on each at-risk area over	DP2.1.2	System to measure moisture on each at-risk area over time (i.e.sensor patch)
FR1.2.1	Attach system to at-risk area (adhere for 7 days)	DP2.1.2.1	Mechanism to attach system to at-risk area (i.e. adhesive)
FR1.2.2	Provide power to system	DP2.1.2.2	Mechanism to provide power to system (i.e. battery)
FR2.1.2.2	Record moisture over time	DP2.1.2.3	System to record moisture over time
FR2.1.2.3.1	Measure moisture	DP2.1.2.3.1	Moisture sensor
FR2.1.2.3.2	Measure time	DP2.1.2.3.2	Component with clock
FR2.1.2.3.3	Save measurements	DP2.1.2.3.3	Component with memory and connection to both moisture sensor and clock (i.e. MCU)
FR2.1.3	Measure temperature on each at-risk area over time	DP2.1.3	System to measure temperature on each at-risk area over time (i.e. sensor patch)
FR2.1.3.1	Attach system to at-risk area (adhere for 7 days)	DP2.1.3.1	Mechanism to attach system to at-risk area (i.e. adhesive)
FR2.1.3.2	Provide power to system	DP2.1.3.2	Mechanism to provide power to system (i.e. battery)
FR2.1.3.3	Record temperature over time	DP2.1.3.3	System to record temperature over time
FR2.1.3.3.1	Measure temperature	DP2.1.3.3.1	Temperature sensor
FR2.1.3.3.2	Measure time	DP2.1.3.3.2	Component with clock
FR2.1.3.3.3	Save measurements	DP2.1.3.3.3	Component with memory and connection to both temperature sensor and clock (i.e. MCU)
FR2.1.4	Display measurements to patient and caregiver(s)	DP2.1.4	System to display measurements to patient and caregiver(s) (i.e. base station)
FR2.1.4.1	Provide power to system	DP2.1.4.2	System to communicate raw measurement data to base station (wirelessly)
FR2.1.4.2.1	Transmit raw measurement data from sensor patches to base station	DP2.1.4.2.1	Tx antenna and circuitry on sensor patches
FR2.1.4.2.2	Receive raw measurement data on base station	DP2.1.4.2.2	Rx antenna and circuitry on base station
FR2.1.4.2.3	Establish connection between Tx and Rx	DP2.1.4.2.3	Shared wireless communications protocol
FR2.1.4.3	Process raw measurement data	DP2.1.4.3	Algorithm to process raw measurement data
FR2.1.4.4	Dispaly processed measurement data	DP2.1.4.4	Graphic user interface (GUI)
FR2.2	Estimate probability of damage based on present status of each factor	DP2.2	Algorithm to estimate probability of damage based on present status of each factor
FR3	Issue warning(s) to appropriate patient(s) and caregiver(s) when damage to tissues in any at-risk area(s) is imminent	DP3	System to issue warning(s) to appropriate patient(s) and caregiver(s) when damage to tissues in any at-risk area(s) is imminient (i.e. software application with graphic user interface)
FR3.1	Identify which at-risk area(s) need to attention	DP3.1	Algorithm to identify which at-risk area(s) need attention
FR3.2	Identify which patient(s) and caregiver(s) need warning	DP3.2	Algorithm to identify which patient(s) and caregiver(s) need warning
FR3.3	Generate warning	DP3.3	System to generate warning (e.g. changes on visual display, audible alarms, text messages)

3.6 Design Matrix

Table 3 through Table 16 show how the design parameters impact the ability of the design to achieve its functional requirements. The only fully coupled matrix deals

with the FRs and the DPs related to wireless communications: The protocol selected determines how the transmitter and the receiver interact and which antenna to select. The matrices that deal with measuring pressure, temperature, moisture, and time are also coupled because the microcontroller determines the accuracy of the values reported to caretakers and patients, in addition to the frequency with which the measurements are recorded. The other matrices are decoupled, meaning the DPs must be adjusted in a certain order to satisfy the FRs whenever changes to the design are made.

Table 3: Top Level FR-DP Matrix

	DP1: Method to identify at-risk areas on patients	DP2: System to determine whether damage to tissues in at-risk areas is imminent	DP3: System to issue warning(s) to appropriate patient(s) and caregiver(s) when damage to tissues in any at-risk area(s) is imminent (i.e. software application with graphic user interface)
FR1: Identify at risk areas on patients	X	O	O
FR2: Determine wheter damage to tissues in at-risk areas is imminent	X	X	O
FR3: Issue warning(s) to appropriate patient(s) and caregivers(s) when damage to tissues in any at-risk area(s) is imminent	X	X	X

Table 4: FR1 Design Matrix

	DP1.1: Education on pressure ulcer formation	DP1.2: Method to predict where pressure ulcer formation might occur on each patient
FR1.1: Understand pressure ulcer formation (when, where, why, and how it happens)	X	O
FR1.2: Predict where pressure ulcer formation might occur on each patient	X	X

Table 5: FR1.2 Design Matrix

	DP1.2.1: Method to identify how patient might be positioned	DP1.2.2: Method to identify how long patient might be in each position
FR1.2.1: Identify how patient might be positioned (e.g. lying on back, sitting in wheelchair)	X	O
FR1.2.2: Identify how long patient might be in each position	X	X

Table 6: FR2 Design Matrix

	DP2.1: Method to monitor influential factors in each at-risk area	DP2.2: Algorithm to estimate probability of damage based on present status of each factor
FR2.1: Monitor influential factors in each at-risk area	X	O
FR2.2: Estimate probability of damage based on present status of each factor	X	X

Table 7: FR2.1 Design Matrix

	DP2.1.1: System to measure pressure on each at-risk area over time (i.e. sensor patch)	DP2.1.2: System to measure moisture on each at-risk area over time (i.e. sensor patch)	DP2.1.3: System to measure temperature on each at-risk area over time (i.e. sensor patch)	DP2.1.4: System to display measurements to patient and caregiver(s) (i.e. base station)
FR2.1.1: Measure pressure on each at-risk area over time	X	O	O	O
FR2.1.2: Measure moisture on each at-risk area over time	O	X	O	O
FR2.1.3: Measure temperature on each at-risk area over time	O	O	X	O
FR2.1.4: Display measurements to patient and caregiver(s)	X	X	X	X

Table 8: FR2.1.1 Design Matrix

	DP2.1.1.1: Mechanism to attach system to at-risk area (i.e. adhesive)	DP2.1.1.2: Mechanism to provide power to system (i.e. battery)	DP2.1.1.3: System to record pressure over time
FR2.1.1.1: Attach system to at-risk area (adhere for 7 days)	X	O	O
FR2.1.1.2: Provide power to system	O	X	O
FR2.1.1.3: Record pressure over time	X	X	X

Table 9: FR2.1.1.3 Design Matrix

	DP2.1.1.1: Pressure sensor	DP2.1.1.3.2: Component with clock	DP2.1.1.3.3: Component with memory and connection to both pressure sensor and clock (i.e. MCU)
FR2.1.1.3.1: Measure pressure	X	O	X
FR2.1.1.3.2: Measure time	O	X	X
Fr2.1.1.3.3: Save measurements	X	X	X

Table 10: FR2.1.2 Design Matrix

	DP2.1.2.1: Mechanism to attach system to at-risk area (i.e. adhesive)	DP2.1.2.2: Mechanism to provide power to system (i.e. battery)	DP2.1.2.3: System to record moisture over time
FR2.1.2.1: Attach system to at-risk area (adhere for 7 days)	X	O	O
FR2.1.2.2: Provide power to system	O	X	O
FR2.1.2.3: Record moisture over time	X	X	X

Table 11: FR2.1.2.3 Design Matrix

	DP2.1.2.3.1: Moisture sensor	DP2.1.2.3.2: Component with clock	DP2.1.2.3.3: Component with memory and connection to both moisture sensor and clock (i.e. MCU)
FR2.1.2.3.1: Measure moisture	X	O	X
FR2.1.2.3.2: Measure time	O	X	X
FR2.1.2.3.3: Save measurements	X	X	X

Table 12: FR2.1.3 Design Matrix

	DP2.1.3.1: Mechanism to attach system to at-risk area (i.e. adhesive)	DP2.1.3.2: Mechanism to provide power to system (i.e. battery)	DP2.1.3.3: System to record temperature over time
FR2.1.3.1: Attach system to at-risk area (adhere for 7 days)	X	O	O
FR2.1.3.2: Provide power to system	O	X	O
FR2.1.3.3: Record temperature over time	X	X	X

Table 13: FR2.1.3.3 Design Matrix

	DP2.1.3.3.1: Temperature sensor	DP2.1.3.3.3: Component with clock	DP2.1.3.3.3: Component with memory and connection to both temperature sensor and clock (i.e. MCU)
FR2.1.3.3.1: Measure temperature	X	O	X
FR2.1.3.3.2: Measure time	O	X	X
FR2.1.3.3.3: Save measurements	X	X	X

Table 14: FR2.1.4 Design Matrix

	DP2.1.4.1: Mechanism to provide power to system (e.g. plug into outlet in wall)	DP2.1.4.2: System to communicate raw measurement data to base station (wirelessly)	DP2.1.4.3: Algorithm to process raw measurement data	DP2.1.4.4: Graphic user interface (GUI)
FR2.1.4.1: Provide power to system	X	O	O	O
FR2.1.4.2: Communicate raw measurement data to base station (wirelessly)	X	X	O	O
FR2.1.4.3: Process raw measurement data	X	X	X	O
FR2.1.4.4: Display processed measurement data	X	X	X	X

Table 15: FR2.1.4.2 Design Matrix

	DP2.4.1.2.1: Tx antenna and circuitry on sensor patches	DP2.1.4.2.2: Rx antenna and circuitry on base station	DP2.1.4.2.3: Shared wireless communications protocol
FR2.1.4.2.1: Transmit raw data from sensor patches to base station	X	O	X
FR2.1.4.2.2: Receive raw measurement data on base station	X	X	X
FR2.1.4.2.3: establish connection between Tx and Rx	X	X	X

Table 16: FR3 Design Matrix

	DP3.1: Algorithm to identify which at-risk area(s) need attention	DP3.2: Algorithm to identify which patients(s) and caregiver(s) need warning	DP3.3: System to generate warning (e.g. changes on visual display, audible alarms, text messages)
FR3.1: Identify which at-risk area(s) need attention	X	O	O
FR3.2: Identify which patient(s) and caregiver(s) need warning	X	X	O
FR3.3: Generate warning	X	X	X

4 Alternative Designs

4.1 Objective

The objective of the chapter is to present the designs that were developed based on the FR-DP decomposition and the design matrix detailed in Chapter 3 and to describe the processes through which the final rigid PCB design and the initial flexible PCB design were realized.

4.2 Conceptual Designs

This pressure ulcer prevention system must ultimately be able to monitor multiple areas at once and alert a caretaker to move the patient in order to minimize the possibility of developing a pressure ulcer. Figure 13 displays a broad overview of the system. The system developed during the PUP MQP consisted of three patches, a base station, and a user interface that could be either a computer or a smartphone. Each patch included a pressure sensor and a relative humidity and temperature sensor. The patch would sense each variable and transmit data to a base station via the built in transceiver within the microcontroller. In future prototypes, these data will then be processed with an algorithm to determine the likelihood of the patient developing a pressure ulcer in each localized area at each point in time. Whenever the algorithm detects a likelihood in excess of a probability of 90%, the base station will communicate wirelessly with the caretakers computer or smartphone to alert them that the patient needs to be repositioned.

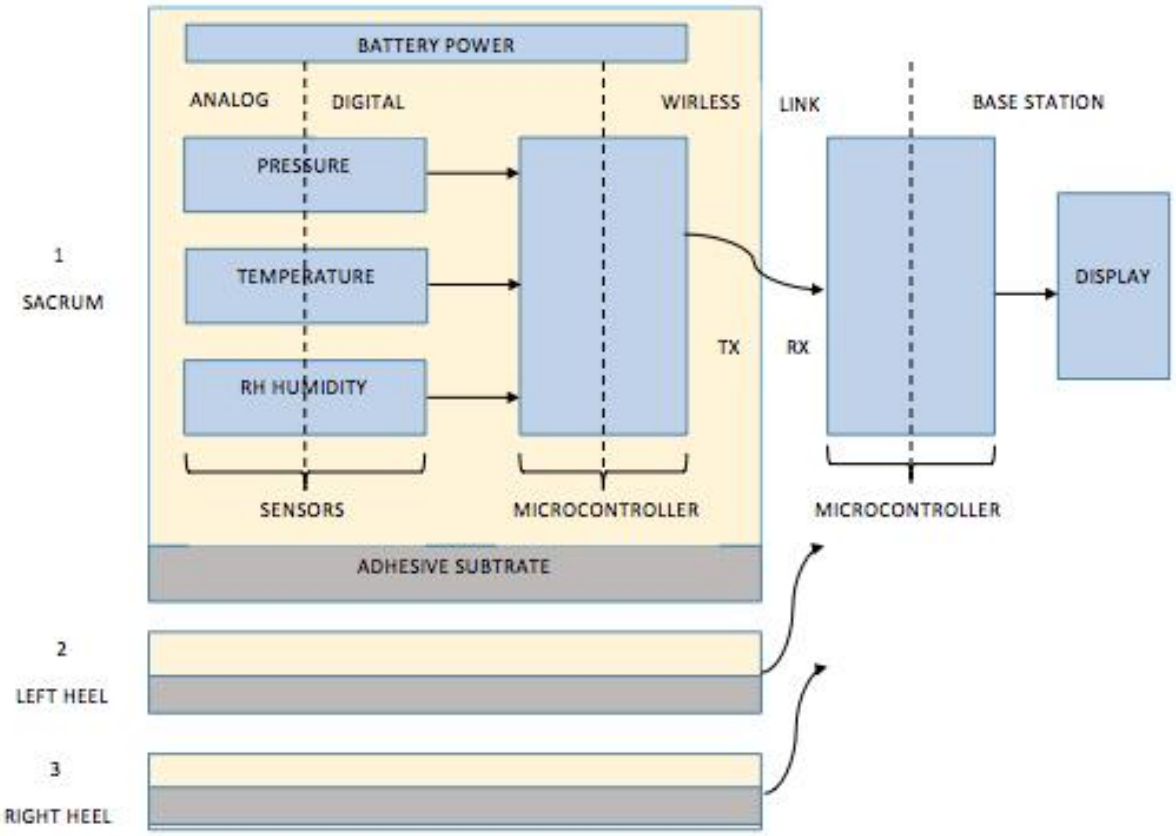

Figure 13: System Block Diagram

During the PUP MQP, three separate patches were implemented to validate the system. Ideally, future prototypes will enable more than three patches to be used to monitor multiple areas of the body simultaneously.

4.3 Component Options

There is a large variety of components currently on the market from which parts must be selected in order to design a patch that can determine the probability of pressure ulcer formation based on the pressure, temperature, and relative humidity of a localized area. However, a number of limitations eliminate the components that cannot be used, helping to narrow the scope of the search. Value analyses were conducted and the top three products for each aspect of the design are shown below.

4.3.1 Encasings and Adhesives

The material used for encasing the sensors and adhering to the skin must meet a number of requirements. The material must be able to create a waterproof environment around the area to protect the sensors. It must also adhere to the skin for at least seven days without causing further damage to the area. Moreover, the material must keep with the requirement of a desired thickness of ≤ 1 mm.

Based on these requirements, three types of wound dressing products were considered. All of these products are currently manufactured by Smith & Nephew. These

products were selected because they met the minimum requirements expected of the patch material and have been proven effective in pressure ulcer care.

Table 17: Product Comparison for Encasings and Adhesives

Design Goals	Cost	Material	Dimensions	Waterproof	Duration of Wear	Bonus (Prevent Pressure Ulcers)
Allevyn Life Patch	$1.99	Soft Silicone dressing, hydro cellular foam, hyper absorbent core	18.29cm x 10.3cm	Yes	7 days	Distributes pressure to prevent pressure ulcers, prevents leakage
Replicare Thin	$5.21	Hydrocolloid dressing	5cm x 7cm x 2.32cm	Yes	21 days	Leaves no residue, adapatable to awkward areas
OPSITE Film	$0.01	Acrylic adhesive	121cm x 997cm	Yes	7 days	Moisture vapor permeable, adaptable to awkward areas

Table 17 compares the selected products based on cost, size, availability, durability, and additional beneficial features of the product. The cost listed was determined after normalizing the area of each bandage to that of a circle with a diameter of 3.5cm. The circle with a 3.5cm diameter is the target shape for the final version of the patch to be made for manufacturing. The products were compared relative to each other instead of a standard for the category of cost. The size was assessed in terms of thickness, as the ideal dimension of the patch is a thickness of ≤ 1 mm. Waterproof and leakage prevention capabilities were also considered, so both the electronics and the patients skin would be protected from further damage. Durability was also an important factor because the ideal operational lifetime time of the patch is at least seven days. Lastly, any bonus features about the product that aided in its function to prevent pressure ulcers, or to prevent factors that contribute to pressure ulcer formation, were considered. According to the value analysis done in Appendix A, the OPSITE Film product was most desirable, followed by the Allevyn Life Patch and the Replicare Thin (ALLEVYN Life; OPSITE Film Dressings; REPLICARE Thin). The product comparison in Table 17 above also supports the results of the value analysis. The sections that are highlighted in green show the desirable qualities of the product relative to each other while the red indicate undesirable qualities. The yellow highlight indicates that the product was satisfactory in that category or that there was not enough information about the product for it to be compared.

Despite the OPSITE Film being the leading product, there are situations where the Allevyn Life patch outrank the OPSITE Film in terms of performance. The Allevyn Life patch is desirable for larger areas, such as the sacrum, where it is currently used in preventing pressure ulcers. The patch itself is also intended for large, flat areas, making it undesirable for awkward areas such as the heel or elbow. On the other hand, the OPSITE

Film has desirable traits such as moisture-vapor permeable characteristic. Moreover, the OPSITE Film is adaptable to awkward areas, as it does not have the foam layer to evenly distribute pressure. Due to its conforming qualities, it could be used as the adhesive for sensors that are placed in areas such as the heel or elbow. Both the Allevyn Life patch and OPSITE Film would be potential products to use as the encasing and adhesive.

While these adhesives were our recommendations, the decision of which adhesive to use was ultimately made by the biomedical engineering team that also worked on this project. After conducting their own tests and research, they determined the top two materials for the adhesive to be Tegaderm and 3M Transpore Tape, and yellow polyurethane foam for the encasing (Ooyama-Searls, Pachucki, & Parent, personal communication, 2016).

4.3.2 Sensors

The following section discusses which sensors were considered and how value analysis was used to find the best sensors for the design.

Pressure Sensors

There were many different types of pressure sensors that could have been used in the implementation of the first prototype. In order to pick the best type of sensor that matched the requirements, a value analysis was conducted for the top sensors selected. Based on the design requirements, the following value criteria were established: cost, size, weight, accuracy, power requirement, familiarity, availability, and, range and repeatability. Each goal was weighted based on its importance in the design. Size and cost were considered the most important factors and were assigned to a weight factor of 100 with the rest relative to them. Appendix A shows the weighted value of each criterion. The score for each design goal was calculated by multiplying the rating and the weight factor. A rating of 5 was excellent, 4 was good, 3 was satisfactory, 2 was mediocre, and 1 was unsatisfactory. The individual scores for the design goals were summed to get a final total score for each design option. The design goal with the highest score was considered the most desirable choice and would be used in the design.

Table 18: Initial Product Comparison for Pressure Sensors

Pressure Sensors	Unit Cost (High Volume)	Pressure Range [kPa]	Sensing Area [mm^2]	Thickness [mm]	Experience with the Product and/or Manufacturer
FlexiForce A401	$17.50	0 - 219.5	506.7	0.203	Prod = HIGH Man = HIGH
FSR 402 Short	$6.16	1.6 - 157.9	12.7	0.46	Prod = HIGH Man = HIGH
FSR 402	$4.24	1.2 - 118.2	14.68	0.46	Prod = LOW Man = HIGH
FSR 400	$3.85	9.9 - 986.7	5.08	0.30	Prod = LOW Man = HIGH
LPS25HB	$1.52	26.0 - 126.0	0.135	0.80	Prod = LOW Man = LOW

According to the value analysis, the FSR 402 Short from Interlink Electronics was the most desirable pressure sensor, as it matched the design requirements best. The table above compares the top five components from the value analysis based on unit cost, pressure range, sensing area, thickness and experience with the product and/or the manufacturer. The green color indicates that the parameter best fits the design requirement, yellow indicates that the parameter is good and can be worked with, whereas, red indicates it to be an undesired parameter and does not match with the design requirement.

Table 19: Final Product Comparison for Pressure Sensors

Company	Interlink	Tangio	Tekscan	Tekscan	Sensitronics
Sensor	FSR-402 Short	TPE-502	A201	A301	1/2 Inch ThruMode
Unit Price	$12.54	$5.00	$19.82	$12.62	$6.00
Device Length	25mm	25mm	57mm**	32mm	50mm
Maximum Thickness	0.46mm	0.25mm	0.203mm	0.203mm	0.4318mm
Sensing Diameter	12.70mm	12.70mm	9.53mm	9.53mm	12.70mm
Connector Type(s)	1. exposed carbon traces 2. solder tabs 3. female contacts 4. female contacts w/ housing	1. exposed carbon traces 2. solder tabs 3. female contacts w/ housing	3-pin male square pin	2-pin male square pin	female contacts w/ housing
Single Part Repeatability	+/−2%	2% (1)	< +/−2.5% (3)	< +/−2.5% (3)	+/−5% (4)
Part-to-Part Repeatability	+/−6%	+/−4% (2)		+/−15% (5)	
Hysteresis	10%	5%	<4.5%	<4.5%	
Long-Term Drift*	<5%	<1%	<5%	<5%	

*per log10 time ** after being trimmed; original length is 197 mm

1. measured as [one standard deviation] / [mean], based on 100 actuations with 1kg
2. measured as [one standard deviation] / [mean], based on 100 sensors in same batch
3. measured as percent of full-scale, using conditioned sensor with 80% of full force applied
4. measured as percent of established nominal resistance, with consistent actuations
5. measured as percent of average resistance, with consistent actuations

The Red-Yellow-Green scale used in Table 19 is based on comparison with the Interlink sensor: Green = same as Interlink or better than Interlink, Yellow = slightly worse than Interlink but still acceptable, Red = much worse.

Relative Humidity Sensors

Beginning with the relative humidity sensors explored and selected in Gutierrez et. al (2011) and Hause et. al (2012), fourteen different options from five different manufacturers were compared based on unit cost, device dimensions, required input power (voltage and current), sensor accuracy, compatibility with microcontrollers, prior experience with the product and the manufacturer, and availability for purchase. Since most relative humidity sensors investigated were digital, and because digital relative humidity measurements factor in ambient temperature, the accuracy of the built-in temperature sensor on each device was also considered. The value analysis conducted to determine the top three options is depicted and explained in Appendix A.

The best relative humidity sensors for the pressure ulcer prevention system are compared more closely in Table 20. The Texas Instruments HDC1010 was determined to be the top option due to its low cost, acceptable size, low input current requirement, and high relative humidity and temperature sensor accuracies.

Once the PUP MQP team realized more progress could be made with an analog relative humidity sensor, the team researched available products on DigiKey.com and selected the only analog sensor less than 1 mm in thickness. Thus the Sensirion SHT31-ARP-B was included in the second iteration of the patch design.

Temperature Sensors

Again, beginning with the temperature sensors explored and selected in Hause et al. (2012) and in Crivello et al. (2016a; 2016b), seven different options from four different manufacturers were compared based on unit cost, size, required input power (voltage and current), sensor accuracy, compatibility with microcontrollers, prior experience with the product and the manufacturer, and availability for purchase. The built-in temperature sensors included with the digital relative humidity sensors were also considered. The value analysis conducted to determine the top three options is depicted and explained in Appendix A.

The best temperature sensors for the pressure ulcer prevention system are compared more closely in Table 21. All three are variants of the Murata NCP15XH resistive temperature detector, which was selected and used in Crivello et al. (2016a; 2016b). The NCP15XH103F03RC was determined to be the top option due to its acceptable cost and accuracy.

However, to reduce design complexity and cost, the built-in temperature sensor included in the Texas Instruments HDC1010 was used in lieu of a separate Murata sensor since the 0.2°C accuracy was almost good enough to be acceptable in the pressure ulcer prevention system.

Table 20: Top Relative Humidity Sensor Options

RH Sensors	Unit Cost (High volume)	Device Height	Device Area	Required Input Voltage	Required Input Current	Sensor Accuracy	Experience with Product and or Manufacturer	Temp Accuracy
Texas Instruments HDC1010	$1.10	0.675 mm	3.3 $5mm^2$	2.7V to 5.5V (3.0V typical)	220uA (on) 0.2uA (sleep)	+/− 2%RH	Prod = LOW Man = HIGH	+/−0.2°C
Sensirion SHWT2	$1.60	0.5 mm	0.91 mm^2	1.62V to 1.98V (1.8V typical)	465 uA (on) 1.5 uA (sleep)	+/−3%	Prod = LOW Man = LOW	+/−0.4°C
Texas Instruments HDC1080	$1.20	0.8 mm	9.00 mm^2	2.7V to 5.5V (3.0V typical)	220 uA (on) 0.2 uA (sleep)	+/−2%	Prod = LOW Man = HIGH	+/−0.2°C

Table 21: Top Temperature Sensor Options

Temperature Sensors	Unit Cost (High Volume)	Sensor Accuracy
Murata NCP15XH103F03RC	$0.04	R:+/−1%, β: +/−1%
Murata NCP15XH103D03RC	$0.16	R:+/−0.5%, β: +/−0.7%
Murata NCP15XH103E04RC	$0.03	R:+/−3%, β: +/−1

4.3.3 Wireless Communication

Bluetooth Low Energy (BLE) and ZigBee are the two most widely used low power protocols out of numerous wireless communication protocols. Manufacturers may also design their transceivers to utilize a protocol specific to their organization. These are usually listed as proprietary protocols.

One benefit of using ubiquitous protocols such as BLE and ZigBee is their scalability. Both operate with a center band frequency around 2.4GHz, which is what most Wi-Fi channels operate at. Thus, for example, the base station designed to communicate via BLE or ZigBee may be reconfigured with minimal efforts to communicate with other devices developed by a different group of engineers as long as their device communicates in the same protocol. One benefit of using non-ubiquitous, proprietary protocols is their security. Because these protocols are usually not openly characterized or widely known, hackers with malicious intent will most likely lack the tools necessary to bypass the security in a timely manner. The most notable differences between BLE and ZigBee applicable to this project are their transmission rate and

their energy consumption. ZigBee has much slower transmission rate compared to that of BLE. As a result, ZigBee has much lower energy consumption.

In conclusion, scalability was considered to be more important than security. Therefore, BLE and ZigBee were chosen over other protocols. BLE was preferred due to its compatibility with existing devices; however, ZigBee should be used in future designs if the energy efficiency proves to be a more critical factor.

4.3.4 Antennas

Two types of antennas were evaluated, each with two configurations and two modes of operation. The first type of antenna considered was a trace antenna. Trace antennas are designed in layout software and printed onto a circuit board much like any other copper trace. One benefit of trace antennas is that they require little to no cost to implement because they are part of the circuit board. One drawback of trace antennas is their increased area. Their performance varies depending on their implementation. While well designed trace antennas may have very good performance, they are often difficult to work with because trace antennas are greatly affected by nearby components. Tuning trace antennas is also difficult because they can only be characterized after implementation, which requires PCB redesign if iteration is necessary.

Another type of antenna considered was a chip antenna. Chip antennas are separate from the circuit board and are often surface mounted on the board. While not providing significant performance advantages, they are guaranteed to work moderately well, and they are smaller compared to other types of antennas.

Two configurations of antennas include monopole and dipole. Monopole antennas are directional, providing high gain towards the direction they are facing but decaying rapidly when the receiver is oriented in the wrong direction. Dipole antennas are omnidirectional, providing moderate gain in all directions. Dipole antennas were considered more suitable to the project because the short distance between the patient and the base station does not require high gain, and there is no guarantee that the antenna will be facing the base station at all times.

The two modes of operation include single ended antennas and differential antennas. In single ended antennas, the transmitting signal is referenced to ground. Its benefits come from simplicity of design and lower energy consumption. In differential antennas, the transmitting signal is referenced to the inverse of itself. Its primary benefit is higher noise tolerances.

A separate value analysis was performed on antennas for different frequencies. For 2.4 GHz, two antennas by Johanson Technology scored the highest. The deciding factor between the two is that one of them has higher gain and lower return loss, and the other higher return loss and lower gain. Given that higher return loss is preferable, 2450AT42A100E ultimately scored the highest. For 915 MHz, two antennas were chosen. The antenna made by Johanson Technology is better in all attributes as reflected in the analysis shown in Appendix A.

A microcontroller module with an embedded antenna was ultimately chosen due to ease of implementation. The microcontroller utilizes the Bluetooth Low Energy protocol and a 2.4GHz chip antenna.

Table 22: Antenna Comparison

Part Number	Manufacturer	Height	Center Band	Return Loss	Gain	Price
2450AT07A0100T	Johanson Technology Inc.	0.37 mm	2.4GHz	6.5dB	1dBi	$0.25
2450AT42A100E	Johanson Technology Inc.	0.37 mm	2.4GHz	9.5dB	0dBi	$0.28
0915AT43A0026E	Johanson Technology Inc.	0.8 mm	915MHz	8.5dB	1dBi	$0.38
W3014	Pulse Electronics Corporation	1.5 mm	915MHz	7dB	-0.5dBi	$0.74

4.3.5 Microcontrollers

Microcontrollers from five manufacturers were considered, which included Texas Instruments, RF Digital Corporation, Nordic Semiconductor, Atmel, and Analog Devices.

Attributes that were considered in the value analysis were cost, size, power required, accuracy, familiarity, and availability. The size value was determined by averaging the height value and the area value because length and width are individually not as important as height, which must meet a 1 mm constraint. The power value was determined by averaging the value for the minimum supply voltage needed and the value for the maximum current draw. The accuracy value was determined by the accuracy of the ADC in the microcontrollers. The familiarity value was determined by prior experience with the manufacturer and the MCU, the tools and software currently available, and external components required to implement the MCU.

The top three choices were the CC2650MODA, CC2640, and ATBTLC1000. The greatest strength of CC2650MODA was that it included all the external components necessary to run the MCU, including clock crystals, lumped elements, and antennas. It was likely to save space and most importantly time. The CC2640 was well-rounded in all respects, and the ATBTLC1000 had exceptionally low current draw. The CC2650MODA scored the highest overall and was chosen as the component.

Table 23: Microcontroller Comparison

MCU	Include Antenna	CPU Current Draw	TX Current Draw	RX Sensitivity	ADC	Supply Voltage	Price	Dimensions (mm)
CC2640	N	1.45 mA + 30.5 uA/MHz	4.71 mA + 1.3 mA/mW	-97dBm	ADC1 - 8ch	1.8V - 3.8V	$3.25	4.25 x 4.25x 1.15
CC2650MOI	Y	1.4 5mA + 30.5 uA/MHz	5. 6mA + 1.2 mA/mW	-97dBm	ADC1 - 8ch	1.8V - 3.8V	$7.57	16.9 x 11 x 1.15
ATBTLC100	N	0.85 mA idle	2.19 mA + 0.81 mA/mW	-95dBm	ADC1 - 2ch	1.8V - 4.3V	$4.65	4x4x0.85

4.3.6 Power Supplies

The power supplies considered for the system included zinc air batteries (which are commonly used in hearing aids), silver oxide batteries (which are used in certain ingestible biomedical devices), primary lithium and lithium polymer batteries, supercapacitors, and thermoelectric generators. Zinc air batteries were concluded to be too thick for this application, since the thinnest ones on the market (size 10) are between 3.3 mm and 3.6 mm from terminal to terminal (Hearing Aid Battery Shop, 2017). Thermoelectric generators (TEGs) were concluded to be electrically insufficient, since most available TEGs required a 5°C temperature differential to operate and needed a DC booster to supply enough voltage to a circuit. With the Micropelt MPG-D655, for example, a device with a 1 mm thickness required a 40°C differential across it to generate 3.3 V.

The best battery options were compared based on unit cost, size, output power (nominal voltage and maximum drain current), nominal capacity, and availability for purchase. The value analysis conducted to determine the top options is depicted and explained in Appendix A. The best power sources for the pressure ulcer prevention system were determined to be lithium button cells, including the CR1616, CR1620, and CR2016, and lithium polymer batteries, which are compared in Table 24.

Table 24: Power Source Comparison

Company	Product	Unit Cost	Thickness	Area	Capacity	Max Drain Current (continuous/pulse)	Flex
VARTA Microbattery	Li Button CR 1616	$0.66	1.6 mm	d = 16.0 mm	55 mAh	3 mA / 8 mA	None
VARTA Microbattery	Li Button CR 1620	$0.86	2.0 mm	d = 16.0 mm	70 mAh	3 mA / 8 mA	None
VARTA Microbattery	Li Button CR 2016	$0.32	1.6 mm	d = 20.0 mm	90 mAh	3 mA / 10 mA	None
PD Battery	Li Polymer PDCP044	?	0.45 mm	45.5 mm x 60 mm	100 mAh	10 mA / 20 mA	HIGH
PD Battery	Li Polymer PDCP053	?	0.5 mm	30 mm x 50 mm	80 mAh	15 mAQ / 30 mA	HIGH
Bright Volt	Li Polymer BV-542229-25	?	<0.54 mm	25 mm x 29 mm	25 mAh	?	HIGH
GM Battery	Li Polymer CP202914	$5.00	2.1 mm	29 mm x 15 mm	65 mAh	5 mA / 15 mA	HIGH
GM Battery	Li Polymer CP142828	$5.00	1.4 mm	28 mm x 28 mm	80 mAh	8 mA / 24 mA	HIGH

All options in Table 24 have 3.0V nominal voltage

Though neither option was considered ideal, both had advantages over other products on the market: The lithium button cells were small in area, widely available, and relatively low in cost. The lithium polymer batteries were very thin and flexible, and they were more available and less expensive than other thin film products that were explored. Both lithium button cells and lithium polymer batteries were able to provide enough voltage, current, and capacity with one cell. However, lithium button cells were thicker, and lithium polymer batteries were more expensive and more difficult to acquire. Both options were explored further in the preliminary design before one was selected for use in the final design. Because batteries slowly lose voltage as they are depleted, a buck-boost converter was initially incorporated in the preliminary design to stabilize the supply voltage. It was soon removed upon discovering the MCUs ability operate

in voltage as low as 1.8 V and to scale the reference voltage, VREF, with the supply voltage.

4.4 Design Overview

4.4.1 Preliminary Design

The image in Figure 14 shows the initial targeted shape of the sensor patch being designed here. Marketable patches are ultimately expected to be approximately the same size and shape as ECG electrodes. However, the components available to the PUP MQP team were too large to compress into such a small area. To prevent stiff components, such as the microcontroller module, from exacerbating pressure on at-risk areas, the patch was designed to wrap around human appendages like KT Tape. The I-shape seemed best able to accommodate all components while maximizing wearability and comfort.

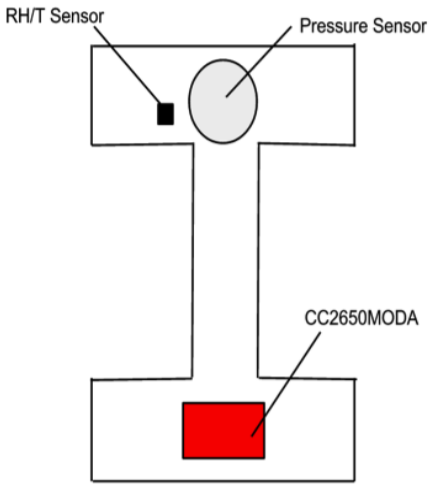

Figure 14: I-Shape Design for Sensor Patch

The detailed system block diagram depicted in Figure 15 shows the original components selected and the original plan for implementation on the rigid PCB. The buck-boost converter was included because the capabilities of the microcontroller module with respect to reference voltage supply were not yet fully understood. Also, the resistance of the resistor in the voltage divider with the pressure sensor was chosen arbitrarily based on graphs provided in the Interlink FSR data sheet.

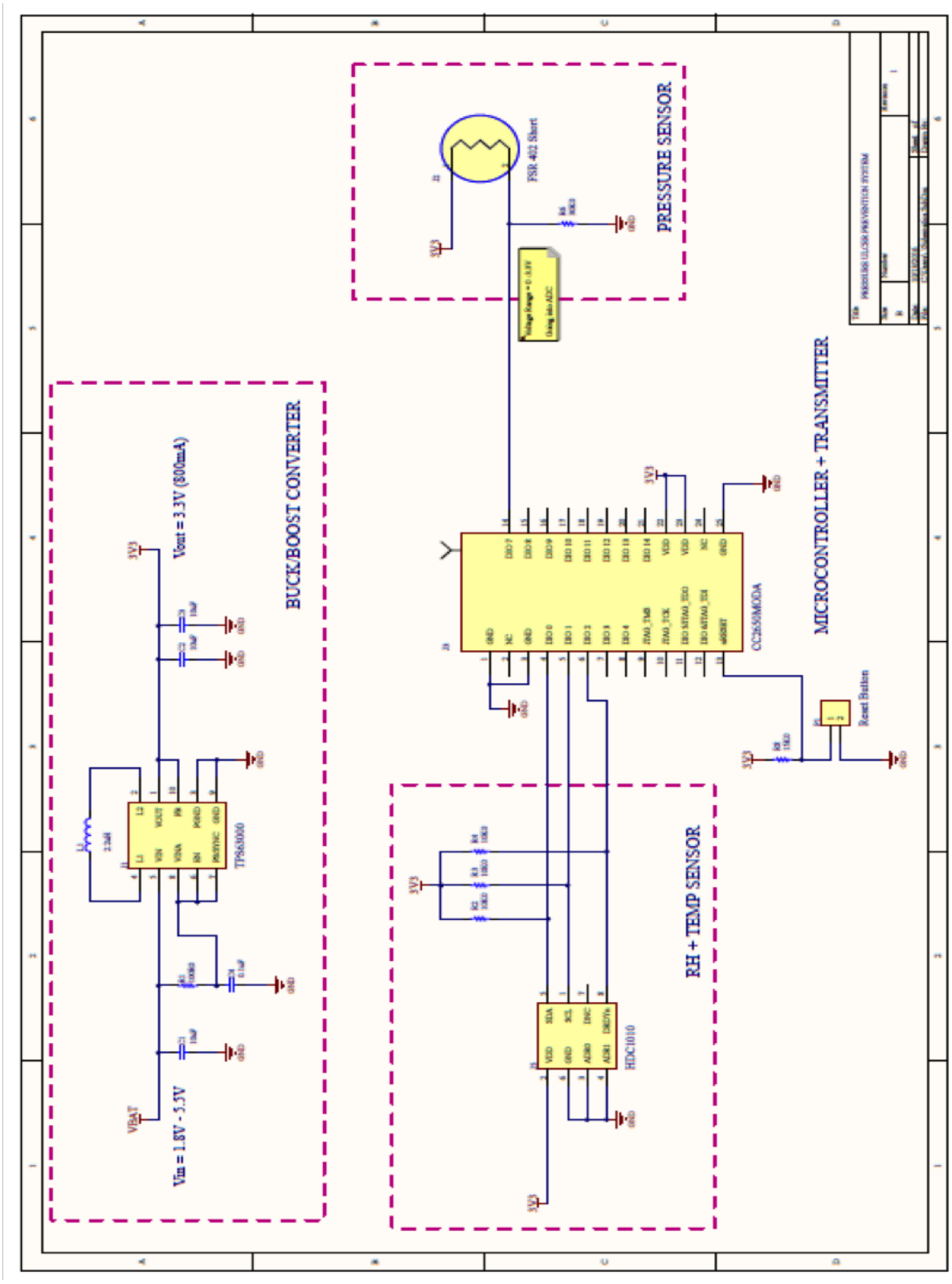

Figure 15: Detailed Schematic of Preliminary Design

4.4.2 First Rigid PCB

The detailed system block diagram depicted in Figure 16 shows the components used in the actual implementation of the first rigid PCB. Note the buck-boost converter was removed,

and the value of the resistor in the voltage divider with the pressure sensor was changed to maximize the resolution at 30 mmHg in accordance with the analyses presented in section 4.5.1. The analog relative humidity and temperature sensor was added as well.

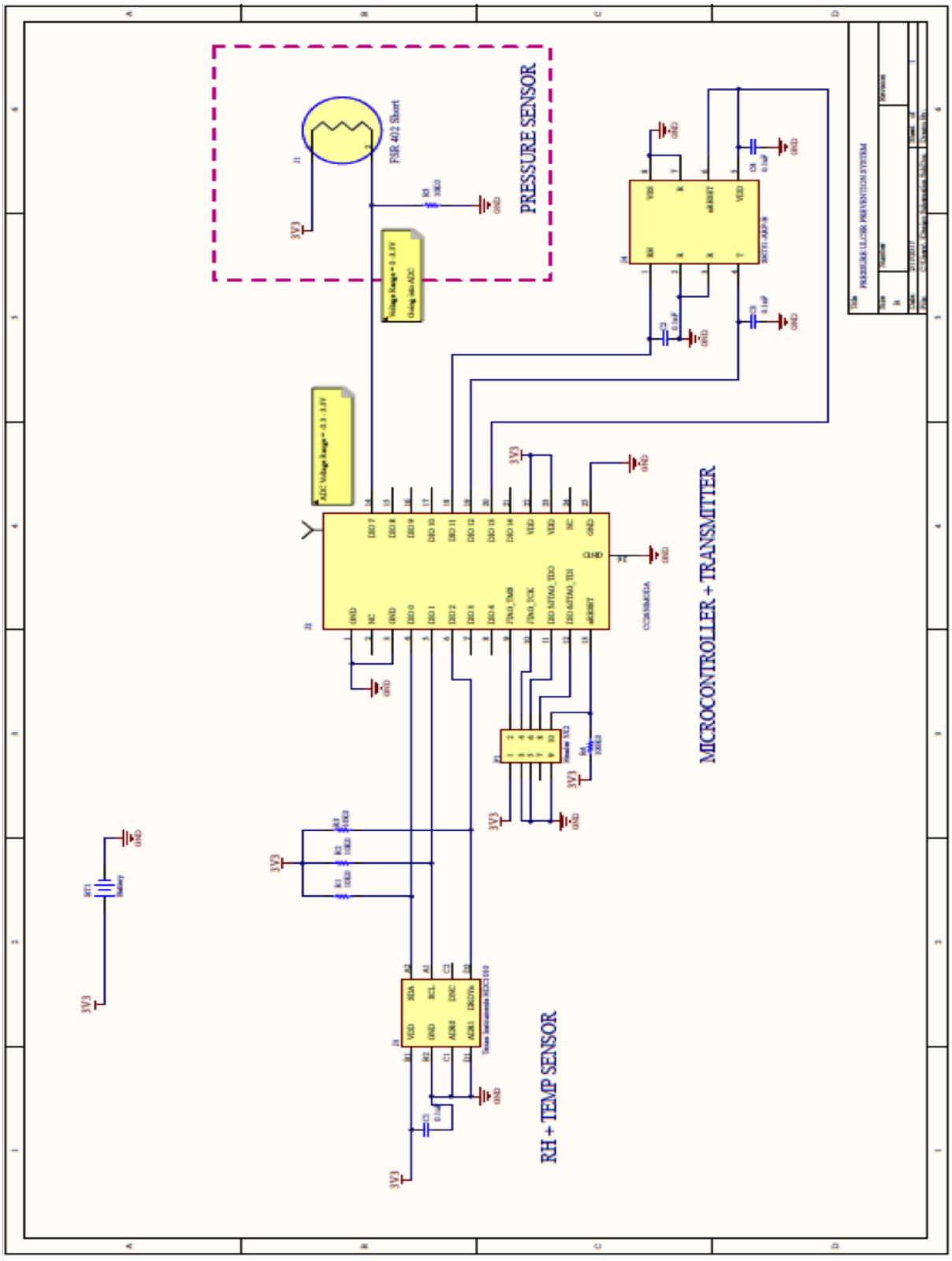

Figure 16: Detailed Schematic of First Rigid PCB

4.5 Rigid PCB Design

Although the final version of the patch was implemented on flexible PCB substrate, there were a number of reasons as to why the first prototypes were designed using rigid PCB substrate. Rigid PCBs are generally cheaper and faster to produce. Moreover, they are better suited for testing the proof of concept of the design, which was the desired application at this stage.

After reviewing the preliminary design discussed in section 4.4, the PCB design was modified to eliminate as many components as possible in order to simplify the design and reduce the cost. By doing so, the buck-boost converter was removed.

The value of the fixed resistor that used in the voltage divider with the pressure sensor was also changed. Beginning with the force-resistance curves in the data sheet of the FSR-402 Short, an analysis was conducted to determine which resistance value would produce the best resolution at 30 mmHg.

4.5.1 Voltage Divider Resistor Selection

Since pressures between 30 mmHg and 40 mmHg are expected to obstruct blood flow in the capillaries that run over bony prominences, the pressure sensor output must achieve its highest resolution at approximately 30 mmHg. When the resistive force sensor is implemented in the voltage divider configuration depicted in Figure 17, the resolution of the output voltage V_{OUT} is determined by the resistance of the fixed resistor R. The relationship between V_{OUT} and R is defined by Equation 1:

$$V_{OUT} = V_{DD}\left(\frac{R}{R + R_{FSR}}\right) \tag{1}$$

where R_{FSR} is derived in Crivello et al. (2016a) as:

$$R_{FSR} = R_0\left(\frac{F}{F_0}^{x}\right) \tag{2}$$

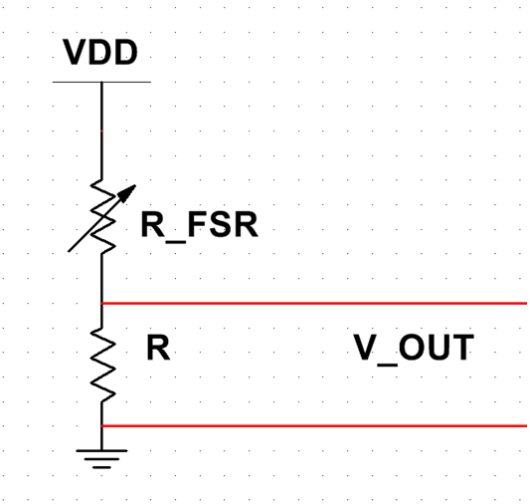

Figure 17: Diagram of FSR Configuration

Combining Equation (1) and Equation (2) and replacing normalized force with normalized pressure yields the overall relationship between output voltage and applied pressure:

$$V_{OUT} = V_{DD}\left(\frac{R}{\left(R + R_0\left(\frac{P}{P_0}\right)^x\right)}\right) \tag{3}$$

Equation (3) is depicted in Figure X with applied pressures ranging from about 0 mmHg to about 120 mmHg and voltage divider resistance values ranging from 3kΩ to 100kΩ.

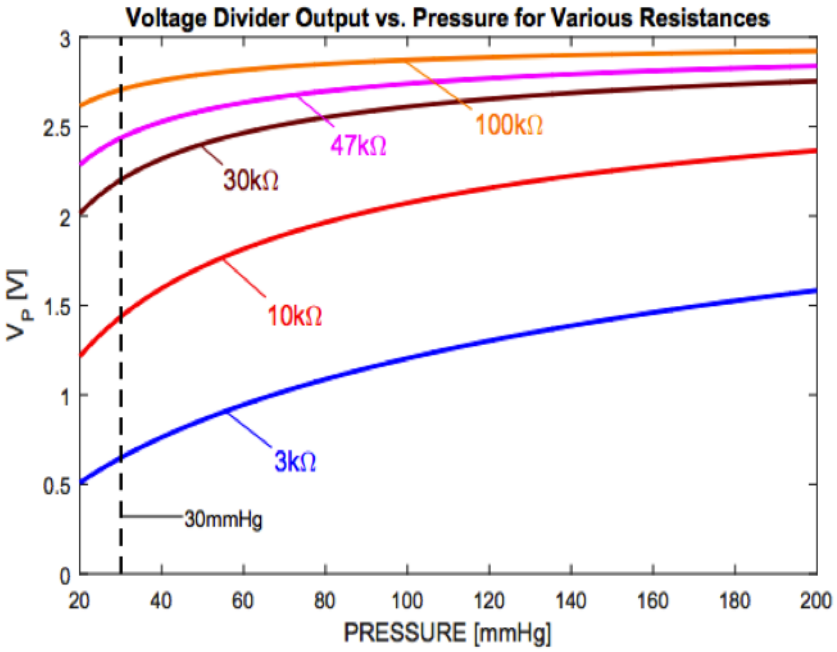

Figure 18: Voltage Divider Output versus Pressure Input

The resolution of the output voltage in Equation (3) is equal to the first derivative of the output voltage with respect to pressure:

$$\frac{dV_{OUT}}{dP} = \frac{-V_{DD}RR_0log(\frac{P}{P_0})(\frac{P}{P_0})x}{P(R + R_0\frac{P}{P_0}x)2)} \tag{4}$$

In a plot of output voltage versus applied pressure, the best resistance value to use in the voltage divider yields the curve in which the slope at 30 mmHg is greatest, as depicted in Figure 19.

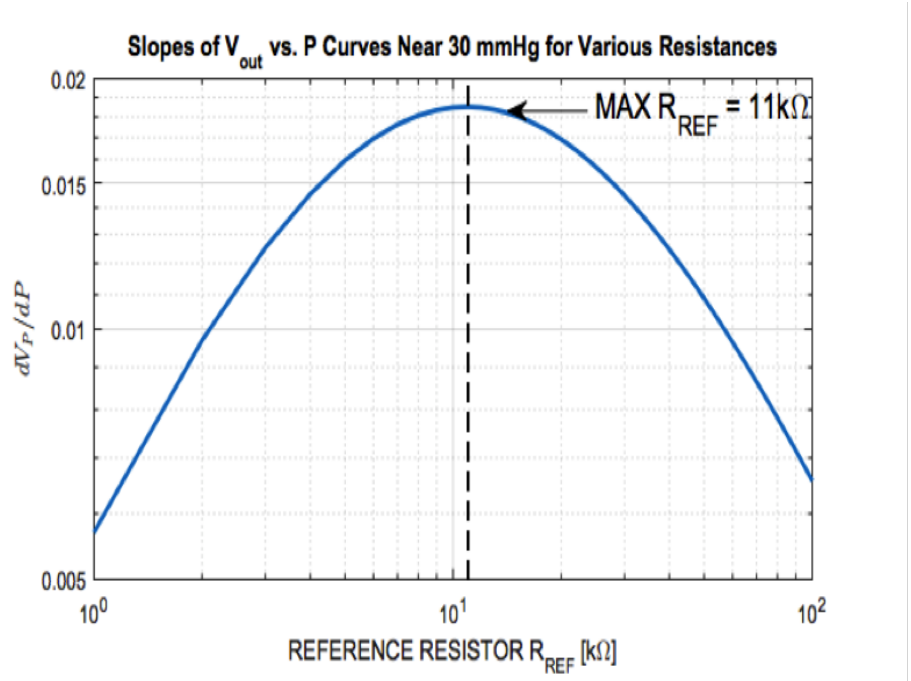

Figure 19: Best Resistor Value for Maximum Resolution at 30 mmHg

The slope of the output voltage versus applied pressure curve achieves its maximum value when the first derivative of Equation 4, taken with respect to resistance, is equal to zero. The resistance value at which the maximum slope occurs is:

$$R = R_0 \left(\frac{P}{P_0} \right)^x \tag{5}$$

Table 25: Summary of Voltage Divider Resistor Analysis

Constants	$R_0 = 200k\Omega$ $P_0 = 0.5807$mmHg x = -0.738
Applied Pressure (mmHg)	Voltage Divider Resistance (kΩ)
30	10.8815
35	9.7114
40	8.8000

In attempt to achieve the best resolution possible at applied pressures near 30 mmHg, the resistance value of the fixed resistor in the voltage divider was chosen to be $10k\Omega$. Although the calculated resistance was $11k\Omega$, a $10k\Omega$ was used in the design due to the time constraints of the project. A $11k\Omega$ resistor had a lead time of at least 10 weeks.

4.5.2 First Rigid PCB

Moreover, a bypass capacitor of 0.1μF was added near the input pin of the HDC 1010 sensor upon recommendation of the data sheet to dampen the noise present at all frequencies.

The PCB was designed using Altium Designer Software due to the familiarity of the tool. Learning to use new software would have taken time and delayed the process.

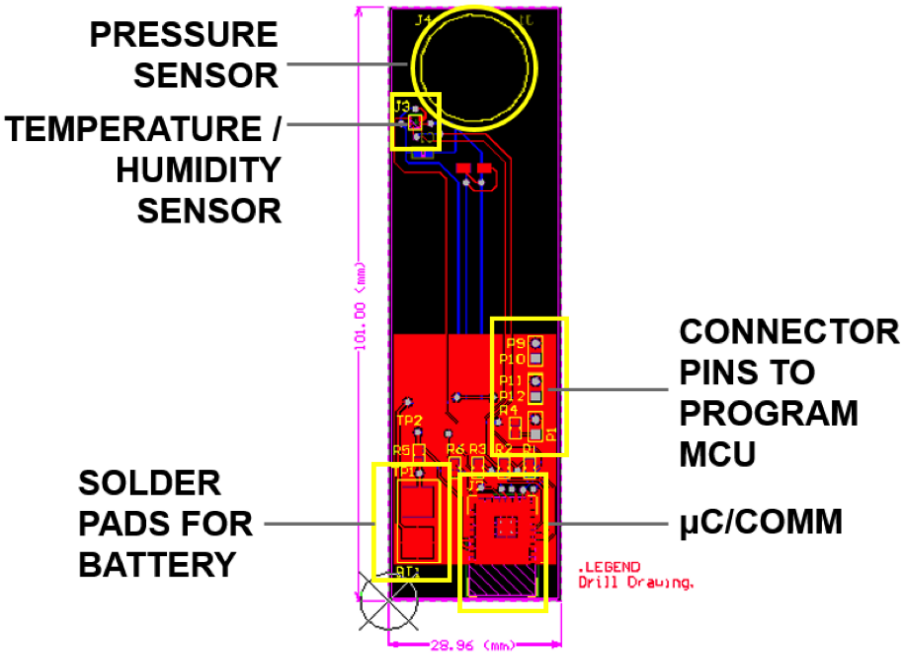

Figure 20: Initial Rigid PCB Design

The PCB depicted in Figure 20 is a two-layered board with components on both sides. By having a two-layered board, the thickness was minimized and was kept at 0.062, which is the standard thickness for Advanced Circuits (PCB manufacturer). Reducing the thickness of a one-layered board would have cost more. Moreover, having two layers allowed for the separation of traces. For instance, the communication and power lines were kept on opposite layers to avoid interference. Furthermore, the electrical components that were not paramount to measuring the desired variables of pressure, relative humidity, and temperature, were located on the side of the board that would not come in contact with the patient. This ensured that there would not be any unnecessary interactions between the patients skin and the electrical components. However, footprints for the pressure sensor were laid on both sides of the PCB, allowing the flexibility to solder the pressure sensor on either side.

The dimensions of the first PCB were 101mm x 28.956mm. These dimensions were acceptable, since the purpose of the prototype was to verify component functionality and to establish wireless communication between the microcontroller and the base station; the simplest and least expensive size and shape would enable the board to fulfill that purpose.

Figure 20 shows the layout of the electrical components. The FSR-402 Short sensor, along with the HDC1010 sensor, were on the one end while other components such as the microcontroller and the resistors, were on the other end. The HDC1010 sensor was soldered on the layer of the PCB that would not be in contact with skin because the relative humidity sensor and temperature sensor are on the bottom side of the package. Such a design protects the sensing elements from exposure to dirt, dust, and other contaminants, making the device as a whole more robust. To enable the device to monitor the side of the PCB in contact with the patient's skin and thus provide both sensors with an adequate sensing environment, vias were included in the PCB near the HDC1010 in accordance with the data sheet of the HDC1010. The design also provided for pads with which an external power supply could be connected and a 2 resistor with which power consumption tests could be conducted.

Originally, the PCB design did not include the CC2650MODA, as the module with a height of 2.49 mm surpassed the desired thickness of 1 mm. Despite attempts to use the CC2650 MCU in the design, the CC2650MODA was desired due to the fact that it did not require the

external components (such as the antenna and crystal oscillators) that the CC2650 MCU did. Upon reviewing the issue of thickness with Dr. Dunn of UMMS, the design was cleared to use the CC2650MODA under the condition that it would not be placed in an area where it could end up between a bony prominence and a hard surface.

The rigid PCB design developed here was intended for areas on the body like the heel and the elbow. For example, the end of the PCB with the FSR-402 Short and the HDC1010 would be attached proximally to the heel while the end with the bulkier components, including the MCU, would be attached distally to avoid any contact with the bed and the patient simultaneously. The patch would then essentially wrap around the patients foot, whether it be on the medial side of the foot or on the bottom surface (assuming that the patient is in supine position).

4.5.3 Second Rigid PCB

The first version of the PCB could not be tested since the HDC1010 and the CC2650MODA were not hand solderable due to small size and numerous pins. After receiving the PCBs and realizing neither the team members nor the resources at WPI were skilled enough to connect the components to the boards, the PUP MQP team determined that all future prototypes using these components would require in-house assembly.

Therefore, another PCB was designed and ordered such that Advanced Circuits soldered the components before shipping the boards. The design, depicted in Figure 21, included some modifications.

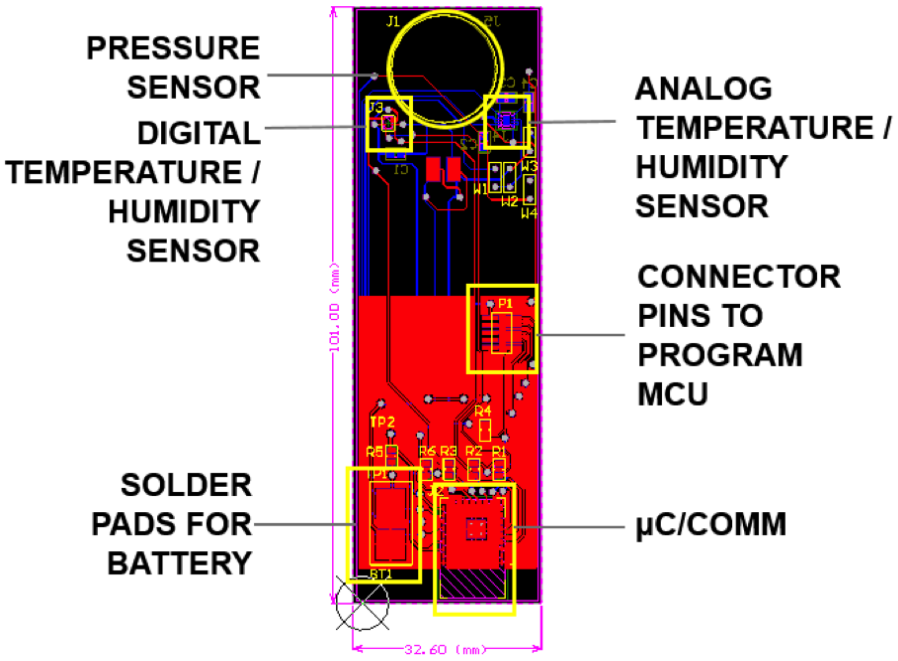

Figure 21: Second Rigid PCB Design

First, a new relative humidity and temperature sensor was added. The SHT31-ARP-B was selected because of its simplicity: It output analog voltages corresponding to the relative humidity and the temperature, which could be read through the ADC of the MCU exactly as the output of the voltage divider with the pressure sensor was being read. The HDC1010 uses I2C to transfer data to an MCU, so it has to be programmed before it can be tested, and the team members decided the project goal would likely not be achieved if they spent more time struggling with code than demonstrating prototypes. The major issue with the new relative

humidity and temperature sensor was that it was not as power efficient as the HDC1010. In order to save power, the team decided to power the SHT31-ARP-B through the MCU so it could be switched on to collect and send data and switched off otherwise.

Second, jumper cables were added to the design. Depending on how they were connected, they could be used to power the SHT31-ARP-B either through the MCU or through the battery. In addition, programming connectors were added to the design. Since the prototype would never be tested on people, the height of the connectors was deemed unimportant. Note the design approach taken with the flexible PCB was much different, since it was expected to be tested on live animals.

The final implementation of the second rigid PCB design is shown below in Figure 22.

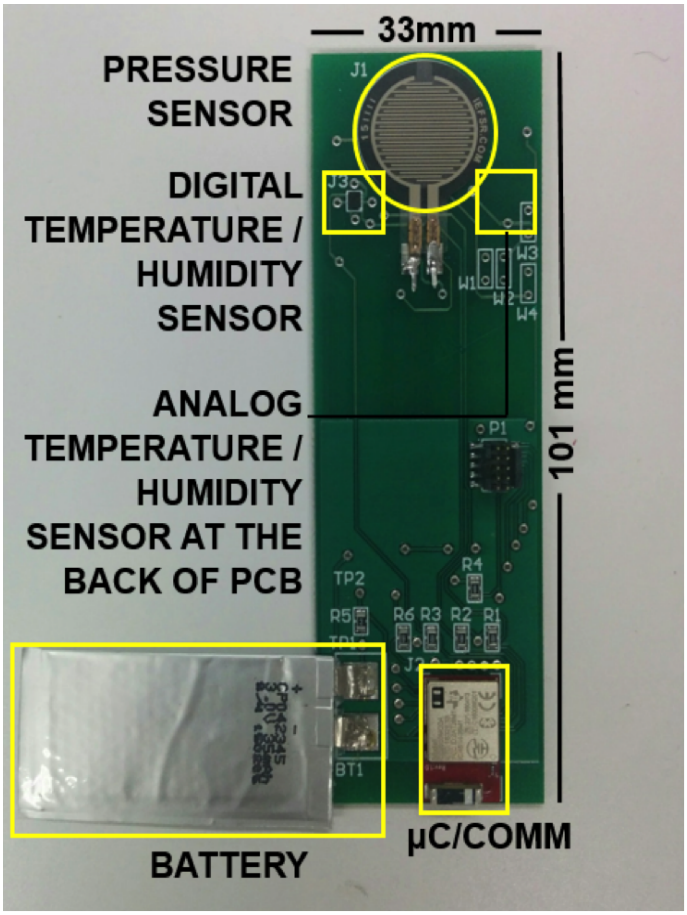

Figure 22: Second Rigid PCB Implementation

4.6 Flexible PCB Design

The final version of the design was implemented on a flexible PCB. The initial plan was to design the flexible PCB for the heels or the elbows, using the I-design introduced in section 4.4.1. Towards the conclusion of the PUP MQP, the team was asked to design the flexible PCB such that it could be used during the UMMS rat experiment. Thus the final design had to be much smaller and could afford to be slightly less flexible.

The flexible PCB substrate was 0.19812 mm thick, and the design was much smaller in size than the second rigid PCB. The package size for resistors and capacitors on the flexible board was 0402 whereas the package size for the same components on the rigid board was 0805. These smaller resistors and capacitors were chosen to accommodate the reduced size of the new

PCB, allowing more room for traces and more flexibility in component placement.

A different approach had to be taken for programming the MCU on the flexible PCB since header connectors could no longer be used. Each flexible board was programmed through a spring pin tag connector that could plug directly into the board and be removed once the MCU was programmed.

The rest of the design was the same as the second rigid PCB.

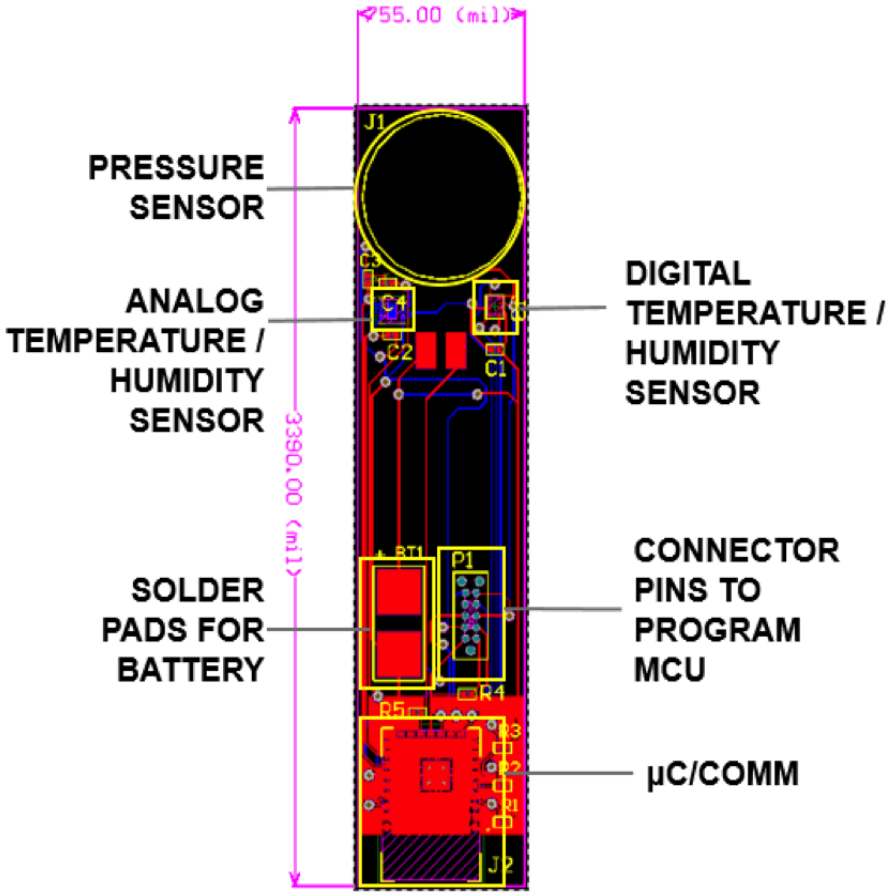

Figure 23: Flexible PCB Design

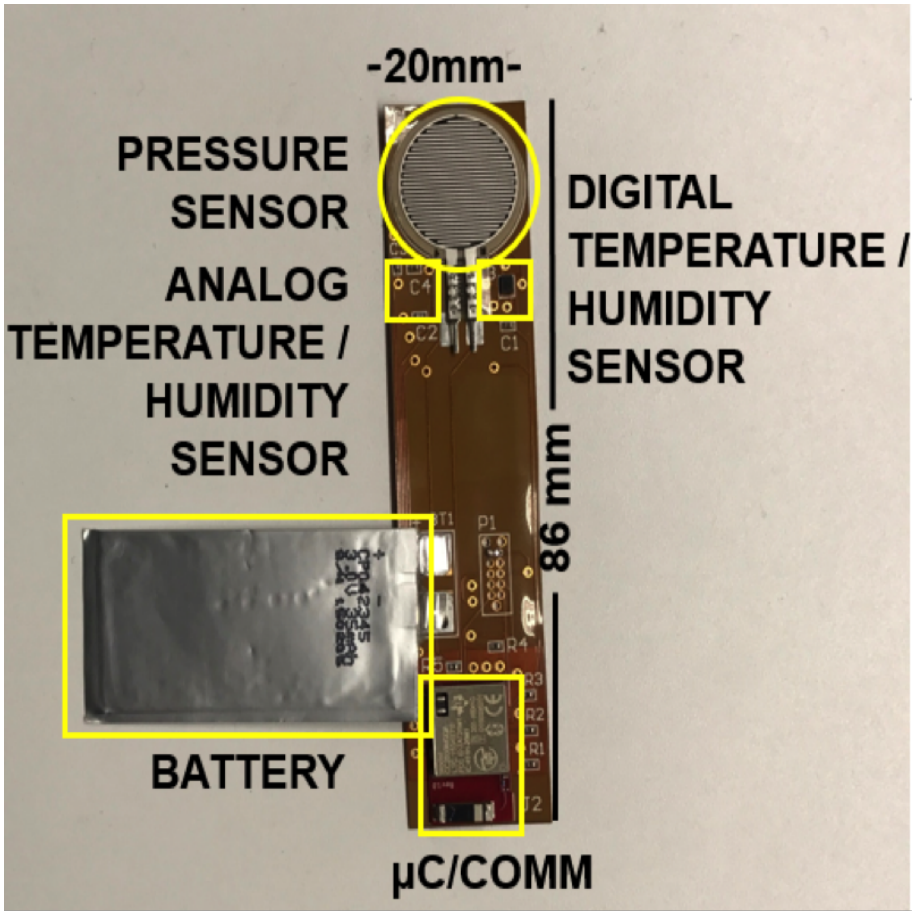

Figure 24: Flexible PCB Implementation

4.7 Software Design

4.7.1 Firmware Design

The following flowchart shows a step-by-step progression of the firmware.

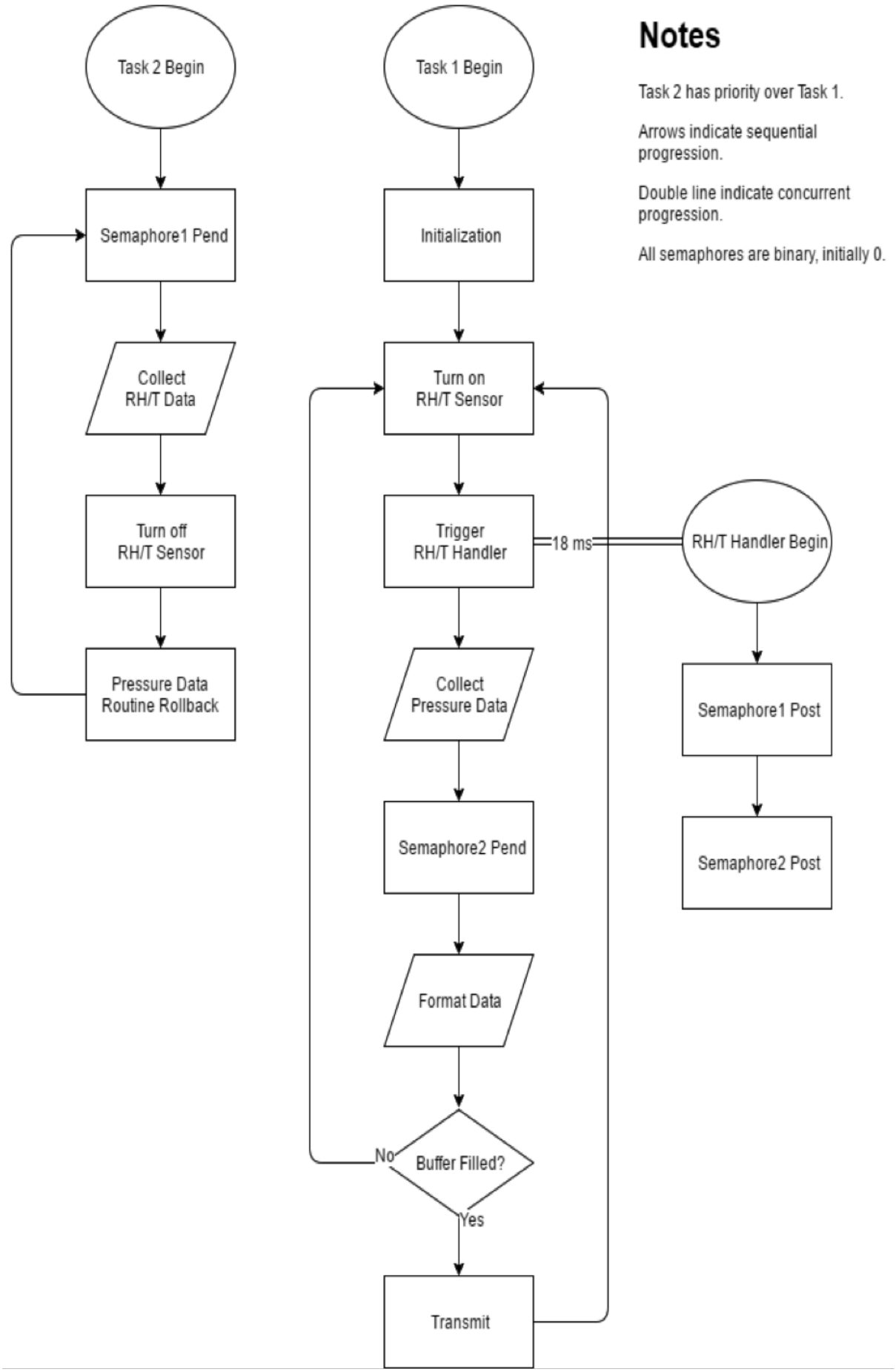

Figure 25: Visualization of Firmware Design

The firmware is implemented as a multitasking scheme as shown in the flowchart. It is because the multitasking scheme increases the code efficiency. For example, because the relative humidity and temperature sensor is powered by the MCU only when the MCU needs the data, there is a start-up time of 18 ms between the MCU supplying power to the sensor and the data being available to the output pins. In a single-tasking scheme, there is not an efficient way of tracking 18 ms. The firmware required in the single-tasking case would need multiple calls in the code, each checking how much time has passed, which are redundant and slow the execution of the firmware in runtime. In a multitasking scheme, a one-shot timer can be set to unblock a higher priority task exactly after 18 ms without requiring repeating checks for elapsed time.

Tools that allow a multitasking scheme to be implemented as described above are semaphores. They can be thought of as global variables denoting whether the code may proceed or not. The semaphores used in the firmware are binary semaphores, where they are either 1 or 0. Pending a semaphore has two outcomes. If the semaphore was 1, the pend will decrement the semaphore to 0 and the code will proceed. If the semaphore was 0, the code will block until another task increments the semaphore to 1. Meanwhile, an unblocked task of lower priority will run. Usually, one of the unblocked tasks of lower priority will post the semaphore at some point, which increments the semaphore to 1. All semaphores in the firmware are initialized as 0s.

To elaborate on the operation of the firmware, task 2 has higher priority over task 1. However, task 2 starts blocked from the beginning of the runtime, which starts the execution of task 1. Right after the firmware provides power to the sensor in the middle of task 1, the task starts a timer, which posts the semaphore blocking task 2 after 18 ms. 18 ms later, task 2 is unblocked and it will preempt task 1 since task 2 has the higher priority. In a single-tasking scheme where task 1 and task 2 are combined, after the task provides power to the sensor, the firmware has to guess how far long the code is 18 ms after or have multiples checks to ensure the relative humidity and temperature data are collected as soon as they are available. It is important to collect the data as soon as they are available because the sensor can be turned off afterwards to lower the current draw.

"Pressure Data Routine Rollback" block in task 2 resolves the shared resource problem. When task 2 is unblocked and preempts task 1, there is no concrete method of knowing exactly where in task 1 is interrupted. Task 2 forwards different GPIO pins to the ADC and overwrites the initial data present at the ADC interrupt service routine. The rollback block returns the original pins and the values to the ADC and the routine at the end of the task. Without the rollback, task 1 runs the risk of collecting data from GPIO pins most recently forwarded to the ADC, which may be the relative humidity and temperature data from task 2.

4.7.2 Power Considerations

The frequency of execution of task 1 and task 2 elaborated in section 4.7.1 depends on the power consumption of each task. There are three different stages in the firmware with differing current draw: sleep, collect, and transmit. In the flowchart, the collect stage is equivalent to the entire task 2 in additional to turning on the RH/T sensor to buffer check. The transmit stage is the transmit block, and the sleep stage is defined as neither the collect stage nor the transmit stage. The following waveform illustrates the cycle as a function of current over time.

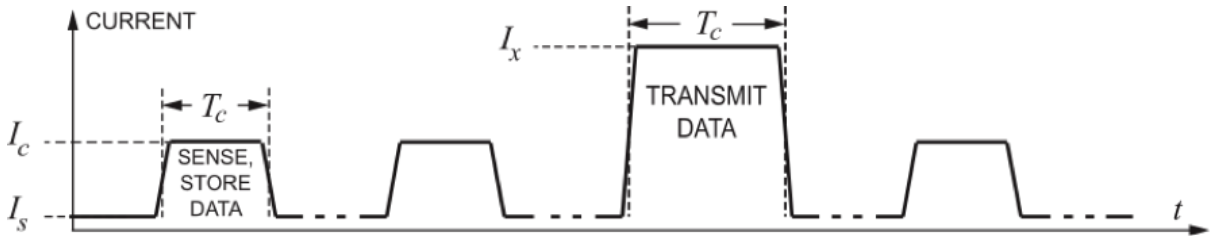

Figure 26: Visualization of Power Draw over Time

I_S denotes sleep current, I_C collect current, and I_X transmit current. T_C denotes collecting interval and T_X denotes transmitting interval. T_S, sleeping interval, is defined as whenever the MCU is not collecting or transmitting. The waveform is not drawn to scale and the actual values for the variables are calculated in the following sections of the report.

The sleep stage is when the MCU is sleeping. It does not collect data from its sensors nor does it transmit the data that has been collected. As a result, it draws the least amount of current out of all the stages. The MCU will spend most of its time sleeping due to the limited capacity of the battery.

The collect stage is when the MCU collects data from its sensors. The data is stored within the MCU and will be transmitted during the transmit stage. Each collect stage collects one instance of pressure, RH, and temperature data.

The transmit stage is when the MCU transmits the data that was collected during the collect stages. There are multiple collect stages before a transmit stage occurs. Because wireless transmission is most taxing in terms of current draw, the transmit stage is required to occur as infrequently as possible. In order to conserve power, the transmit stage does not include collecting data.

These stages alternate to form one cycle, and the cycle repeats itself until the battery runs out, after which the patch must be replaced. The following section of the report addresses key aspects in each stage.

Sleep Stage

The current draw in the sleep stage is as follows:

Table 26: Current Draw During Sleep Stage

Component	**Current Draw (mA)**
MCU	0.003
FSR 402 Short Pressure Sensor	0.235
HDC1010 RH/Temperature Sensor	2 x 10^{-4}
Total	0.238

The duration of the sleep stage depends on the sampling rate, which is the frequency of the collect stage.

Collect Stage

The current draw in the collect stage is as follows:

Table 27: Current Draw During Collect Stage

Component	**Current Draw (mA)**
MCU	2.950
ADC	0.660
FSR 402 Short Pressure Sensor	0.235
HDC1010 RH/T Start Up	0.300
RH Sensor	7.1 x 10^{-4}
Temperature Sensor	5.9 x 10^{-4}
Total	0.238

The duration of the collect stage is as follows:

Table 28: Duration of Collect Stage

Componen Activity	**Duration (ms)**
ADC Sampling	2.7 x 10^{-3}
ADC Conversion	1.042 x 10^{-3}
ADC Total	3.742 x 10^{-3}
HDC1010 RH/T Start Up	15
RH Sensor	3.850
Temperature Sensor	3.650
Total	22.50

The power consumption of the collect stage is as follows:

Table 29: Power Consumption Calculations

Calculations	**Power Consumption**
$U_{MCU} = I_{MCU}$ x t_{total}	66.38[uAs] = 18.44[nAh]
$U_{PRESSURE} = I_{PRESSURE}$ x t_{total}	5.288[uAs] = 1.469[nAh]
$U_{ADC} = I_{ADC}$ x $t_{ADC_{total}}$	2.470[nAs] = 0.686[pAh]
$U_{RHTstart} = I_{RHTstart}$ x $t_{RHTstart}$	4.500[uAs] = 1.250[nAh]
$U_{RH} = I_{RH}$ x t_{RHconv}	2.734[nAs] = 0.759[pAh]
$U_T = I_T$ x t_{Tconv}	2.154[nAs] = 0.598[pAh]
U_{TOTAL}	21.16[nAh]

Note that the pressure sensor component exists in both sleep and collect stage. This is because the pressure sensor is configured in a voltage divider, which continuously draws current. This component will be present in the transmit stage as well.

Transmit Stage

The current draw in the transmit stage is as follows:

Table 30: Current Draw During Transmit Stage

Component	**Current Draw (mA)**
MCU	3.175
FSR 402 Short Pressure Sensor	0.235
TX	2 x 6.800
Total	10.21

Note that the MCU current draw is slightly higher than that from the collect stage. This is because activation of the RF core draws additional current, not included in the current draw of the actual transmission.

The duration of the transmit stage mostly depends on the receivers capability to establish a connection and receive data. While it requires further research, 10 seconds was chosen as an approximation for the remainder of this section.

Due to the large number of variables involved in the analysis, several values are predetermined and many assumptions are made. Firstly, the firmware will collect 5 sets of data before transmission, meaning 5 collect stages per transmit stage. Battery capacity is assumed to be 60 mAh. The primary variable affecting the longevity is the length of the entire cycle, or transmission interval. The total duration of sleep stages in a cycle is defined as transmission interval minus the collect stages and the transmission stage; thus the following equation describes the relationship between the transmission interval and the patch longevity.

$$T_l = \frac{U_b}{\frac{T_s}{T_p} * I_s + \frac{T_c}{T_p} * I_c + \frac{T_x}{T_p} * I_x} \tag{6}$$

where T_l denotes the longevity of the patch in hours (converted to days in the below plot), U_b is the battery capacity, T_s is the total sleep stages duration, T_c is the total collect stages duration, T_X is the total transmit stages duration, and T_P is the total duration of a cycle.

The following figure is a graphical representation of relationship between the patch longevity and the transmission frequency.

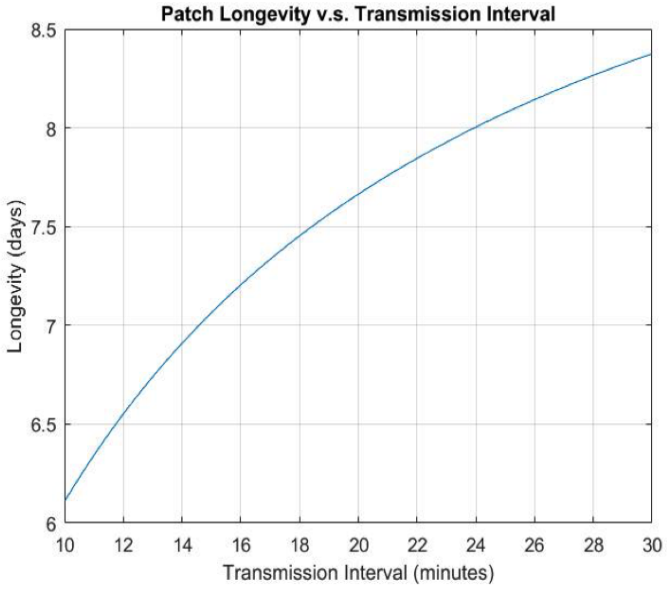

Figure 27: Modeled Longevity of System

Patch longevity denotes the number days the device is going last. Transmission interval denotes the number of minutes between each transmit stage.

The numbers indicated in the plot represent the time elapsed between each transmission in minutes. It is clear that it is possible to have the patch last 7 days and there exists a proportional relationship between the transmission interval and the transmission rate.

4.7.3 Data Display Design

The following screenshot shows preliminary data display with actual data sent from three devices.

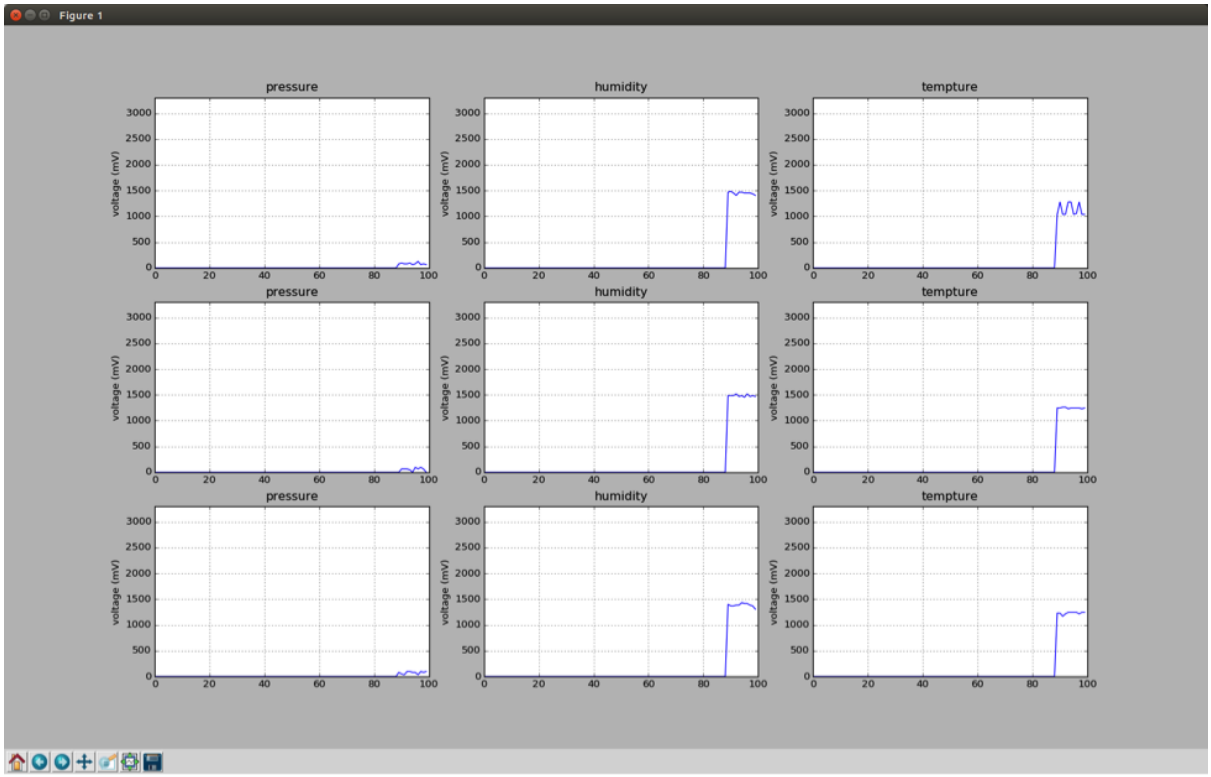

Figure 28: Python Graphic Display

The code is written in Python with a library that mimics the API and plotting scheme of MATLAB. It dynamically generates data structure to fit a number of data types from a number of devices. The number of data types, their names, and the number of devices must be defined by the user.

Because the BLE library for Python is buggy, the connection is often lost in seconds and a stable connection is rarely sustained for more than a minute. The code mitigates this problem by iterating until a stable connection is made. However, the connection can still be lost after the connection is deemed stable by the code. As a result, the data display is riddled with random delays (non-fatal) and stalls (fatal).

As shown above, the data display serves its purpose as proof that there are multiple active devices and a possibility of retrieving data from them.

5 Design Verification

5.1 Objective

The objective of the chapter is to describe the protocols used to test the sensors and the power consumption, to analyze the results, and to discuss the implications.

5.2 Testing Protocol

The rigid PCB used to verify the functionality of the overall design and the individual components is depicted below.

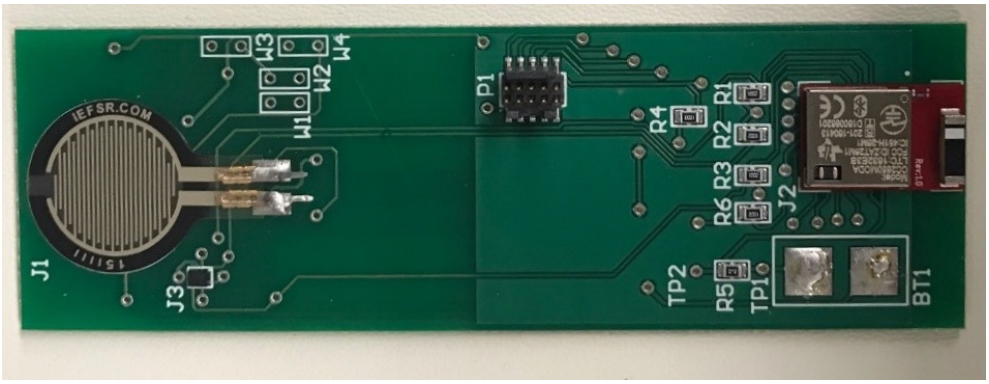

Figure 29: Rigid PCB Used During Testing

The pressure sensor soldered on the board (J1, left) was the Interlink FSR-402 Short. It was tested using the protocol described in section 5.2.1. The digital relative humidity sensor (J3, lower left) was not tested before the PUP MQP got submitted; however, the analog relative humidity and temperature sensor, which was soldered to the other side of the board (not shown), was tested in January 2017 using the protocol described in section 5.2.2 and 5.2.3. The microcontroller (J2, right) was connected to the launchpad, programmed, and powered through the port (P1, center). Its ability to communicate with the sensors and with the base station were verified when the Interlink pressure sensor and the analog relative humidity and temperature sensor were tested using the protocol describe below. Its consumption of power was measured using the protocol described in section 5.2.4.

5.2.1 Pressure Sensor

Figure 30 shows the apparatus used to test both the Interlink and the Tangio pressure sensors. Together, the two tubes were used to contain and support the weights with which pressures were applied and to immobilize the devices under test. The paper tube (left in Figure 30) was used to confine the weights, while the clear plastic tube (center in Figure 30) was used to hold them straight up on the sensor during each test. The paper tube was slightly smaller in diameter than the clear plastic tube, allowing it to easily slide in and out while ensuring it remained upright and stable within the plastic tube. The plastic tube could also be detached from the orange base, allowing the device under test (an individual pressure sensor or an assembled PCB) to quickly and easily be positioned on the apparatus. The procedure used to test the FSR402 Short and the TPE-502, either detached or soldered on a PCB, is detailed below (see Appendix B and Appendix C for results).

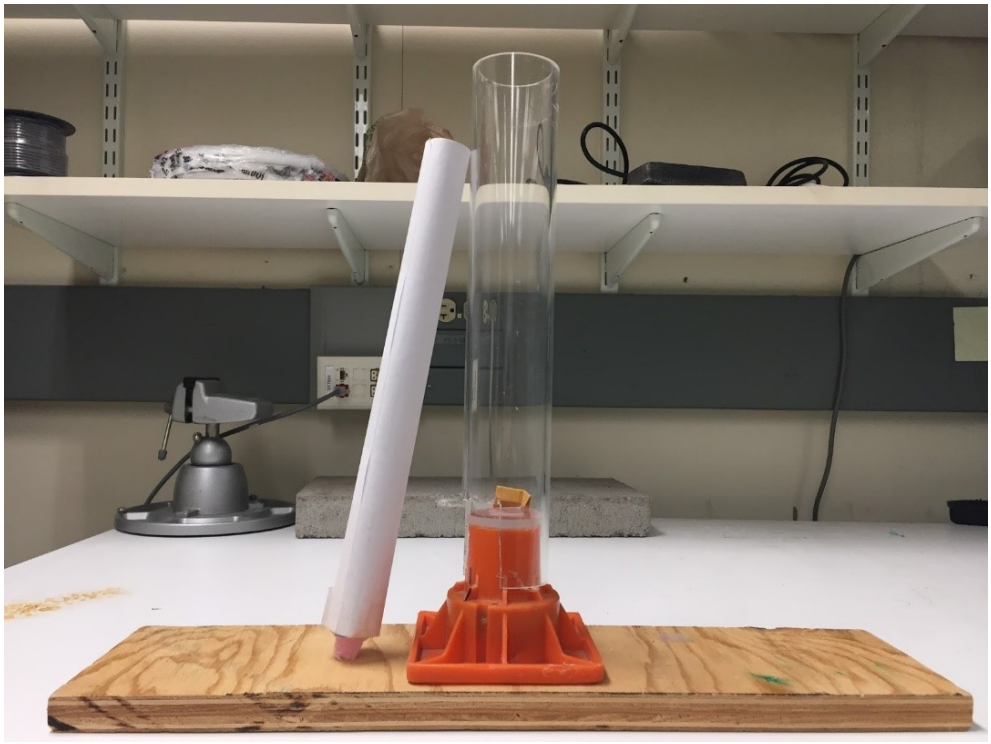

Figure 30: Testing Apparatus for Pressure Sensor

1. Quarters and dimes were used to make the weights with which the force sensors were tested, since the U.S. Department of Treasury and the U.S. Mint make information on what coins weigh readily available, and these weights vary little between coins of the same type. Moreover, quarters and dimes are very easily accessible. The combinations of coins used during the pressure sensor tests and the corresponding weights are shown in Table 31.

2. The Interlink FSR402 Short and the Tangio TPE-502 were tested. Each sensor was inserted into the testing apparatus in one of two configurations:

   (a) The sensor was soldered on to a rigid PCB between a supply voltage line and the fixed resistor of the voltage divider, as discussed in section 4.5. The PCB was then placed on the orange base of the testing unit, as shown in the figure above.

   (b) The sensor was secured the orange base of the testing unit, and its leads were connected to a digital multi-meter (DMM) set to measure the resistance across the sensor.

   Scotch Tape was used as needed to secure either the board or the sensor to the base of the testing unit. The tape was never allowed to contact or cover the sensing area (the best way to attach the tape was to put a double sided strip on the side of the board or the sensor that would be in contact with the base, as well as to apply strips to the corners of the board).

3. The coins were stacked in the paper tube.

4. The pink sponge attached to the bottom of the tube was used to simulate skin and was placed in direct contact with the sensor on the sensing area. The exact position of the pink sponge, in addition to the weight distribution of the coins in the paper tube, had a significant impact on voltage and resistance readings (attempts were made to return the sponge to the same position on the sensor each time the weight was changed).

5. The PCB was powered through one of two sources:

   (a) laptop computer, connected to the PCB via the Texas Instruments launchpad for the CC2650 microcontroller, setting the VDD on the board to 3.3V

   (b) DC voltage supply set to 3.0V, connected to the PCB via two color-coded wires (red = positive, black = negative) soldered to its power supply terminals

   Unattached sensors did not require voltage supply.

6. The microcontroller on the PCB was used to digitize and transmit the voltage values output by the voltage divider on the PCB. The BLE Scanner app from Bluepixel Technologies was downloaded onto an android phone, which served as the base station on which the sensor data were received. Note the microcontroller transmits one hex value corresponding to each ADC output voltage, recorded in millivolts.

7. Ten different weights were used, corresponding to ten different pressures in and around 30 - 35 mmHg. Table 31 below shows the different coin combinations used as weights and the corresponding pressure values used to test each pressure sensor. Note the Tangio sensor was not tested with the 3 quarters + 1 dime combination. Each weight was tested for 5 minutes in total, during which the read function in the BLE Scanner app was used to collect a hex value every 30 seconds. Therefore, 10 data points were acquired for each weight.

Table 31: Weights Used for Pressure Sensor Testing

Coin Combination	Weight (g)	Pressure (mmHg)
3 quarters + 1 dime	19.278	11.194
7 quarters	39.690	23.046
8 quarters + 2 dimes	49.896	28.972
8 quarters + 3 dimes	52.164	30.289
8 quarters + 4 dimes	54.432	31.606
10 quarters	56.700	32.923
10 quarters + 1 dime	58.968	34.240
10 quarters + 2 dimes	61.236	35.557
14 quarters	79.380	46.093
21 quarters	119.070	69.139
28 quarters + 1 dime	161.028	93.502

8. The data were calibrated according to the nonlinear relationship between force and resistance that is typical of shunt-mode force sensing resistors such as the Interlink FSR-402 Short and the Tangio TPE- 502. The calibration procedure and the calibrated data are discussed in section 5.3.

The protocol described above was developed using the ASTM D57720-95 test standard for static calibration of electronic transducer-based pressure measurement systems. The test standard was modified according to the particular needs of the PUP MQP team and to calibrate these pressure sensors for biomedical purposes.

5.2.2 Temperature Sensor

The temperature sensor in the SHT31-ARP-B analog relative humidity and temperature sensor soldered on the PCB was tested using the VWR Symphony CO2 Incubator. The images in Figure 29 below show the setup of the test system. The microcontroller on the PCB was used to digitize and transmit voltage values output by the sensor, and the data were received on an android phone via the BLE Scanner app.

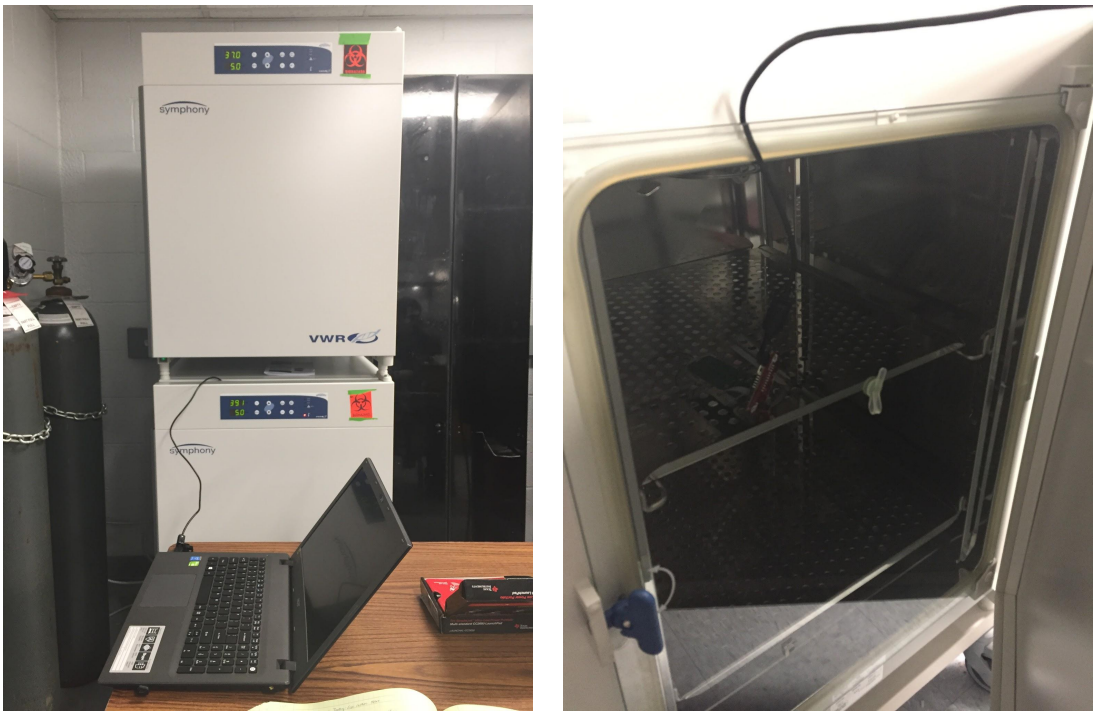

Figure 31: Setup for Temperature Sensor Test Using VWR Symphony CO2 Incubator

1. A laptop was used to provide a 3.3V power supply to the PCB via the launchpad.
2. Both the launchpad and the PCB were placed inside the incubator, and the incubator was shut as tight as possible.
3. The internal temperature of the incubator was set to the target temperatures 35°C, 36°C, 37°C, and 40°C. At each target temperature, data was collected over 5 minutes. Both the actual temperature in the incubator and the hex value from the microcontroller were recorded every 30 seconds, resulting in 10 data points total for the incubator readings and for the microcontroller readings at each target temperature.
4. The data were calibrated according to the linear relationship between voltage and temperature provided in the SHT31-ARP-B data sheet. The calibration procedure and the calibrated data are discussed in section 5.4.

5.2.3 Relative Humidity Sensor

The relative humidity sensor in the SHT31-ARP-B analog relative humidity and temperature sensor soldered on the PCB was tested using the protocol described below. The image in Figure 30 below show the setup of the test system. As in the testing of the temperature sensor, the microcontroller on the PCB was used to digitize and transmit voltage values output by the sensor, and the data were received on an android phone via the BLE Scanner app.

1. The Vernier RH-BTA probe was used to sense the relative humidity of the environment and thus to provide measurements with which the relative humidity measured by the sensor could be compared. The probe was connected to a computer equipped with the LoggerPro software application. Then LoggerPro was opened and set up to record new data.

2. A glass 500 mL beaker was filled with about 500 mL of water. Using a hot plate, the water in the beaker was brought to a boil.

3. While the water heated, the testing apparatus shown in Figure 30 below was set up:

   (a) The PCB was encased in saran wrap so all exposed parts except the SHT31-ARP-B sensor were protected in attempt to prevent moisture damage from occurring.

   (b) A cardboard box was used to simulate a closed system. The PCB was secured to the top part of the box, with the exposed SHT31-ARP-B sensor inside and the rest of the board outside. The Vernier probe was secured to the top of the box, as well, with the sensing area inside and the rest of the probe outside so the probe sensor would be close enough to the analog sensor to experience approximately the same sensing environment. The seams in the box and the openings near the PCB and the probe were then sealed with packaging tape.

   (c) A laptop was used to provide a 3.3V power supply to the PCB via the launchpad.

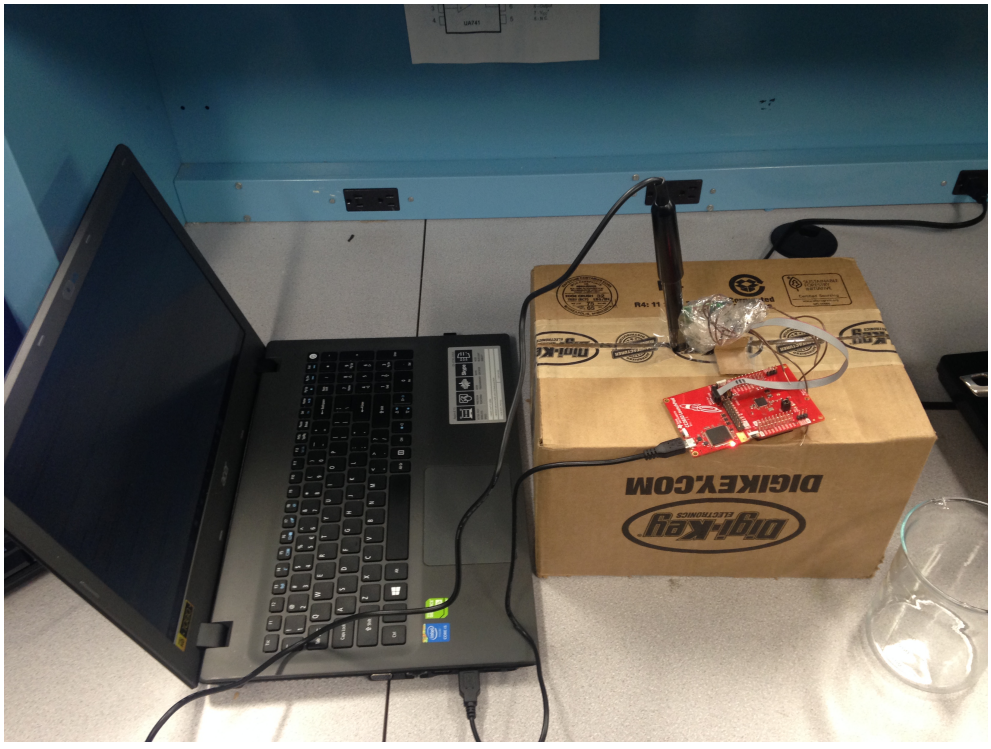

Figure 32: Testing Apparatus for RH Sensor

4. A baseline relative humidity measurement was recorded. Using LoggerPro, relative humidity data were recorded at a sampling rate of 0.1 Hz for a duration of 2 minutes. Using the android phone, hex values were read from the microcontroller every 10 seconds for 2 minutes, as well, so each value recorded with LoggerPro would be obtained at the same time as each value on the phone.

5. Once the water was steaming and boiling, the beaker was removed from the hot plate and set on the table. A second 500 mL beaker was obtained, and about 100 mL of boiling water were poured into it.

6. With the PCB and the probe attached to the box, the beaker of 100 mL of boiling water was covered with the box, such that both sensors were placed directly above it.

7. Data were recorded from the probe with LoggerPro and from the PCB with the android phone every 10 seconds for 5 minutes.

8. The beaker with the boiling water were removed from under the box.

9. Additional data were recorded from the probe with LoggerPro and from the PCB with the android phone every 10 seconds for 5 minutes. Note readings between 40% - 60% relative humidity were most important, since changes within this range impact pressure ulcer formation.

10. The data were calibrated according to the linear relationship between voltage and relative humidity provided in the SHT31-ARP-B data sheet. The calibration procedure and the calibrated data are discussed in section 5.5.

The protocol described above was developed using the ASTM D7191 - 10 test standard for determination of moisture in plastics by relative humidity test sensor. The test standard was modified according to the particular needs of the PUP MQP team and to calibrate this relative humidity sensor for biomedical purposes

5.2.4 Power Consumption

In Figure 33 below is the block diagram of the circuit used for testing power consumption. The block labeled VDD encompasses all of the components on the PCB, including the sensors and the microcontroller. Thus the current drawn by the entire circuit can be determined using the voltage drop across the 2Ωresistor, Ohms Law, and Kirchhoff's Voltage Law.

The following procedure was used to test the power consumption of the system in the multiple stages of the microcontroller, which are described in section 4.6.

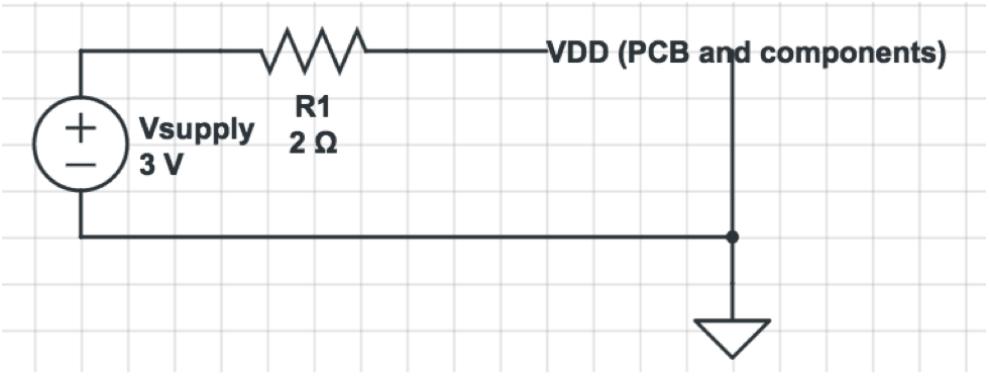

Figure 33: Block Diagram for Circuit Used in Testing Power Consumption

1. 3V supply voltage was provided to the PCB.

2. A digital multimeter (DMM) was used to measure the voltage drop across the 2Ωresistor.

3. The total current of the circuit was calculated according to Ohms Law by dividing the voltage across the 2Ωresistor by the resistance of the resistor.

4. The voltage across VDD was calculated according to Kirchhoff's Voltage Law by subtracting the voltage across the 2Ωresistor from the supply voltage.

5. The overall power consumption of the PCB was calculated by multiplying the current from step 3 with the voltage from step 4.

6. The test was repeated using multiple settings for sampling rate and transmission rate of the microcontroller in order to optimize the power consumption.

5.3 Pressure Sensor Testing Results

Data collections occurred between December 2016 and February 2017 using various weights with two different force sensing resistors, as described in Table 32 below. Recorded values are tabulated in Appendix B for the Interlink FSR-402 Short sensor and in Appendix C for the Tangio TPE-502 sensor. Using the protocol described in Section 5.2.1, voltage-time measurements were recorded for multiple weights on each date. The same sensor was used throughout each test, so its responses to various forces could be observed.

Table 32: Pressure Sensor Data Collection Summary

Date (mm/d-d/yy)	Sensor Tested	Number of Weights	Weight Range (g)	Pressure Range (mmHg)
11/30/16	Interlink FSR-402 Short	5	190.06 - 590.30	110.36 - 342.76
12/01/16	Interlink FSR-402 Short	4	102.06 - 408.24	59.26 - 237.05
12/03/16	Interlink FSR-402 Short	11	51.030 - 204.12	29.63 - 118.52
12/06/16	Interlink FSR-402 Short	3	119.07 - 181.44	69.14 - 105.35
1/25/17	Interlink FSR-402 Short	9	51.030 - 72.576	29.63 - 42.14
1/31/17	Interlink FSR-402 Short	11	19.278 - 161.028	11.19 - 93.05
2/01/17	Interlink FSR-402 Short	11	19.278 - 161.028	11.19 - 93.05
2/17/17	Tangio TPE-502	10	39.690 - 158.760	23.05 - 92.15

5.3.1 Interlink FSR-402 Short Measurement Data

The data recorded on January 31, 2016, and on February 1, 2017, included the weight of the coin column, the hex value output by the microcontroller, and the time at which the microcontroller output was sampled. These data were combined and processed in MATLAB using the script and the function in Appendix B to calibrate the FSR-402 Short.

As mentioned in Chapter 4, shunt-mode force sensing resistors experience a nonlinear relationship between the output resistance and the applied pressure. The measured pressure can be derived from the voltage output by the microcontroller according to Equation 6 (McNeill et al., 2017):

$$P = P_0 \left(\frac{R_{Ref}}{R_0 \left[\frac{1-n}{n} \right]} \right)^{\frac{1}{x}} \tag{7}$$

where n is defined as $\frac{V_{OUT}}{V_{SUPPLY}}$.

With respect to the data recorded for the FSR-402 Short, P_0 was defined as the actual applied pressure closest to 30 mmHg, and R0 was defined as the average FSR resistance recorded at P_0.

The figure below displays a log-log plot of normalized sensor resistance ($\frac{R_{FSR}}{R_0}$) versus normalized applied pressure ($\frac{P}{P_0}$) for the Interlink FSR-402 Short. According to Equation 7, the relationship between log resistance and log pressure is linear. The 2-point calibration method was thus used to find the line along which most data points in the relevant range (25 mmHg to 35 mmHg) fell. The x value in Equation 7 was defined as the slope of the line.

The 2-point calibration method allowed the team to predict how the sensor would behave over a range of applied pressures. To perform the calibration, data were collected in the relevant range (25 - 35 mmHg), at the low extreme (11 mmHg), and at the high extreme (118 mmHg). The same technique was used by Crivello et al. in "Modeling of force sensor nonlinearity for time-domain-based pressure measurement in biomedical sensors" (2016).

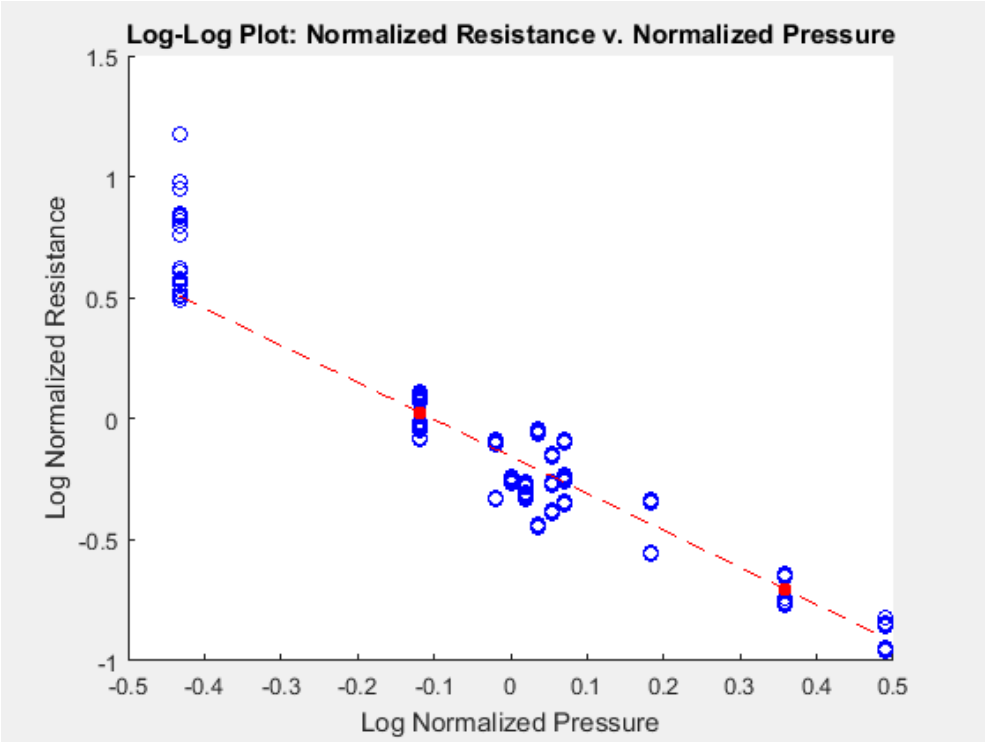

Figure 34: Log Resistance versus Log Pressure

In the above plot, the blue circles represent the data recorded on January 31, 2016, and on February 1, 2017. The same Interlink FSR-402 Short sensor was used on both dates. The red dots represent the averaged data points that were used in the 2-point calibration. From these data, P_0 = 30.2894 mmHg, R_0 = 5.9311 x $10^4\Omega$, and x = -5.298.

Next, recorded voltage values were input into Equation 7 with these P0, R0, and x values, and the pressures sensed by the FSR-402 Short were calculated. The calculated pressure values were then compared to the actual applied pressure values, and linear regression was used to calibrate the data and reduce the error.

The figure below displays the data before and after calibration. Ideally, the pressure measured by the sensor should equal the pressure applied to the sensor, and the data in the plot should lie along a straight line with slope = 1 and a y-intercept = 0 (i.e. line of identity).

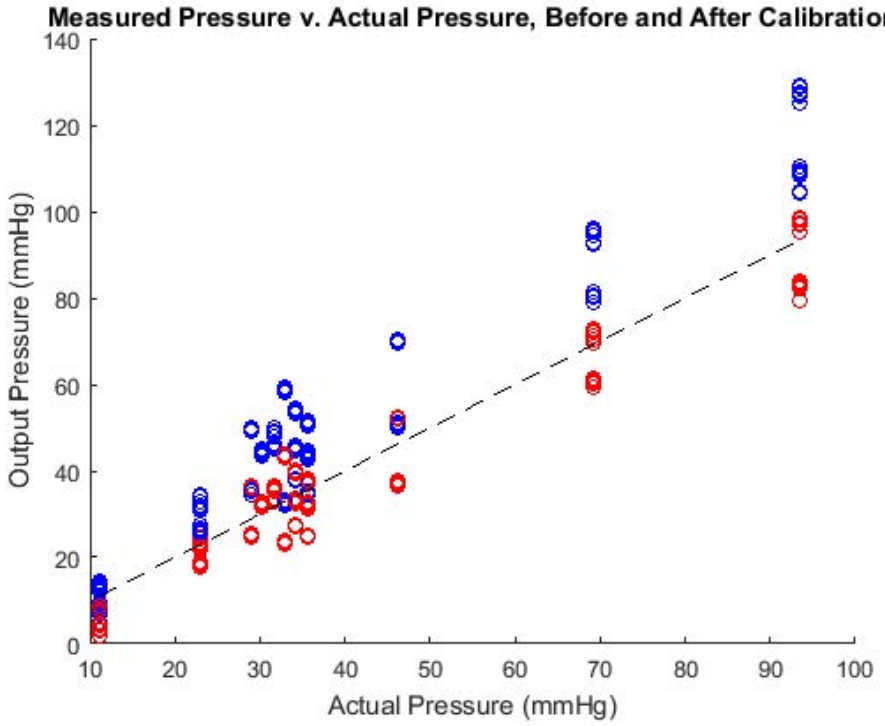

Figure 35: Measured Pressure versus Actual Pressure

In the figure above, the line of identity is represented by the black dashed line. The blue circles represent the output pressure values calculated using Equation 7 with the P_0, R_0, and x derived in the 2-point calibration. The red circles represent the calculated output pressure values after linear regression calibration:

The linear regression analysis on these data produced the following results: r = 0.9636, m = 1.2820, b = 2.2330. The r value represents the regression coefficient, which quantifies the nature of the relationship between two variables. Here, r is close to 1, indicating very strong positive linear correlation between the calculated output pressure and the actual applied pressure. The m value represents the slope of the line of fit. The m value is slightly greater than 1, meaning the line of fit (along which recorded data lie) is not perfectly parallel to the line of identity (along which ideal data would lie). The b value represents the y-intercept of the line of fit. Here, the b value indicates the calculated output pressure is consistently greater than the actual applied pressure by at least 2.2330 mmHg.

The sensor output was calibrated by adjusting each value as follows:

1. To make the slope of the line of fit equal to the slope of the line of identify, each calculated output pressure value was multiplied by factor $\frac{1}{m} = 0.7800$.

2. To make the y-intercept of the line of fit equal to the y-intercept of the line of identity, each product in (1) was reduced by b = 2.2330.

In the plot above, the red circles appear to follow the line of identity much more closely than the blue circles, especially between 25 mmHg and 35 mmHg, suggesting the linear regression calibration greatly improved the accuracy of the output pressure calculation.

The figure below depicts the difference between the calculated output pressure and the actual applied pressure. The blue circles represent the error before linear regression calibration, and the red circles represent the error after linear regression calibration.

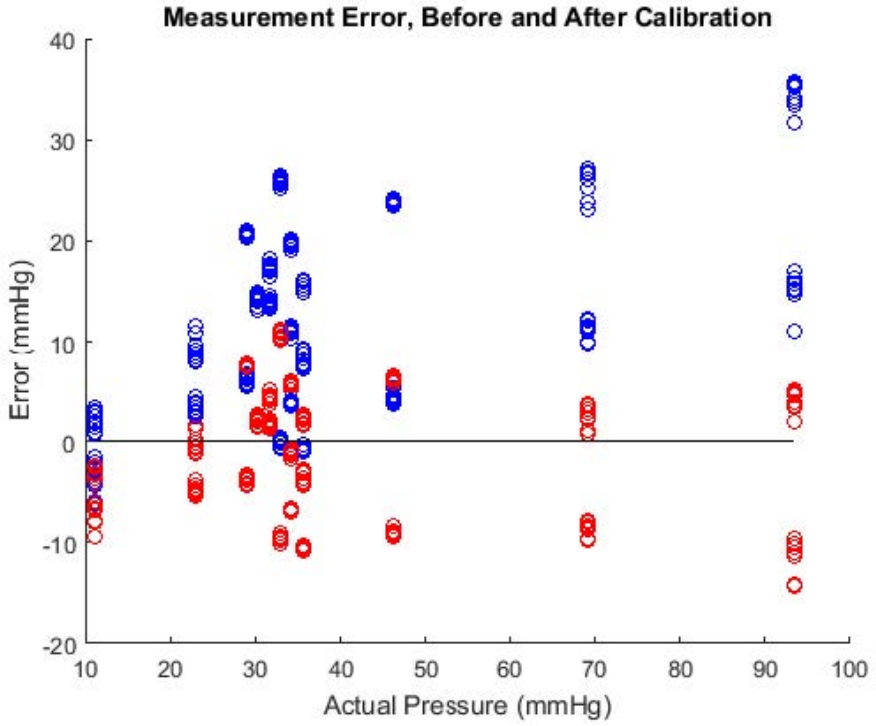

Figure 36: Pressure Sensor Error

The error before the linear regression calibration is almost always positive and seems to be greater at higher pressures. Such results suggest issues in the equation derived with the 2-point calibration: It produces inaccurate output values with all input values, and its performance worsens as pressure increases.

The error after the linear regression calibration is more evenly distributed around zero, suggesting the linear regression calibration succeeded in eliminating the issues described in the previous paragraph.

These results are summarized in Figure 37 below, in which the average calculated output pressure value at each actual applied pressure is plotted versus the actual applied pressure. Again, the blue circles represent data before the linear regression calibration, and the red circles represent data after the linear regression calibration.

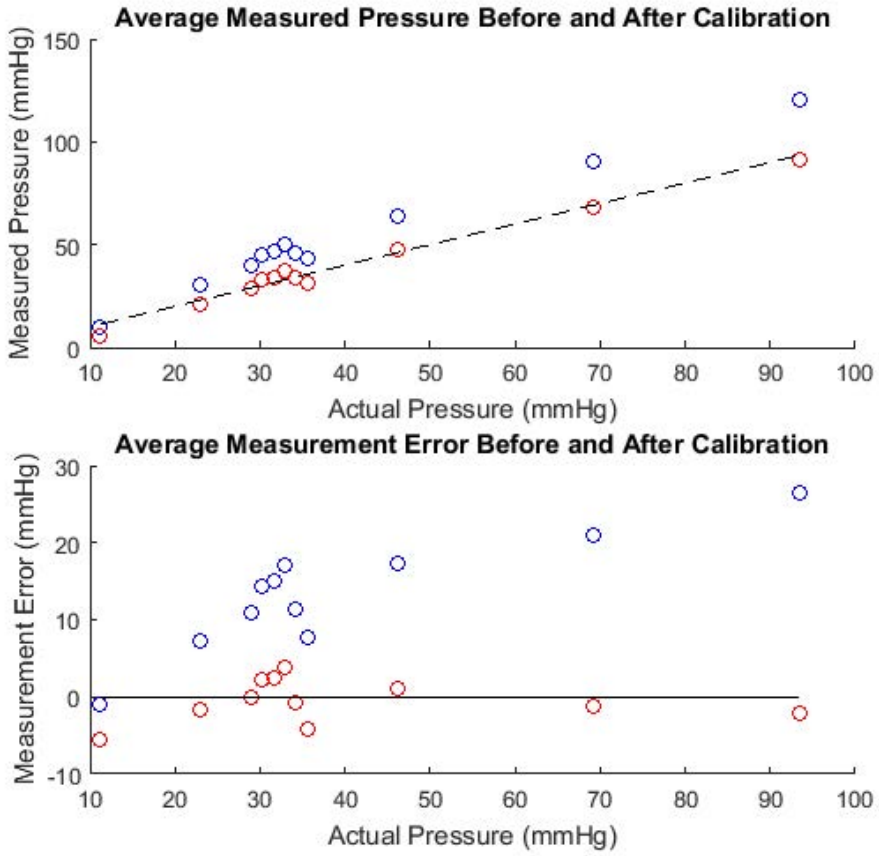

Figure 37: Average Pressure Measurements and Corresponding Errors

The average pressures in Figure 37 were used to assess the accuracy of the FSR-402 Short. Sensor error is summarized in Table 33 below. Linear regression calibration reduced average error by over 25% and reduced maximum error by about 3%.

The mean absolute deviation (MAD) in the average calculated output pressure after linear regression calibration was calculated to be 2.301 mmHg, suggesting the algorithm derived here to determine the pressure sensed by the FSR-402 Short may be more accurate than +/- 3 mmHg. However, the Interlink FSR series is known to have a very high part-to-part variability (Crivello et al., 2016b), so other methods of calibration may have to be considered to accommodate outputs from multiple sensors with the same algorithm.

Table 33: Interlink FSR-402 Short Error Summary

	Average % Error	Max % Error	Error at P_0 (mmHg)	Error at P_0 (%)	MAD (mmHg)
Before Linear Regression Calibration	32.24	52.21	14.37	47.44	13.61
After Linear Regression Calibration	9.50	49.04	2.313	7.64	2.301

5.3.2 Tangio TPE-502 Measurement Data

The data recorded on February 17, 2017, included the weight of the coin column, the resistance displayed by the digital multi-meter, and the time at which the digital multi-meter was sampled. These data were combined and processed in MATLAB using the script and the function in Appendix C to calibrate the Tangio TPE-502.

The measured pressure was once again calculated using Equation 7. With respect to the data recorded for the TPE-502, P0 was defined as the actual applied pressure closest to 30 mmHg, and R0 was defined as the average FSR resistance recorded at P_0.

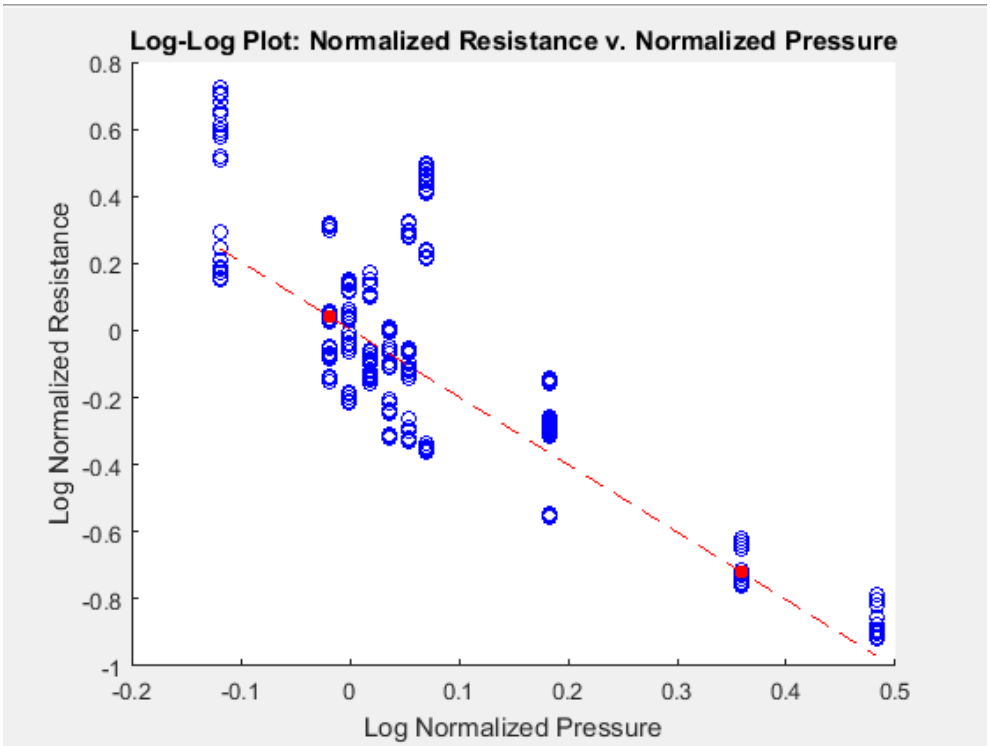

Figure 38: Log Resistance versus Log Pressure

The figure above displays a log-log plot of normalized sensor resistance (RFSR / R0) versus normalized applied pressure ($\frac{P}{P_0}$) for the Tangio TPE-502. The blue circles represent the data recorded on February 17, 2017. The red dots represent the averaged data points that were used in the 2-point calibration. From these data, P_0 = 30.2894 mmHg, R_0 = 1.6572 x $10^4\Omega$, and x = -2.0171.

In comparison to the FSR-402 Short, the TPE-502 appears to have a higher sample-to-sample variability, a much lower R_0, and a small magnitude x.

Next, recorded voltage values were input into Equation 7 with these P_0, R_0, and x values, and the pressures sensed by the TPE-502 were calculated. The calculated pressure values were then compared to the actual applied pressure values, and linear regression was used to calibrate the data and reduce the error, as with the FSR-402 Short.

The figure below displays the data before and after calibration. The line of identity is represented by the black dashed line. The blue circles represent the output pressure values calculated using Equation 7 with the P_0, R_0, and x derived in the 2-point calibration. The red circles represent the calculated output pressure values after linear regression calibration:

The linear regression analysis on these data produced the following results: r = 0.9284, m = 0.8982, b = 1.8693. The r value is somewhat close to 1, indicating strong positive linear correlation between the calculated output pressure and the actual applied pressure. The m value

is slightly less than 1, meaning the line of fit (along which recorded data lie) is not perfectly parallel to the line of identity (along which ideal data would lie). The b value suggests the calculated output pressure is consistently greater than the actual applied pressure by at least 1.8693 mmHg.

The sensor output was calibrated by adjusting each value as follows:

1. To make the slope of the line of fit equal to the slope of the line of identify, each calculated output pressure value was multiplied by factor $\frac{1}{m} = 1.113$.
2. To make the y-intercept of the line of fit equal to the y-intercept of the line of identity, each product in (1) was reduced by b = 1.8693.

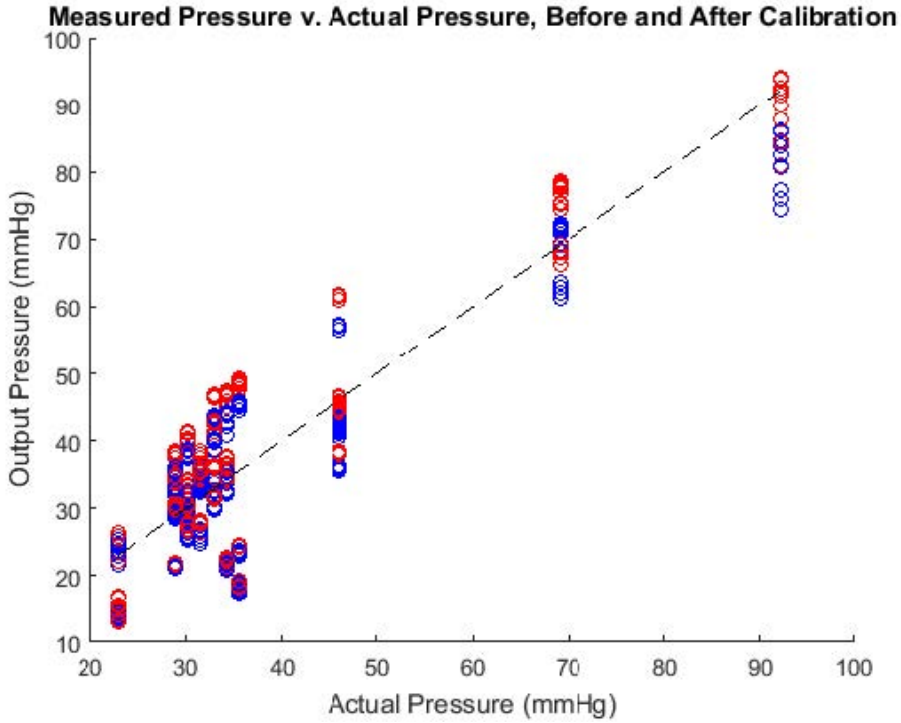

Figure 39: Measured Pressure versus Actual Pressure

In the plot above, both the red circles and the blue circles appear to follow the line of identity. The blue circles appear to follow the line of identity more closely than the red circles between 25 mmHg and 35 mmHg, suggesting the linear regression calibration did not improve the accuracy of the output pressure calculation.

The figure below depicts the difference between the calculated output pressure and the actual applied pressure. The blue circles represent the error before linear regression calibration, and the red circles represent the error after linear regression calibration. Note how the blue circles in the relevant range (25 - 35 mmHg) are more evenly distributed around zero than the red circles. Such results suggest the equation derived with the 2-point calibration was good enough without the additional calibration.

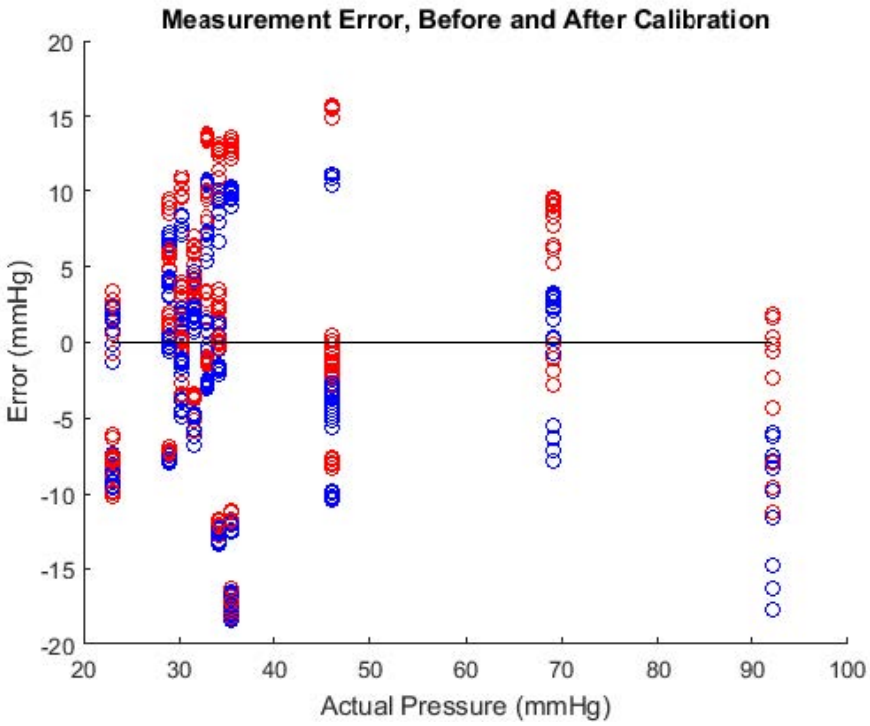

Figure 40: Pressure Sensor Error

These results are summarized in Figure 36 below, in which the average calculated output pressure value at each actual applied pressure is plotted versus the actual applied pressure. Again, the blue circles represent data before the linear regression calibration, and the red circles represent data after the linear regression calibration.

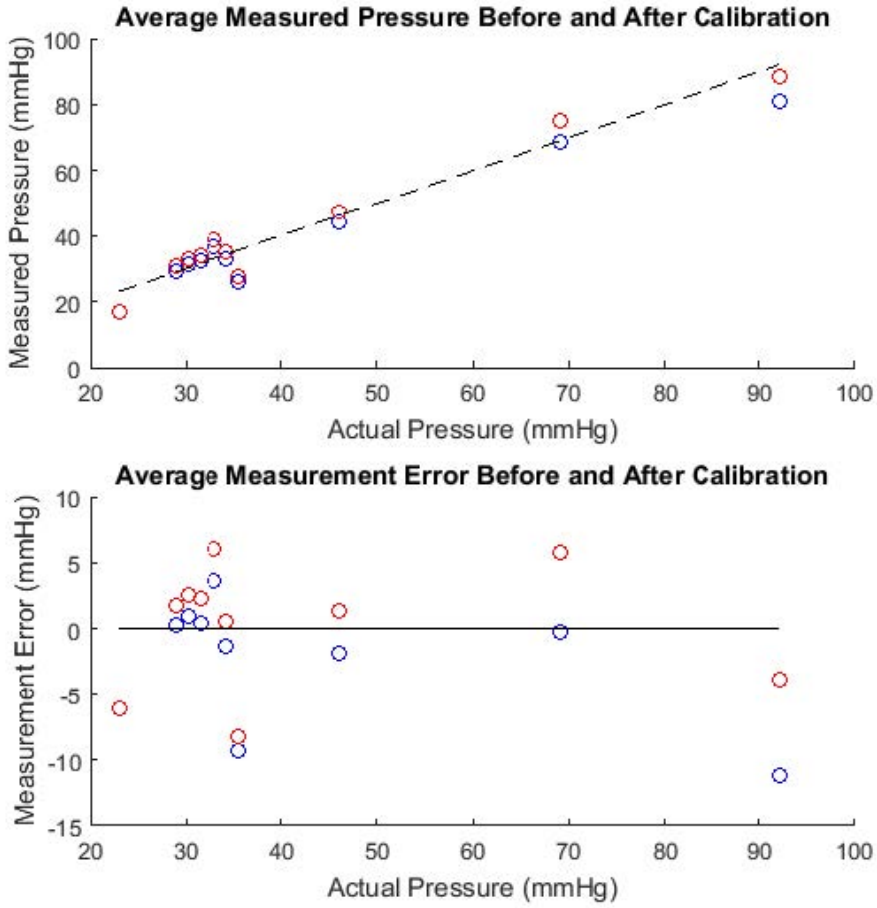

Figure 41: Average Pressure Measurements and Corresponding Errors

The average pressures in Figure 41 were used to assess the accuracy of the TPE-502. Sensor error is summarized in Table 34 below. Linear regression calibration increased average error by about 1%, suggesting the additional linear regression calibration was not necessary with these data.

The mean absolute deviation (MAD) in the average calculated output pressure before linear regression calibration was calculated to be 3.552 mmHg, suggesting the algorithm derived here to determine the pressure sensed by the TPE-502 may be more accurate than +/- 4 mmHg. The part-to-part variability in the Tangio sensor is expected to be much lower than the part-to-part variability in the Interlink sensor; with luck, the algorithm derived here will work for multiple Tangio TPE-502 sensors.

Table 34: Tangio TPE-502 Error Summary

	Average % Error	Max % Error	Error at P_0 (mmHg)	Error at P_0 (%)	MAD (mmHg)
Before Linear Regression Calibration	9.04	26.76	10.90	3.10	3.552
After Linear Regression Calibration	10.71	26.57	2.609	8.61	3.857

5.4 Temperature Sensor Testing Results

The data from the temperature sensor test were collected on February 15, 2017 and can be found in Appendix D. In this experiment, the SHT31-ARP-B analog relative humidity and temperature sensor was tested in the VWR Symphony CO2 Incubator using the protocol discussed in section 5.2.2. The incubator was set to four different target temperatures: 35°C, 36°C, 37°C, and 40°C. The output temperature of the sensor was then compared to the output temperature of the incubator. Using MATLAB, the data were plotted and calibrated based on linear regression results in order to improve the accuracy of the readings. The linear regression calibration process is described below.

The raw data from the sensor were initially plotted against the outputs of the incubator at each target temperature from 35°C to 40°C. Figure 42 below shows the temperature sensor testing results before calibration.

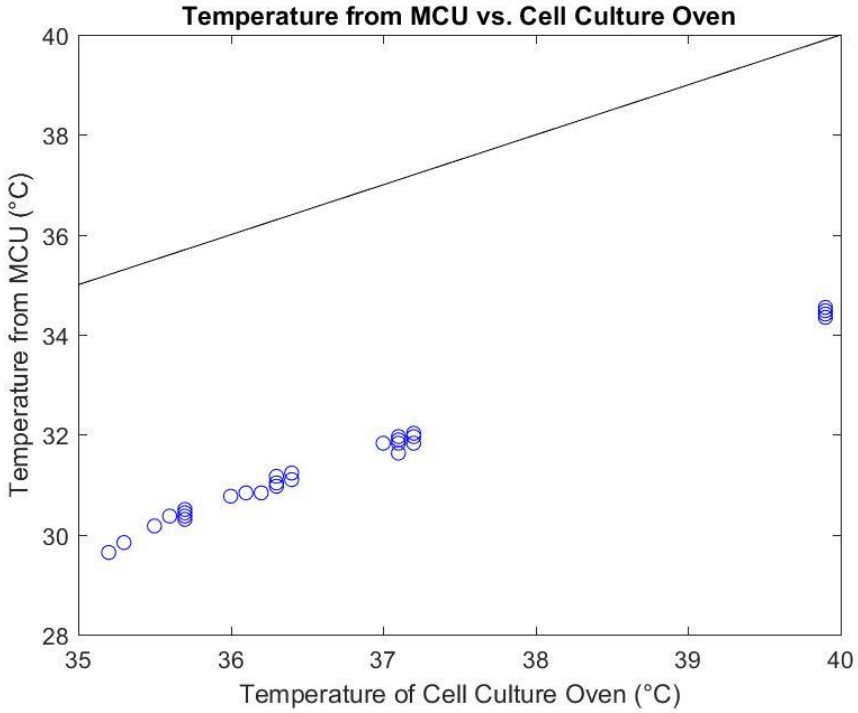

Figure 42: Temperature Reading from MCU vs. Temperature Reading from Incubator Oven

The blue circles represent the individual data points that were sampled from the microcontroller, while the black line represents the line of identity, along which the output of the sensor equals the output of the incubator. Note how the data points lie below the line of identity, seemingly along a straight and parallel line.

Figure 43 below shows the differences between the temperature value output by the incubator oven and the temperature value output by the MCU. Note how consistent the error values are across all temperatures. The maximum error, which occurred at target temperature 36°C, was calculated to be 6.3598°C below the ambient temperature in the incubator oven, which equates to about 18% error.

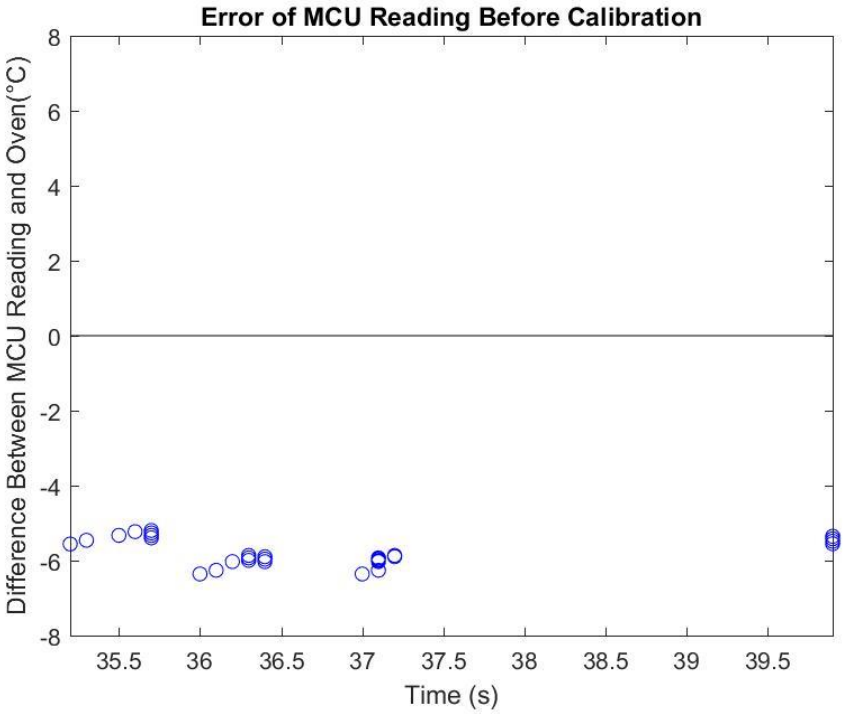

Figure 43: Error Before Calibration

Next, linear regression analysis was conducted to assist in calibrating the data. The values for r, m, and b were 0.9979, 0.9632, and -3.9466, respectively. The r value quantifies the very strong positive linear correlation between the sensor output and the incubator output. The m value is very close to 1, suggesting the line of fit (along which recorded data lie) is approximately parallel to the line of identity (along which ideal data would lie). The b value indicates the sensor output is consistently less than the incubator output by at least 3.9466°C.

The sensor output was calibrated by adjusting each value as follows:

1. To make the slope of the line of fit equal to the slope of the line of identify, each sensor output value was multiplied by factor $\frac{1}{m} = 1.0382$.

2. To make the y-intercept of the line of fit equal to the y-intercept of the line of identity, each product in (1) was increased by 3.9466°C.

Figure 44 below shows the temperature sensor testing results after calibration. Note how the data are distributed along the line of identity, as compared to under it as in Figure 40.

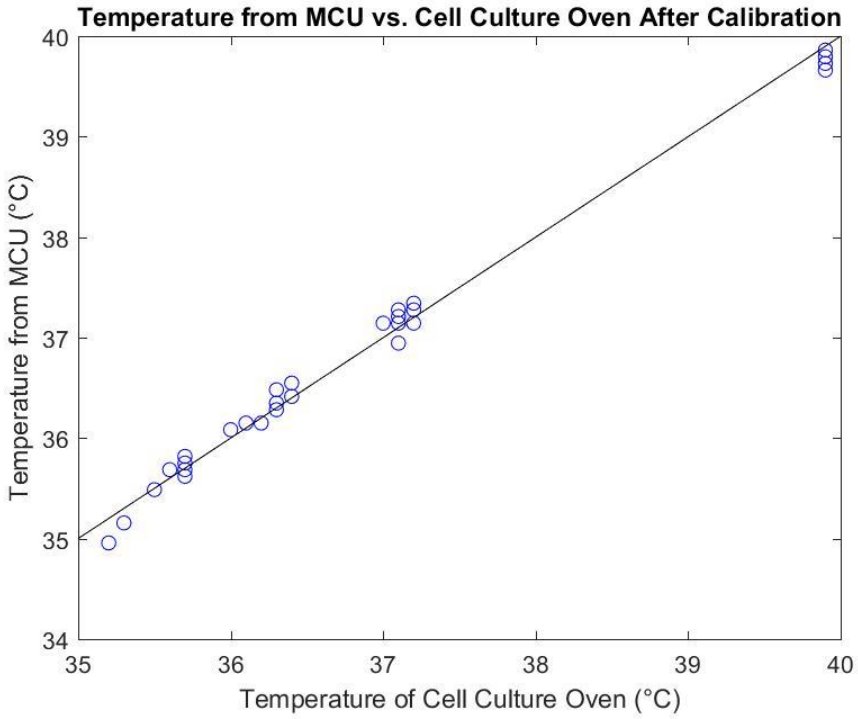

Figure 44: Temperature Reading from MCU vs. Temperature Reading from Incubator Oven After Calibration

The error after calibration was calculated as the difference between the calibrated sensor output and the incubator output. These values are portrayed below in Figure 43. After calibration, the maximum error, which occurred at 35°C, was 0.2437°C, which equates to less than 1% error. Calibration effectively reduced the error by 96%.

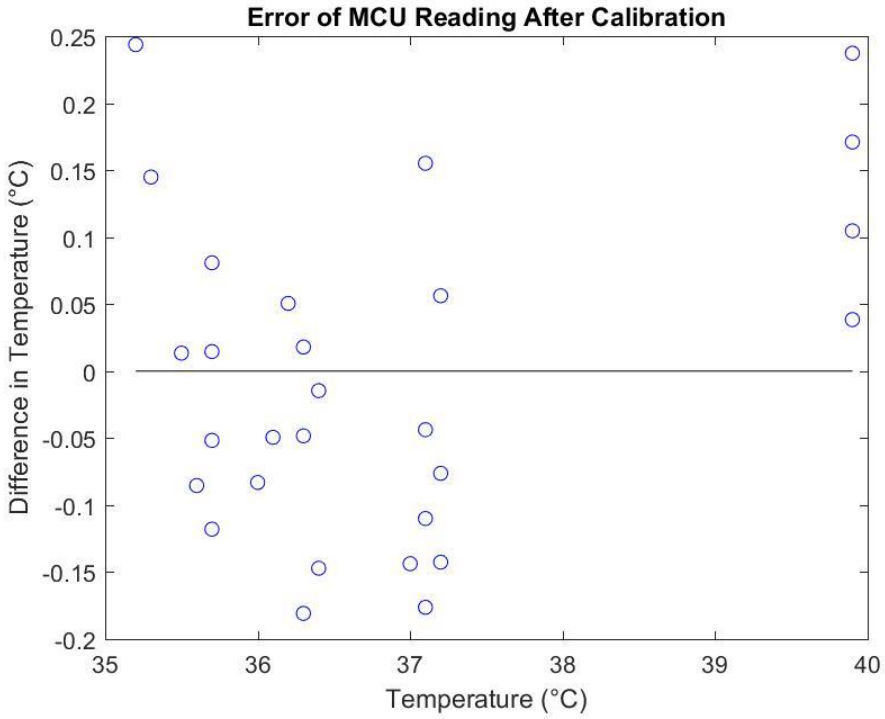

Figure 45: Error After Calibration

In order to reduce the amount of error even further, the last five data points recorded at each target temperature with respect to time were averaged together, and the resulting mean value was used as a singular data point. As a result, there were only four data points, one for each target temperature. The points were then processed with a linear regression that resulted in r, m, and b values of 0.9998, 0.9560, and -3.6591, respectively. Figure 46 below shows the averaged data points after linear regression calibration.

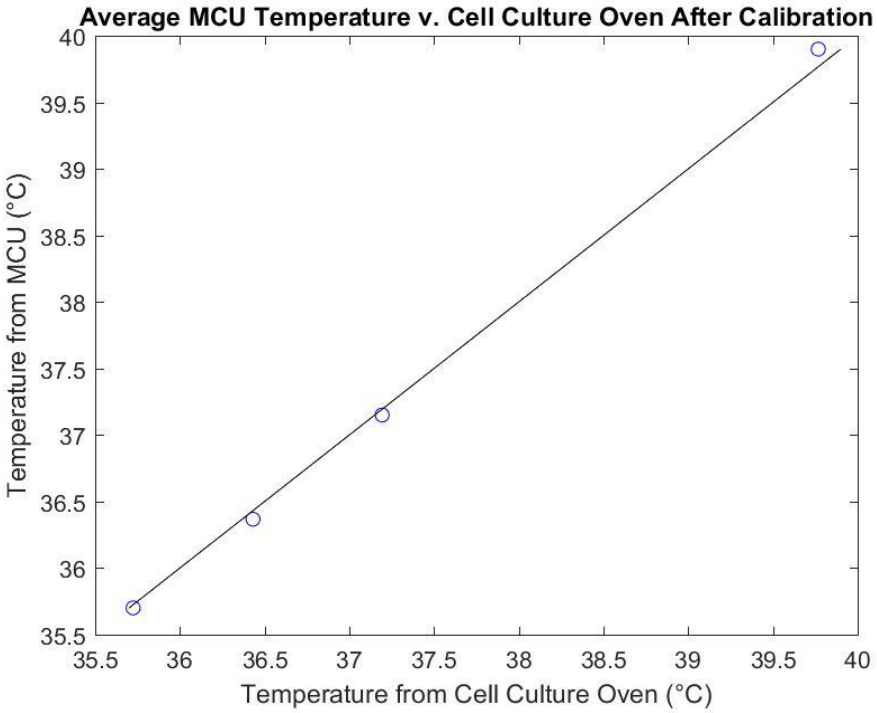

Figure 46: Average Temperature from MCU vs. Average Temperature from Incubator Oven

The error between the average calibrated data points and the average output temperature of the incubator oven was also calculated. Figure 47 below shows the error resulting from differences between these values. After averaging and calibration, the maximum error, which occurred at 40°C, was 0.1323°C, which equates to 0.3% error. The error was reduced by 98% with respect to the original uncalibrated data.

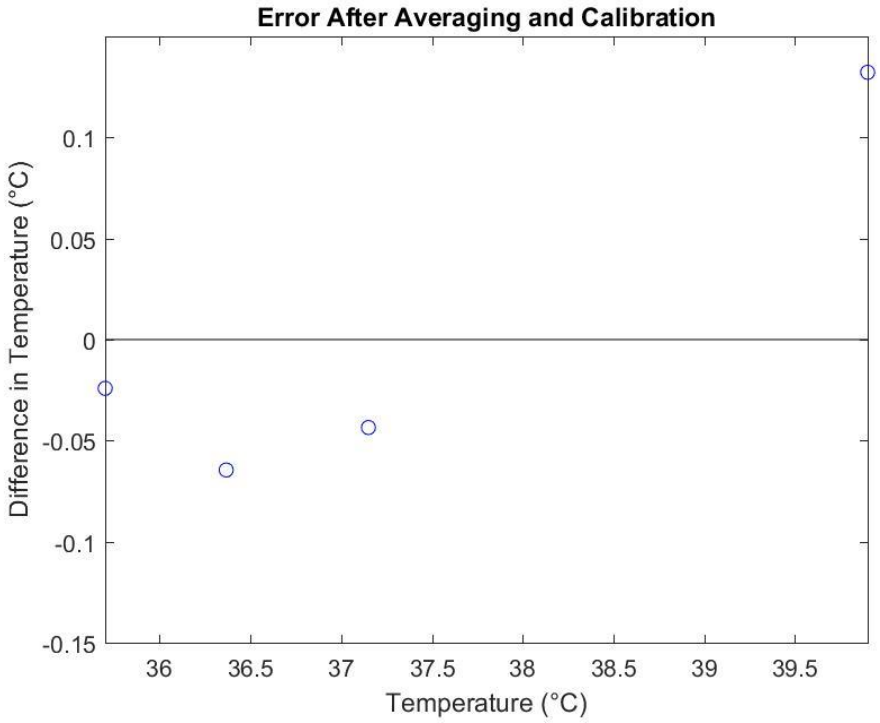

Figure 47: Error After Averaging Temperature and Calibration

Overall, averaging the last five data points and applying linear regression calibration technique was effective in reducing the error experienced by the sensor. However, the analog temperature sensor in the SHT31-ARP-B was still not accurate enough to meet the +/-0.1°C requirement. Thus more accurate temperature sensors must be tested in future.

5.5 Relative Humidity Sensor Testing Results

The data from the relative humidity sensor test were collected on January 25, 2017 and can be found in Appendix E. In this experiment, the SHT31-ARP-B analog relative humidity and temperature sensor was tested against the Vernier RH-BTA probe using the protocol discussed in section 5.2.3. Using MATLAB, the data were plotted and calibrated based on linear regression results in order to improve the accuracy of the readings. The MATLAB script is included in Appendix E. The linear regression calibration process is described below.

The raw data from both the sensor and the probe were initially plotted over time. Figure 48 below shows the results of the baseline relative humidity test. Figure 49 below shows the results of the increasing relative humidity test, and Figure 50 shows the results of the decreasing relative humidity test. The blue circles in each plot represent the relative humidity output by the SHT31-ARP-B sensor, and the red circles represent the relative humidity output by the Vernier RH-BTA probe.

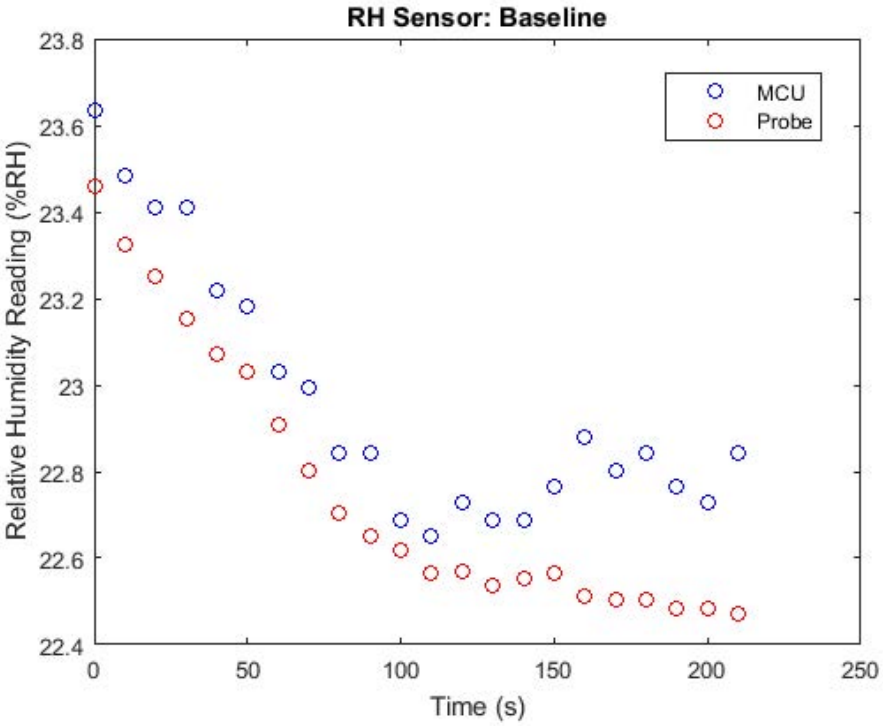

Figure 48: Baseline Relative Humidity

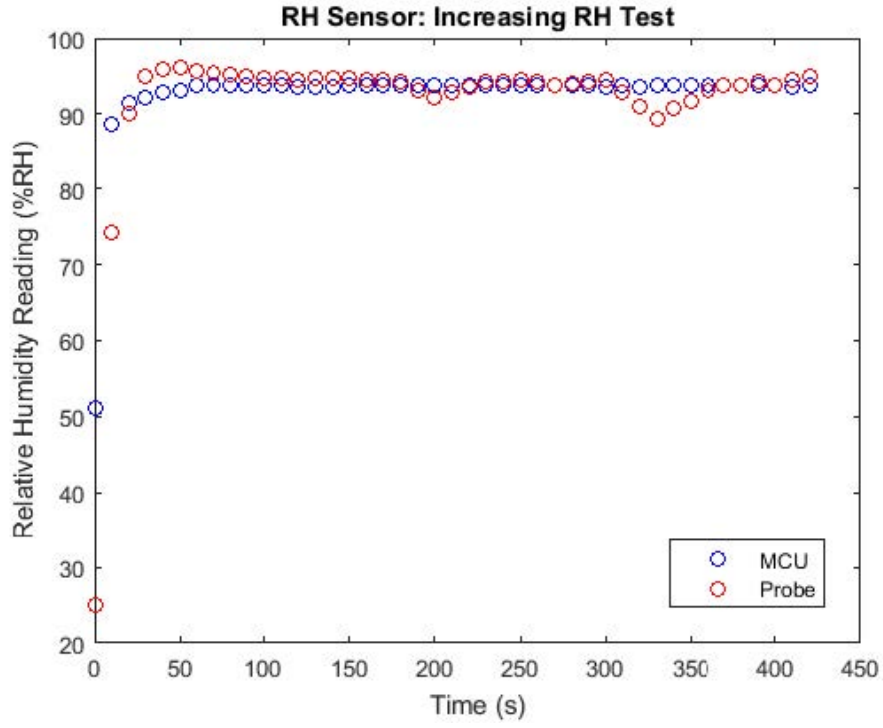

Figure 49: Increasing Relative Humidity Test Result

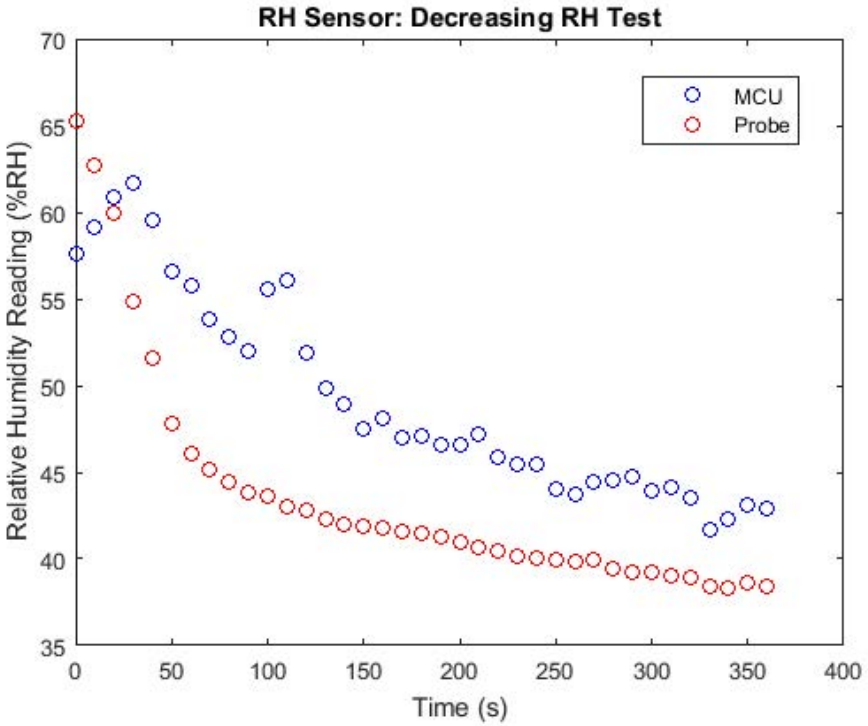

Figure 50: Decreasing Relative Humidity Test Result

In Figure 48-50 above, the output of the sensor on the PCB appears to behave like the output of the probe; however, these values are consistently higher throughout the operational range of the sensor (10 %RH - 90 %RH). These observations are confirmed in the relative humidity versus relative humidity plots and the corresponding error plots below.

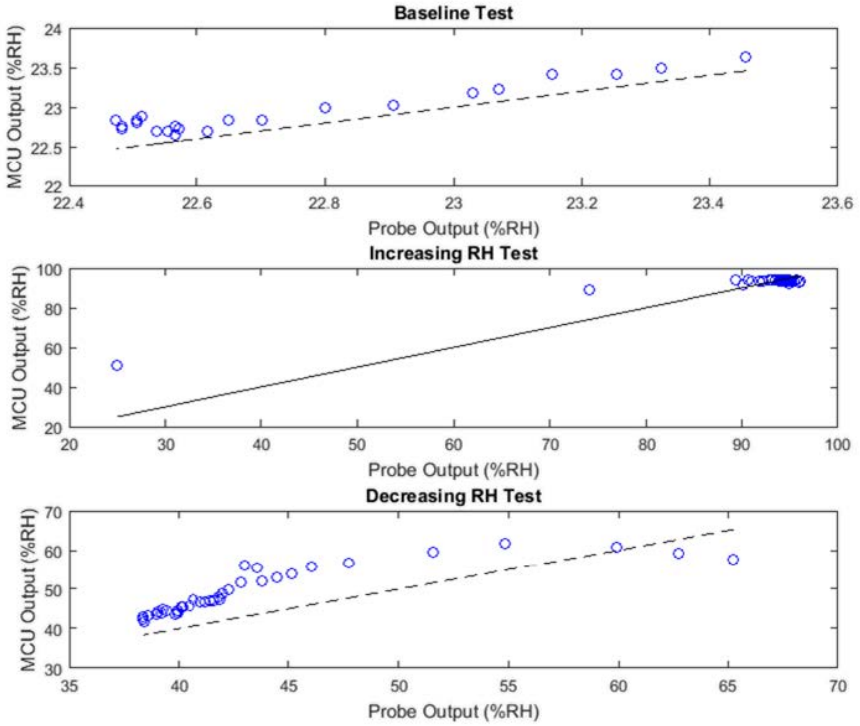

Figure 51: Relative Humidity Sensor versus Relative Humidity Probe versus Line of Identity

The plots in the figure above and the figure below better depict how closely the relative humidity sensor measurements mimic the relative humidity probe measurements.

According to the data sheet, the sensor is supposed to be accurate to +/-2 %RH. The MAD during the baseline test, the increasing relative humidity test, and the decreasing relative humidity test are 0.20 %RH, 2.08 %RH, and 6.20 %RH, respectively. Assuming the probe recorded the exact relative humidity of the sensing environment, the analog sensor exceeded its expectations during the baseline test, barely met its expectations during the increasing relative humidity test, and performed below standard during the decreasing relative humidity test.

The differences between the readings are clearly lowest during the baseline test. These results suggest the sensor is most accurate before exposure to high-relative-humidity conditions and least accurate during significant or rapid changes in relative humidity. The sensor should not often experience violent fluctuations in relative humidity while monitoring areas in which pressures ulcers are most likely to develop on patients; thus its responses during these tests will likely be acceptable in real scenarios.

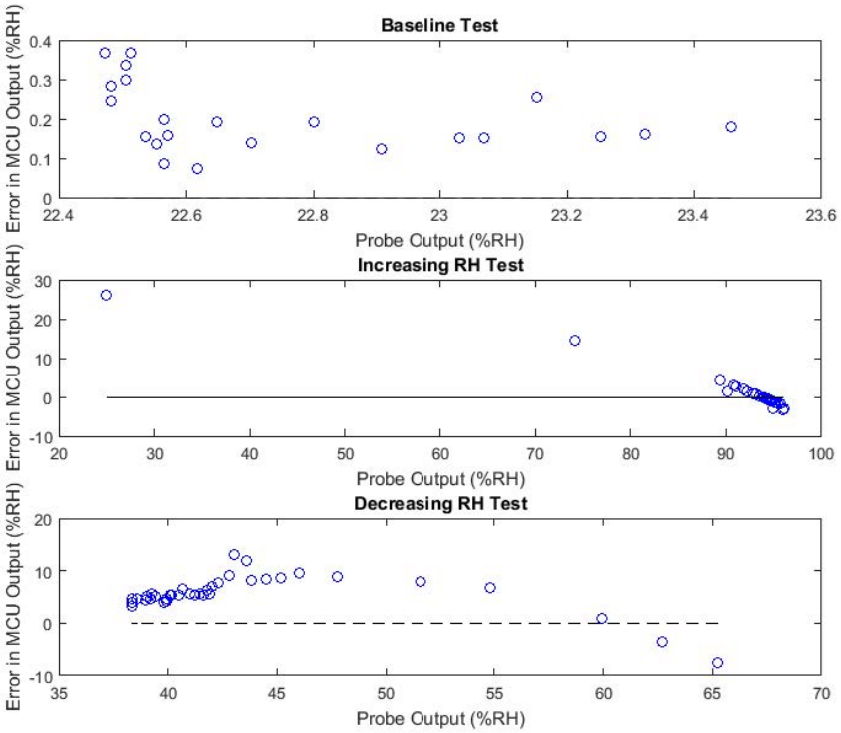

Figure 52: Relative Humidity Sensor versus Relative Humidity Probe versus Line of Identity Error

Note linear regression calibration was attempted on these data; however, the data were less accurate after calibration than before calibration. Since the relationship between the sensor output and the probe output is not perfectly linear, as seen in the preceding plots, and since the results of the attempt were unsuccessful, linear regression calibration was concluded to be inappropriate for these data.

5.6 Current Draw Analysis

The following figure shows a segment of the power draw belonging to the data transmission, measured as the voltage drop across the 2Ωresistor in millivolts over time.

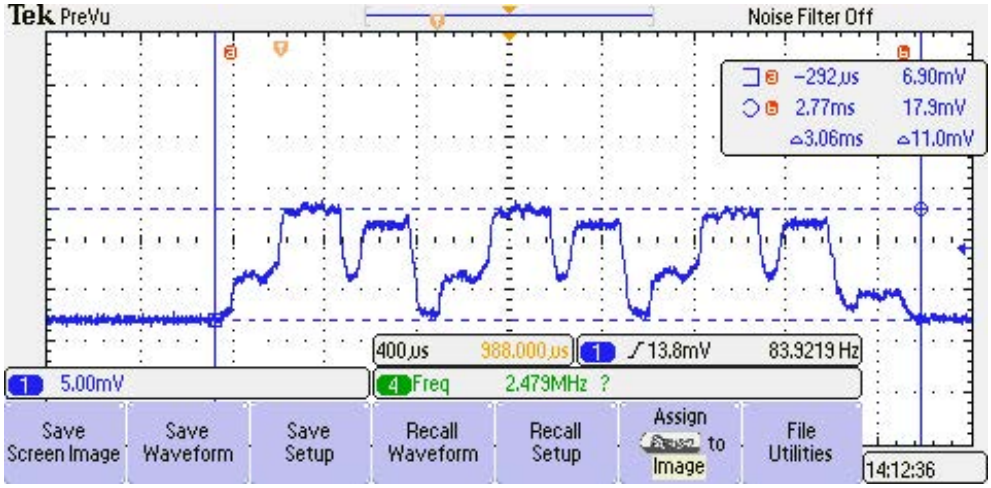

Figure 53: Voltage Waveforms During Transmission

As seen in the figure above, each transmission takes about 3.06 ms. The upper voltage bound, caused by the transmission, is around 17.9 mV and the lower voltage bound is around 6.9 mV. Since these potential differences occur across 2-ohm resistance, the expected current draw of the entire circuit on each patch ranges between around 3.5 mA on the low end and around 9 mA on the high end.

The upper expected current draw value approximately aligns with the preliminary calculation done earlier, which concluded the peak current draw during the transmission should be little above 10 mA. Given 10 mA was obtained using maximum values, as provided in the data sheet, not typical values, measuring a slightly lower value during an actual test is permissible. The lower expected current draw value, which represents the ambient current draw, is higher than what would be allowable in a patch meant to operate for seven days on one battery. The ambient current draw can be reduced by updating the firmware to be power efficient.

5.7 Preliminary Rat Experiment

With the assistance of Dr. Raymond Dunn and Dr. Kelli Hickle from UMass Memorial, the PUP MQP team was able to conduct preliminary tests on a rat using the FSR402 Short sensor. The procedure used during the preliminary rat experiment is described below. These specific steps were taken because:

- operating on the dorsal plane of the rats ensures that live and active rats will not tamper with the magnets or the patch during the actual experiment in May.
- performing a midline incision is ideal because of the avascular environment. The latissimus dorsi muscle in rats are similar to humans (it is important to note that the muscle is the most ischemic tissue in the body).

1. A 330g lab rat that was approximately 24cm from the tip of the nose to the base of the tail was obtained and euthanized. The rat was laid down on a blue towel with the dorsal side facing up.

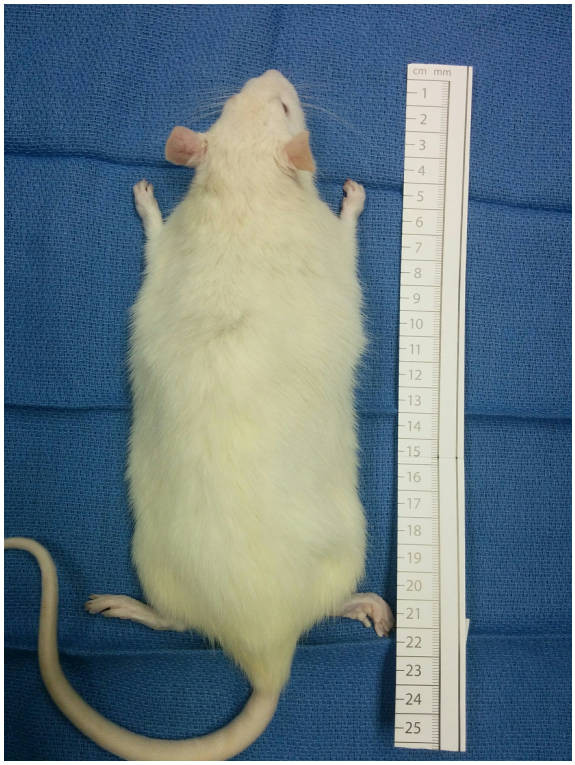

Figure 54: 330g Lab Rat

2. The dorsal side of the rat was shaved in order to expose the skin. The rat was secured to a board beneath the towel via push pins in each of its feet.

    - Operating on the dorsal plane of the rats ensures that the rats cannot tamper with the magnets or the patch.
    - Performing a mid line incision is ideal because of the avascular environment. The latissimus dorsi muscle in rats are similar to humans (it is important to note that the muscle is the most ischemic tissue in the body).

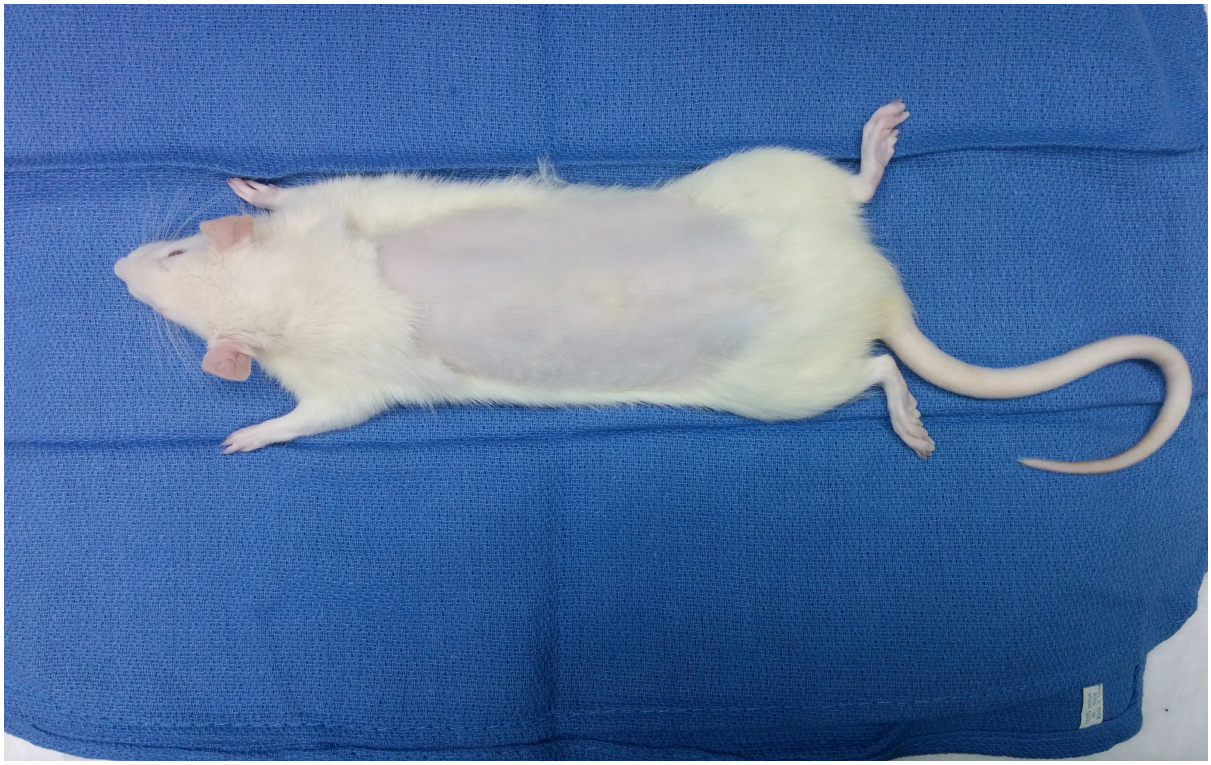

Figure 55: Dorsal View of Shaved Rat

3. A mid line incision was performed and the right latissimus dorsi was disected.

Figure 56: Dissection of latissimus dorsi

4. A 2cm x 2cm galvanized steel plate was implanted beneath the right sub latissimus dorsi.

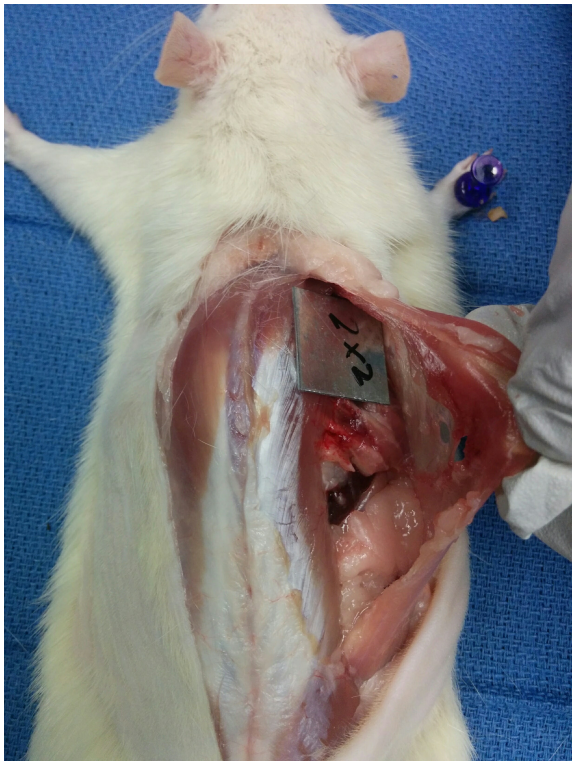

Figure 57: Galvanized Steel Plate Implant

5. A caliper was used to measure the thickness of the skin which was 2.12mm. The thickness of both the skin and muscle was 3.52mm. The muscle and skin layers were then placed over the implant area. The pressure sensor was then placed between the skin and the applied magnet. During this process, different magnets were applied and different areas of steel plates were tested in order to determine which combination yielded the best results. The following table shows the preliminary results. The magnet corresponds to the number labeled on the plastic bags holding the magnet (in this case, magnet 4 was the smallest magnet) and GS refers to the galvanized steel. In some cases, the magnet section is blank because the magnet used was unknown

Table 35: Pressure Data of Right Latissimus Dorsi

Magnet	# of Magnets	Plate Size (cm)	Material	Hex	Pressure (mmHg)
n/a	n/a	2x2	GS		1.1333
	1	2x2	GS	B7F	253.9877
	1	2x2	GS	9D3	138.3269
	1	2x2	GS	76E	79.7531
4	1	2x2	AS	179	17.5338
3	1	2x2	GS	A35	154.4602
3	1	2x2	GS	AAA	179.1349
2	1	2x2	GS	994	129.4991
	1	2x2	GS	881	100.1427
4	1	2x2	GS	2C7	28.5043
4	2	2x2	GS	7D8	86.8779
4	1	2x3	GS		21.8754
4	1	2x3	GS	26B	25.4598

6. Next, the left latissimus dorsi was dissected and the steel plate was implanted under the muscle. The thickness of both the skin and muscle was 2.66mm. The same procedure of applying different magnet and steel plate combinations was conducted. Table 2 shows the results of this experiment.

Table 36: Pressure Data of Left Latissimus Dorsi

Magnet	# of Magnets	Plate Size (cm)	Material	Hex	Pressure (mmHg)
4	1	2x3	GS	38F	35.2026
4	2	2x3	GS	7AB	83.7568
5	1	2x3	GS	750	77.8716
	1	2x3	GS	A75	167.0626
	1	2x3	GS	7A9	83.6215
4	3	2x3	GS	A1E	150.367

7. Lastly, Steri-Strips were stacked together to create a thickness of 1.38mm. The Steri-Strips were placed between the pressure sensor and the magnet and the same procedure of applying magnets to the skin was conducted on the right latissimus dorsi.

Table 37: Pressure Data of Right Latissimus Dorsi with Steri-Strips

Magnet	# of Magnets	Plate Size (cm)	Material	Pressure (mmHg)
4	1	2x3	GS	23.834
4	1	2x3	GS	13.4636

6 Final Design and Validation

6.1 Objective

The purpose of the chapter is to describe how the flexible PCB was tested and verified and to explain the implications of the results.

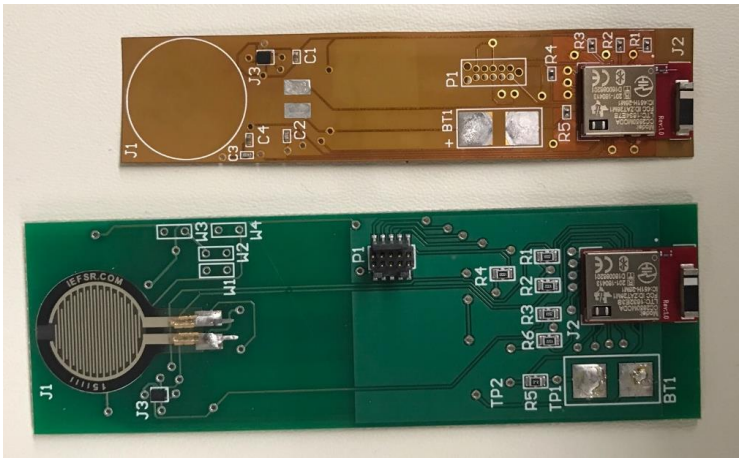

Figure 58: Final Design on Flexible PCB

6.2 Testing Protocol

The testing protocol will be outlined and submitted in the D-Term version of this paper.

6.3 Testing Results

The testing results will be discussed and submitted in the D-Term version of this paper.

7 Financial Analysis

7.1 Objective

The purpose of the section is to estimate the potential economic value of the pressure ulcer prevention system as it is used in one hospital over five years.

7.2 Rationale

Unlike business professors, very few engineering professors challenge students to assess projects or products based on the value to the customer. The electrical and computer engineering design class, ECE2799, is one exception: It provides students with one lecture on return-on-investment and requires students to calculate the initial investment and the return-on-investment associated with the products they develop. Simple financial analyses such as these enable students and professors alike to estimate how much projects might benefit customers and to determine whether or not projects are worth pursuing. The advisors of the PUP MQP, in particular, could use financial analyses to assist them in attracting both government and corporate sponsors, whose funding would enable them to conduct testing on animals and continue preparing for future clinical trials.

7.3 Net Present Value

The value of the pressure ulcer prevention system to its target market can be estimated as the difference between how much consumers would spend on it and how much consumers would save with it over time as it assists in reducing pressure ulcer rates. The net present value of the system at some future point in time can be calculated according to Equation 8 (Investopedia, n.d.):

$$NPV = \sum_{t=1}^{T} \frac{C_t}{(1+r)^t} - C_0 \tag{8}$$

where

C = the net cash flow during the time period t, which is equivalent to the difference between money saved by the system and money spent on the system per day or per year in the net present value analysis below;

r = the discount rate, which accounts for the time value of money and which is equivalent to the hurdle rate, or the minimum rate of return expected by the consumer, in the net present value analysis below;

C_0 is the initial investment, which is equivalent to the total costs associated with purchase, installation, setup, and personnel training in the net present value analysis below.

Once these variables are known, cash flow diagrams can be used to show the magnitude of the costs and the spacing of the costs over time.

7.3.1 Estimated Savings

Three different methods were used to estimate how much medical care facilities, such as hospitals and nursing homes, could save per prevented pressure ulcer per day. The expected length of stay for a patient with a hospital-acquired pressure ulcer was computed based on average length of stay values reported in case studies and national data sets. These data and sources are reported in Appendix F. The average length of stay calculated for a patient with a

hospital-acquired pressure ulcer was 15.5 days, and the average excess length of stay calculated for a patient with a hospital-acquired pressure ulcer was 7.5 days.

The first method used to estimate savings per prevented pressure ulcer per day relied on studies in which both excess charge and average stay per hospital-acquired pressure ulcer case were reported. The estimated savings per hospital-acquired pressure ulcer case per day were calculated according to Equation 9:

$$S = AVERAGE\left(\frac{EXC_I}{LOS_I}\right) \tag{9}$$

where

S = estimated savings per hospital-acquired pressure ulcer case per day

EXC_i = excess charge per hospital-acquired pressure ulcer case, as reported in source i

LOS_i = average length of stay, as reported in source i

Each EXCi / LOSi ratio was adjusted for inflation. Then all ratios were averaged to determine S in 2017 dollars. The original data are reported in in Appendix G, and the manipulated data are shown in Table 38.

Table 38: Savings Per Pressure Ulcer Case Per Day

	Data Collection Time Period	Average Stay	Excess Charge	Savings Per Case Per Day	Adjusted Savings Per Case Per Day
(Zhan & Miller, 2003)	2000	9.98	$10,845	$1,090	$1,530
(Russo et al., 2008)	2006	12.7	$10,500	$827	$996
(Goudie et al., 2015)	2009 - 2011	11.8	$19,740	$1,670	$1,810
Estimated savings per case per day	$1,440				

The second method and the third method used to estimate savings per prevented pressure ulcer per day relied on annual hospital-acquired conditions data compiled by the Agency for Healthcare Research and Quality. Annual savings were reported in two ways each year: based on differences between the hospital-acquired pressure ulcer rate of the present year and the 2010 baseline rate, as shown in Table 38, and based on changes in the hospital-acquired pressure ulcer rate over a multi-year time period, as shown in Table 39.

The estimated savings per hospital-acquired pressure ulcer case per year were calculated according to Equation 10:

$$S_{pC} = \frac{S_{pY}}{\Delta N} \tag{10}$$

where S_{pC} = estimated savings per hospital-acquired pressure ulcer case S_{pY} = estimated savings per year due to change in hospital-acquired pressure ulcer rate over time ΔN = change in annual number of hospital-acquired pressure ulcer cases over time

Each S_{pC} value was adjusted for inflation. The estimated savings per hospital-acquired pressure ulcer case per day were determined by dividing the average savings per case in 2017 dollars by the expected length of stay, which was 15 days once rounded.

Table 39: Yearly Data from Agency for Healthcare Research and Quality

	2010	2011	2012	2013	2014	2015
Number of cases	1,319,825	1,320,000	1,300,000	1,060,000	1,010,000	1,190,000
Change in number cases versus 2010		175	(19,825)	(259,825)	(309,825)	(129,825)
Cost savings versus 2010 baseline			$4,420 M	$5,270 M		
Estimated savings per case per year			$17,011	$17,010		
Adjusted savings per case per year			$17,733	$17,448		
Estimated savings per case per day	$1,170					

Table 40: Marginal Changes in Yearly Data from Agency for Healthcare Research and Quality

	2011 - 2013	2011 - 2014	2011 - 2015
Total reduction in hospital acquired conditions over time period	1,317,800	2,115,800	3,097,400
Percent due to reduction in hospital acquired pressure ulcers	21.2%	27.9%	23.2%
Estimated cost savings due to reduction in hospital acquired pressure ulcers	$4,760 M	$10,030 M	
Estimated savings per hospital acquired pressure ulcer per year	$17,038	$16,991	
Adjusted savings per hospital acquired pressure ulcer per year	$17,761	$17,429	
Estimated savings per hospital acquired pressure ulcer per day	$1,173		

It is important to note these estimates are derived from averages of costs incurred due to stage 1-4 pressure ulcers. These averages are inherently skewed, since stage 3 and stage 4 pressure ulcers are less common than stage 1 and stage 2 pressure ulcers yet require significantly more time and more money to heal.

7.3.2 Estimated Costs

Base Station

The price per base station is going to depend on which computational platform is used. The researchers have not yet decided whether the marketable system will include the complete base station (hardware and software) or the software alone.

The initial concept for the complete base station has been modeled after patient monitors used in critical care units and intensive care units today. These monitors handle one patient each and display multiple physiological parameters. Most can also wirelessly access electronic medical records. They cost between $200 and $12,000, with an average at $1,866 each (Medical Price Online, 2017). Thus base stations modeled after existing patient monitors and sold as complete units would likely cost hospitals about $2,000 each up front.

The alternative option for the base station would take advantage of existing devices, including smartphones, tablets, and laptops. The application through which the base station and the patches would communicate would likely be free to download. For a hospital in which caretakers have already been issued work devices to monitor patients, and for a hospital in which caretakers may interact with patients via personal devices, the up-front cost associated with the base station would be zero, since the required devices are on-hand already. Otherwise, the up-front cost associated with the base station would be around $300 to $600 per device: Smartphones cost about $300 each on average (Consumer Technology Association), while tablets cost between $50 each and $2,200 each (Tabletmonkeys, 2017), and good laptops cost between $500 each and $4,000 each (Domingo & Murray, 2017).

When the BLE wireless communication protocol is used, the base station can only connect to one sensor patch at a time. If the base station requires 5 seconds to retrieve data from each sensor patch, and if each sensor patch advertises once every 5 minutes, then the base station can interface with up to 60 patches. The microcontrollers on the sensor patches can be programmed to advertise more or less often to accommodate less or more patches, respectively.

Sensor Patches

The price per patch is expected to be approximately $10 (McNeill, personal communication, 2017). Each patient will use between one and twenty patches simultaneously, depending on how many at-risk areas caretakers identify. Each patch will be used up to seven consecutive days before it must be removed and replaced.

Other Expenditures

Other expenses a hospital should expect to incur when implementing the pressure ulcer prevention system are costs associated with personnel training, base station power supply, sensor patch inventory storage, and used sensor patch disposal.

7.3.3 Estimated Value

The net present value analyses below rely on the assumptions presented in section 7.6.1. These assumptions will likely not hold true when applied to real-life situations, but they illustrate how these systems might be implemented in hospitals, highlight which variables should be considered, and provide a solid framework in which reasonable predictions about costs and benefits can be made.

Assumptions

- Average length of stay for a patient who acquires a pressure ulcer is 15 days, and average length of stay for a patient who is spared from a pressure ulcer is 7 days.
- Average savings per prevented pressure ulcer per day is $1,000.
- Each complete system costs $5,000 up front, which accounts for expenditures associated with base station, installation, set-up, training, etc.
- Each base station serves 10 patients.
- Each patient uses 6 patches (2 heel, 1 sacrum, 2 elbow, 1 head) at all times.
- Each patch costs $10.
- All patches have a 25% prevention rate and a 100% adhesion rate.
- Hurdle rate, i.e. minimum rate of return on investment, is 10%.
- Interest period is one year.
- The average patient considered in the analysis here can be used to represent all patients in the hospital.

Success Case

If the system succeeds in preventing pressure ulcers, then the patient stays 7 days, and the hospital saves approximately $6,430. Associated cash flows are depicted in Figure 59.

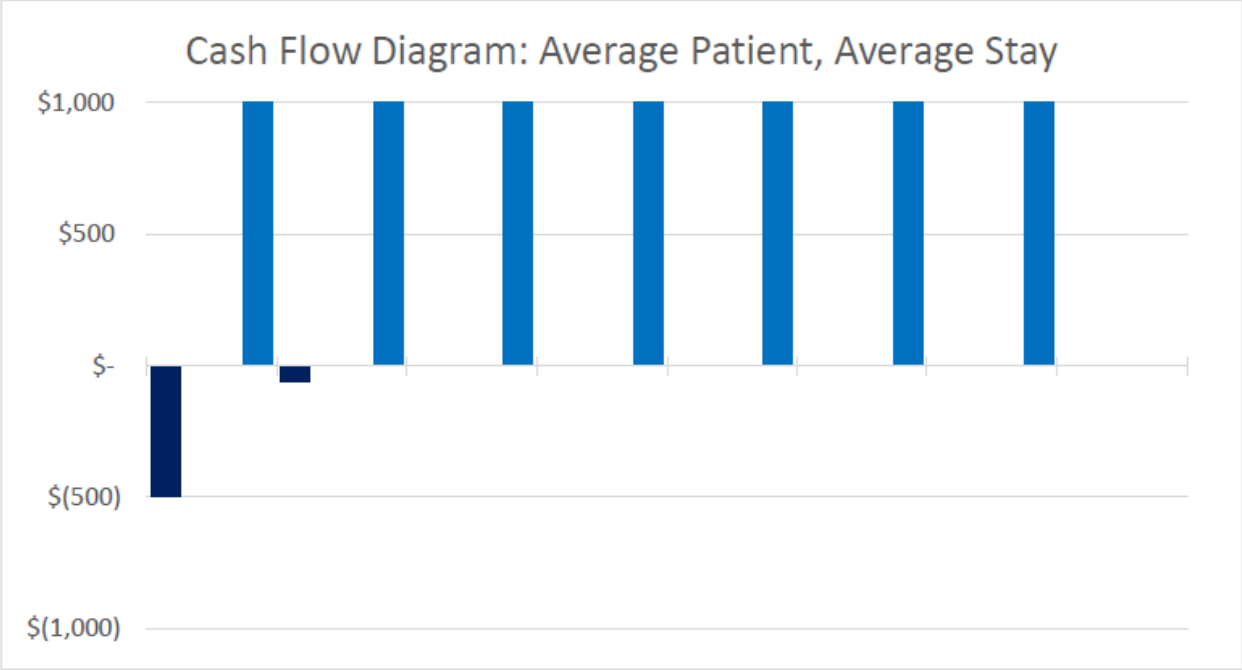

Figure 59: Cash Flow in Success Case

The right-most cash outflow is associated with the initial investment per patient, which equals the up-front cost of one complete system divided by the number of patients served by that system. The next cash outflow is associated with the patches used by the patient. Since all patches are operational for up to 7 days, they only need to be acquired once. The cash inflows are associated with the expected savings per prevented pressure ulcer per day.

Failure Case

If the system fails in preventing pressure ulcers, then the patient stays 15 days, and the hospital loses approximately $680. Associated cash flows are depicted in Figure 60.

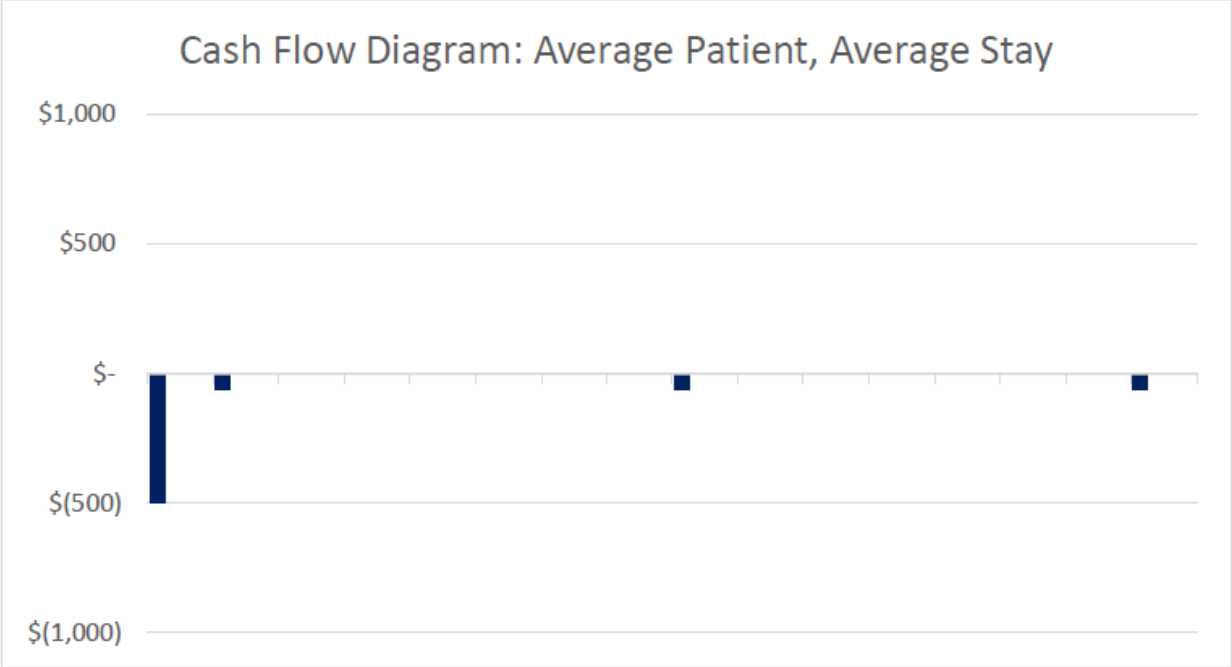

Figure 60: Cash Flow in Failure Case

As in Figure 59, the right-most cash outflow represents the initial investment per patient. The remaining cash outflows are associated with the expenditures on the patches. Since patches operate for up to 7 days, and since the length of stay for the patient with hospital-acquired pressure ulcers is 15 days, patches need to be acquired three times. There are no cash inflows because there are no prevented pressure ulcers.

Average Case

When one success case occurs with every three failure cases, the average net present value of the pressure ulcer prevention system becomes about $1,000 per patient per stay.

For a hospital such as UMass Memorial Medical Center, which reported 38,444 discharges in 2016 (UMass Memorial Health Care, 2017), how much money could the pressure ulcer prevention system save over five years?

If the hospital-acquired pressure ulcer rate at UMass Memorial were equal to the national hospital-acquired pressure ulcer rate in 2016, which is given in Table 41, then approximately 1,200 patients would have acquired pressure ulcers while staying there. Thus UMass Memorial should invest in at least 120 base stations to accommodate that many patients.

Table 41: Annual Hospital-Acquired Pressure Rates from Agency for Healthcare Research and Quality

	2010	2011	2012	2013	2014	2015	2016
Hospital-acquired pressure ulcer rate per 1000 discharges	40.3	40.41	39.43	32.5	30.9	36.3	33.2*

*2016 rate was predicted with a three-year moving average.

If the assumptions listed in section 7.6.1 hold true, then the pressure ulcer prevention system will enable the hospital to save $3,710,000 over 5 years. Associated cash flows are depicted in Figure 61.

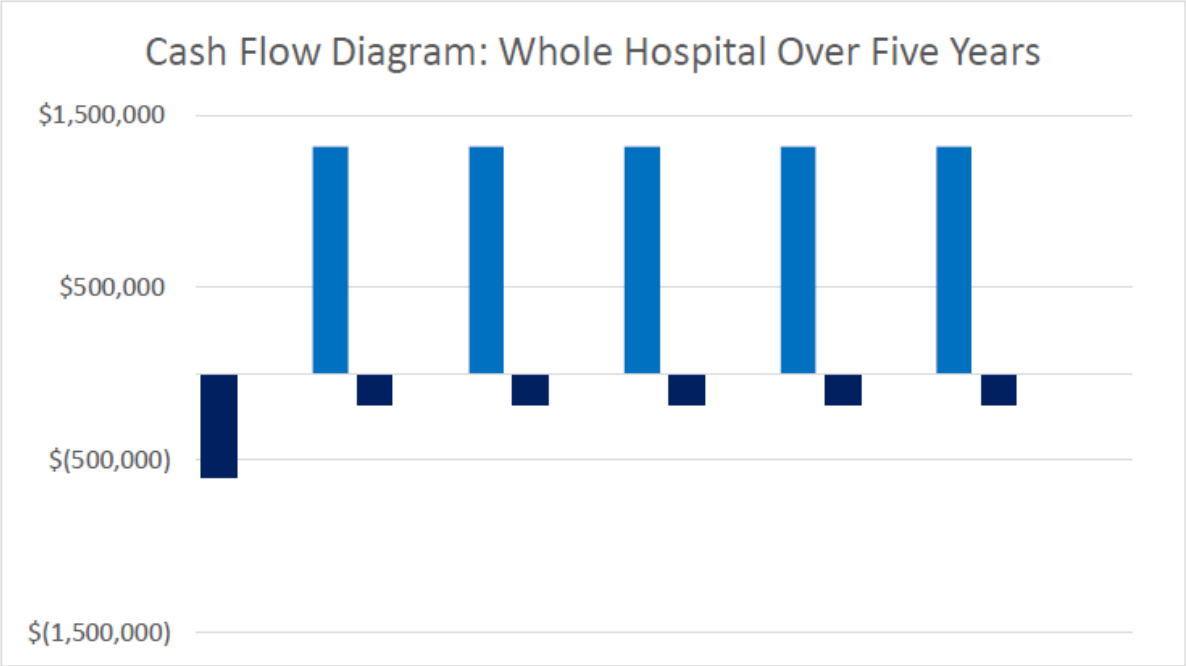

Figure 61: Cash Flow for Whole Hospital

7.4 Return on Investment

To commercialize the pressure ulcer prevention system, the owners of the intellectual property rights will likely enter into a licensing agreement with a medical device manufacturer. In that case, returns on research and development costs will come as royalties and lump sum payments. The break-even analyses below are used to estimate how many sensor patches must be sold before the owners of the intellectual property rights can overcome a 10% hurdle rate. These analyses rely on the assumptions presented in section 7.7.3.1. Base station sales are not considered (as stated in section 7.3.2.1, any software application used to transform an existing portable device into a base station will probably be free to download).

7.4.1 Estimated Initial Investment

The total research and development cost of the pressure ulcer prevention system will probably equal about $3 million. Expenditures incurred over the course of the PUP MQP alone added up to over $5,000. The phase I application submitted to the OTCV Technology Development Fund in January 2017 proposed spending $25,000 on experiments with rats between May 2017 and June 2017, while the application submitted to the Presidents Science & Technology Initiatives Fund estimated the total costs of the same tests to be as much as $100,000 (McNeill, personal communication, 2017). Expenditures on research and development through human trials are expected to be another $1 million to $2 million,obtained through NIH R01 grant funding (McNeill, personal communication, 2017). Additional costs incurred before the system reaches the market will be associated with patenting the technology, modifying the system to conform to FDA regulations and standards and to prepare it for large-scale manufacturing, obtaining

then maintaining FDA approval, and negotiating a licensing agreement. All in all, expenditures made between the inception of the project and the completion of the project will likely add to up approximately $3 million.

7.4.2 Break-Even Point and Target Sales Quantity

Assumptions

- Sensor patch retail price is $10.
- Retailer markup is 30% (Michalson, 2016).
- Distributor markup is 30% (Michalson, 2016).
- Royalty rate is defined as either 6.40% of manufacturer revenue, which is the typical rate in the medical products and equipment industry (Zipkin, 2014) or between one quarter and one third of manufacturer profits, which is the general rule of thumb amongst licensing professionals (World Intellectual Property Organization, 2015; Zaharoff, 2012).
- Hurdle rate is 10%.
- Licensing agreement directs licensee to compensate licensor via royalty payments only.

Manufacturer Revenue and Profit Calculations

Three different supply chain possibilities exist to bring the pressure ulcer prevention system from manufacturer to customer:

1. Direct to Distributor

The manufacturer will sell the product to the distributor, who in turn will sell the product to the retailer, who will finally sell the product to the customer. Both the retailer and the distributor will markup the price in order to profit.

Profit margin is defined as (Investopedia, n.d.):

$$PROFITMARGIN = \frac{PROFIT}{REVENUE} = \frac{RETAILPRICE - PURCHASEPRICE}{RETAILPRICE} \quad (11)$$

Solving for PURCHASE PRICE, Equation 11 becomes:

$$PURCHASEPRICE = (RETAILPRICE) * (1 - PROFITMARGIN) \quad (12)$$

If the retail price of the sensor patch must be $10.00 each, and if the retailer expects 30% profit margin, then the retailer must buy the sensor patch from the distributor for $7.00 each. Similarly, if the distributor expects 30% profit margin, then the distributor must buy the sensor patch from the manufacturer for $4.90.

The manufacturer would also markup the price before selling to the distributor. The maximum possible manufacturing cost to achieve the target retail price is calculated in column 2 of Table 42 for five different manufacturer profit margins.

2. Direct to Store

The manufacturer will sell the product directly to the retailer, bypassing the distributor. The retailer will markup the price before selling the product to the customer.

If the retail price of the sensor patch must be $10.00 each, and if the retailer expects 30% profit margin, then the retailer must buy the sensor patch from the manufacturer for $7.00 each.

The maximum possible manufacturing cost to achieve the target retail price is calculated in column 3 of Table 42 for five different manufacturer profit margins.

3. Direct to Customer

The manufacturer will sell the product directly to the customer, bypassing both the distributor and the retailer.

The maximum possible manufacturing cost to achieve the target retail price is calculated in column 4 of Table 42 for five different manufacturer profit margins.

Table 42: Manufacturer Profit Margin and Associated Manufacturing Cost

Desired Profit Margin	Maximum Possible Manufacturing Cost to Achieve $10.00 Retail Price			
	Direct to Distributor	Direct to Store	Direct to Customer	
10%	$ 4.41	$ 6.30	$9.00	
15%	$ 4.17	$ 5.95	$8.50	
20%	$ 3.92	$ 5.60	$8.00	
25%	$ 3.68	$ 5.25	$7.50	
30%	$ 3.43	$ 4.90	$7.00	

Lump Sum Payment and Royalty Calculations

When a licensor licenses intellectual property rights to a licensee, three main options for reimbursement exist (World Intellectual Property Organization, 2015):

1. Lump Sum Payments

The licensee pays the licensor in lump sums, usually at the very beginning of the agreement or at some later date. Depending on the terms in the agreement, these payments may be made in installments (World Intellectual Property Organization, 2015).

2. Royalty Payments

The licensee pays the licensor royalties based on per unit sales or on net revenues. The licensing agreement may establish a cap, restricting licensor earnings when sales are exceptional, or a minimum, ensuring licensor income when sales are disappointing. The licensing agreement may also allow the rate to fluctuate, depending on sales and other variables (World Intellectual Property Organization, 2015).

3. Combination of Lump Sum Payments and Royalty Payments

The licensee compensates the licensor via lump sum payments and royalties in accordance with the licensing agreement.

As stated in section 7.4.3.1, the break-even analysis conducted here assumes the licensing agreement calls for royalties only. Both royalties based on revenues and royalties based on profits are assessed.

Royalties based on revenues are defined as the product between the royalty rate and the licensee revenue. The values in Table 43 use the medical products and equipment industry average royalty rate, 6.40% (Zipkin, 2014), and the unit revenue seen by the manufacturer for each case in section 7.4.3.2.

Table 43: Unit Royalties Based on Manufacturer Unit Revenue

Supply Chain Setup					
Direct to Distributor		Direct to Store		Direct to Customer	
Manufacturer Unit Revenue	Licensor Unit Royalties	Manufacturer Unit Revenue	Licensor Unit Royalties	Manufacturer Unit Revenue	Licensor Unit Royalties
$ 4.90	$ 0.31	$ 7.00	$ 0.45	$ 10.00	$ 0.64

Royalties based on profits are defined as the product between the royalty percentage and the licensee profits. The values in Table 44 use the rule of thumb amongst licensing professionals, "which provides that the licensor should receive around one quarter to one third of the benefits accruing to the licensee (World Intellectual Property Organization, 2015), and the unit revenue seen by the manufacturer for each case in section 7.4.3.2. The top value in each Licensor Unit Royalties column corresponds to one quarter of manufacturer profits, and the bottom value corresponds to one third of manufacturer profits.

Table 44: Unit Royalties Based on Manufacturer Unit Profit

	Supply Chain Setup					
	Direct to Distributor		Direct to Store		Direct to Customer	
Manufacturer Profit Margin	Manufacturer Unit Profit	Licensor Unit Royalties	Manufacturer Unit Profit	Licensor Unit Royalties	Manufacturer Unit Profit	Licensor Unit Royalties
10%	$0.49	0.12 0.16	$0.70	0.18 0.23	$1.00	0.25 0.33
15%	$0.74	0.18 0.25	$1.05	0.26 0.35	$1.50	0.38 0.50
20%	$0.98	0.25 0.33	$1.40	0.35 0.47	$2.00	0.50 0.67
25%	$1.23	0.31 0.41	$1.75	0.44 0.58	$2.50	0.63 0.83
30%	$1.47	0.37 0.49	$2.10	0.53 0.70	$3.00	0.75 1.00

Break-Even Analysis

The break-even point occurs where total revenues equal total costs. Total revenues and total costs are defined as:

$$TOTALREVENUE = (UNITREVENUE) * (TOTALUNITSSOLD) \tag{13}$$

$$TOTALCOSTS = (TOTALFIXEDCOSTS) + (UNITVARIABLECOST) * (TOTALUNITSSOLD) \tag{14}$$

Setting Equation 13 equal to Equation 14 and solving for TOTAL UNITS SOLD yields:

$$TOTALUNITSSOLD = \frac{TOTALFIXEDCOSTS}{UNITREVENUE - UNITVARIABLECOST} labeleq : 15 \tag{15}$$

To the licensor of the pressure ulcer prevention system, the numerator in Equation 15 is equivalent to the initial investment in research and development, and the denominator in Equation 15 is equivalent to the unit profit seen by the licensor (i.e. unit royalties). In Table 44, break-even quantities of sensor patches are calculated for each in Table 42 and Table 43.

Table 45: Break-Even Quantities of Sensor Patches

		Supply Chain Setup		
		Direct to Distributor	Direct to Store	Direct to Customer
Manufacturer Profit Margin	Licensor Royalty Rate	Break-Even Quantity	Break-Even Quantity	Break-Even Quantity
	6.40% of revenues	9,566,327	6,696,429	4,687,500
10%	25% of profits	24,489,796	17,142,857	12,000,000
	30% of profits	18,367,347	12,857,143	9,000,000
15%	25% of profits	16,326,531	11,428,571	8,000,000
	30% of profits	12,244,898	8,571,429	6,000,000
20%	25% of profits	12,244,898	8,571,429	6,000,000
	30% of profits	9,183,673	6,428,571	4,500,000
25%	25% of profits	9,795,918	6,857,143	4,800,000
	30% of profits	7,346,939	5,142,857	3,600,000
30%	25% of profits	8,163,265	5,714,286	4,000,000
	30% of profits	6,122,449	4,285,714	3,000,000

Note that the minimum break-even quantity is 3 million units, which can be achieved with a 30% royalty rate on licensee profits when the manufacturer delivers the sensor patches directly to the customer and takes a 30% profit margin. The maximum break-even quantity is 24.5 million units, which occurs with a 25% royalty rate on licensee profits when the product must go through both the distributor and the retailer before it reaches the customer and the manufacturer takes a 10% profit margin.

Return-on-Investment Analysis

Return on investment (ROI) is defined as (Investopedia, n.d.):

$$ROI = \frac{GAINFROMINVESTMENT - COSTOFINVESTMENT}{COSTOFINVESTMENT} labeleq : 16 \quad (16)$$

where GAIN FROM INVESTMENT is equivalent to the product of the unit royalties and the total units sold, and COST OF INVESTMENT is equivalent to the initial investment in research and development. Substituting these variables and solving Equation 15 for total units sold yields:

$$TOTALUNITSSOLD = \frac{(1 + ROI) * COSTOFINVESTMENT}{UNITROYALTIES} labeleq : 17 \quad (17)$$

The quantities calculated in Table 46 are derived with a 10% target ROI and a $3 million initial investment.

Table 46: Target Quantities of Sensor Patches to Achieve 10% ROI

		Supply Chain Setup		
		Direct to Distributor	Direct to Store	Direct to Customer
Manufacturer Profit Margin	Licensor Royalty Rate	Target Quantity	Target Quantity	Target Quantity
	6.40% of revenues	10,522,959	7,366,071	5,156,250
10%	25% of profits	26,938,776	18,857,143	13,200,000
	30% of profits	20,204,082	14,142,857	9,900,000
15%	25% of profits	17,959,184	12,571,429	8,800,000
	30% of profits	13,469,388	9,428,571	6,600,000
20%	25% of profits	13,469,388	9,428,571	6,600,000
	30% of profits	10,102,041	7,071,429	4,950,000
25%	25% of profits	10,775,510	7,542,857	5,280,000
	30% of profits	8,081,633	5,657,143	3,960,000
30%	25% of profits	8,979,592	6,285,714	4,400,000
	30% of profits	6,734,694	4,714,286	3,300,000

Note that the minimum target quantity is 3.3 million units, and the maximum target quantity is 26.9 million units. These occur under the same conditions as the minimum break-even quantity and the maximum break-even quantity, respectively.

7.5 Conclusions

The pressure ulcer prevention system will likely enable medical care facilities to reduce hospital-acquired pressure ulcer rates and save significant sums of money over time. The initial up-front costs associated with base stations, installation, setup, and training, may be high compared to the repeated annual costs associated with sensor patches; however, the savings from prevented pressure ulcers will almost definitely outweigh the costs from system use, suggesting the pressure ulcer prevention system described here will eventually meet high demand in the medical supplies market.

The owners of the intellectual property rights can use the return-on-investment analyses to assist them in finding the right manufacturer and negotiating the right licensing agreement based on how soon they intend to break even. Based on the average royalty rate in the medical products and equipment industry, the owners should expect between 5 million and 10 million sensor patches to be sold before they break even. Considering the size of the market, combined with aging population and increasing demand for affordable and effective pressure ulcer prevention techniques, sensor patch sales should surpass these targets in very little time: Returning to the hospital example presented in section 7.3.3.4, in which approximately 18,000 sensor patches are used each year, and assuming 100 identical hospitals invest in the product in the year the product is launched, 10 million patches could be sold in less than 6 years. The preliminary return-on-investment analyses presented here suggest a promising future for the pressure ulcer prevention system.

8 Conclusions and Recommendations

8.1 Overall

The PUP MQP benefited greatly from combining insights from electrical engineering, biomedical engineering, and business. The team not only developed a working prototype of the pressure ulcer prevention system, but also assessed the value of the product and predicted future return on investment, which reassured the team that the system would one day be much appreciated by its users and reasonably profitable to its creators. The team also practiced a new approach to engineering design and learned both how to define a problem and how to decompose a problem in order to develop a solution that succeeds in achieving its functional requirements.

8.2 Pressure Ulcer Prevention System Design

8.2.1 Summary of Progress and Setbacks

Introducing axiomatic design to the PUP MQP enabled the team to make good progress during the initial design phase. The FR-DP decomposition greatly facilitated the component selection and the schematic drawing. However, the FR-DP decomposition was not CEMEmin when the original schematic was drawn, and neither the size constraints nor the power constraints were understood very well until after most components had been selected and ordered. Thus extraneous and inappropriate components were acquired: The buck-boost converter, which would have been used to maintain a constant supply voltage, was unnecessary because neither the ADC in the microcontroller nor the digital relative humidity and temperature sensor required a constant voltage supply to output consistent and accurate values. The very first resistors and capacitors were ordered based on package size. Once the parts came in, the team realized the selected package size (imperial 0201, metric 0603) was way too small for them to solder on to the boards themselves. To eliminate extraneous components and replace inappropriate parts, the sensor patch had to be redesigned, and the schematic had to be redrawn. These modifications set the team back about one week.

After the microcontroller was programmed to interact with the analog pressure sensor, the team decided to add the analog relative humidity sensor and to delay programming the microcontroller to interact with the digital relative humidity sensor. Since the code for the analog sensor was already written and working, and the code for the digital sensor would have to be written from scratch, the team assumed it would save time with the analog sensor. However, researching various analog relative humidity sensors, selecting the best one, waiting for the order to be delivered, and redesigning the PCB to accommodate the new component set the team back again.

The axiomatic design method came in handy once more, this time as a means to help the team get back on schedule. The objective for the term (to finish MQP) was decomposed into well-defined, manageable tasks, and each task was assigned a due-date and a team member. This decomposition better enabled the team to set weekly goals, distribute work, and track progress.

Late in January, two major changes were made: First, new project objectives were presented, along with new constraints. The flexible PCB would no longer be sized to fit humans and would no longer be required to last 7 days; instead, it would have to be stuck to rats, and it would need to record data for up to 8 hours. Second, the Interlink FSR-402 Short, which had been selected to sense pressure back in September, was confirmed to be too inaccurate and too unpredictable to be used in the pressure ulcer prevention system, so it had to be replaced. The flexible PCB had to be redesigned to meet the new size and shape constraints, and the replacement sensor had to be selected and obtained, which set the team back once more.

8.2.2 Summary of Lessons Learned

Axiomatic design was very useful to the PUP MQP team, especially during the design phase of the project. In the end, the pressure ulcer prevention system and the sensor patches were never poorly designed; the problem these were meant to solve was always poorly defined.

In the beginning, expectations related to power, size, and shape were somewhat vague, so the team assumed certain constraints existed, such as constant voltage supply and smallest possible size. The team incorporated these constraints into the initial design without questioning them and selected components before completing the original FR-DP decomposition. Thus the initial design both included extraneous components and called for components that could not be used.

Similar mistakes resulted in similar setbacks, which might have been avoided if the team had more frequently discussed design expectations, requirements, and constraints with the project advisors and completed a CEMEmin decomposition before getting the initial design approved and ordering parts.

The setbacks experienced by the team enabled them to realize how important problem definition was to the success of the project. Throughout the PUP MQP, neither the scope nor the constraints were ever fully defined, and both continually evolved. The team thus repeatedly updated the project goals and the design. These iterations, though necessary to achieve all functional requirements and meet all constraints, resulted in lost time and late delivery.

8.2.3 Conclusions and Recommendations

The axiomatic design method really should be used in future projects sponsored by the ECE department and the BME department to guide students in designing systems to meet constraints and achieve functional requirements. Before the FR-DP decomposition and the design matrix are deemed complete, project teams would be wise make sure the constraints and the requirements associated with the design problem have been, first, as fully defined as possible and, second, fully met. Project teams should also make sure the decomposition is CEMEmin. Nothing can be overlooked, or else the design may fail to meet the top-level functional requirement, and non-productive iterations may be necessary, as in the PUP MQP.

Future designs of the patch should aim to have the shape mimic that of ECG electrodes. Such a design minimizes the area of skin covered with adhesive for 7 days. The electrode-like shape is also familiar to the medical community, which increases the ease of use of the product and reduces the likelihood of human error when applying the patch. The current patch looks similar to an adhesive bandage and has the pressure sensor at one end. Those who are unfamiliar with the product may apply the patch like an adhesive bandage (i.e. placing the middle of the patch over the at-risk area) and cause the sensors, particularly the pressure sensor, to monitor the wrong areas of the body.

The method of sensing pressure should also be modified for the final version of the patch. It would be beneficial to have an array of pressure sensors covering a somewhat larger area instead of a single sensor pinpointing a small location. Having an array would likely reduce the repeatability error of the FSR-402 Short sensor, as well.

8.3 Financial Analysis

Simple financial analyses, such as net present value analysis and return-on-investment analysis, should be used in future projects at WPI whenever the objective of the project team is to develop a new product or a new process. These analyses enable designers, investors, and customers alike to assess how much a product or a process might be worth to its buyers and to its sellers once it enters the market. These analyses also enable designers to determine whether or not designs are worth pursuing; thus unprofitable designs can be scrapped long before too

much time, energy, and money are invested in them, and worthwhile designs, like the pressure ulcer prevention system, can be pursued with even greater urgency and passion.

Appendix A - Value Analysis Details

Sensors, microcontrollers, antennas, and power sources were ranked according to the following 1-5 systems, in which 1 was lowest and 5 was highest, and the product with the greatest weighted total was the considered best.

Pressure Sensor Comparison

NOTE: The value analysis on the pressure sensors was conducted before the limitations of the Interlink FSR-402 Short were known and before the Tangio TPE-502 was discovered. Thus the Tangio sensor is not included.

Pressure Sensors														
	Cost	Height	Area	Size	V	I	Power Required	Comp	Exp	Familiarity	Availability	Range and Repeatability	WEIGHTED TOTAL	RANK
FlexiForce A401	2	5	2	3.5	5	3	4	5	5	5	5	4	1810	
FlexiForce A301	3	5	3	4	5	3	4	5	5	5	5	4	1960	
FlexiForce A201	3	5	3	4	5	3	4	5	5	5	5	4	1960	
FlexiForce A101	4	5	1	3	5	3	4	5	5	5	5	4	1960	
FSR 400	5	5	1	3	5	3	4	5	5	5	5	5	2155	#2 choice
FSR 400 Short	4	5	1	3	5	3	4	5	5	5	5	5	2055	
FSR 402	4	5	3	4	5	3	4	5	5	5	5	4	2060	#3 choice
FSR 402 Short	4	5	5	5	5	3	4	5	5	5	5	4	2160	#1 choice
FSR 406	4	5	1	3	5	3	4	5	5	5	5	3	1865	
FSLP - 34 - 00022	3	5	3	4	5	3	4	5	4	4.5	5	3	1832.5	
LPS25HB	5	5	1	3	4	5	4.5	3	3	3	5	4	1977.5	
	Cost			Size			Power Required			Familiarity	Availability	Range and Repeatability		
WEIGHTS	100			100			95			65	35	95		
NOTES	1=expensive 5=cheap			size =avg(height+area) 1=big 5=small			P =avg(V+I) (typ values) 1=high 5=low			familiarity =avg(compatibility + experience) 1=low 5=high	1=low 5=high	1=not in range, low repeatabiltiy 5=in range, high repeatability		

Relative Humidity Sensor Comparison

RELATIVE HUMIDITY SENSOR CRITERA		5	4	3	2	1
Cost		≤ $1	≤ $2	≤ $3	≤ $4	≤ $5+
Size	Height	≤ 0.8 mm	≤ 0.9 mm	≤ 1.0 mm	≤ 1.5 mm	≤ 2mm +
	Area	≤ 1 mm^2	≤ 4 mm^2	≤ 9 mm^2	≤16 mm^2	≤25 mm^2
Power	V (typ)	≤ 1.5V	≤ 2.5V	≤ 3.5V	≤ 4.5V	≤ 5.5V +
	I (typ on)	≤ 1uA	≤ 250uA	≤ 500 uA	≤ 750 uA	≤ 1mA +
Accuracy		≤ +/- 1%	≤ +/- 2%	≤ +/- 3%	≤ +/- 4%	≤ +/- 5%
Familiarity	Compatibility	Output is analog voltage		Output is SPI or I2C		Other
	Experience	Used previously	Manufacturer and product known	Product known	Manufacturer known	Neither known
Availability		No wait time, many available	No wait time, few available	Wait time is < 1 week	Wait time is 1-2 weeks	Wait time is > 2 weeks
Bonus	Temperature sensor accuracy	≤ +/- 0.1°C	≤ +/- 0.2°C	≤ +/- 0.3°C	≤ +/- 0.4°C	≤ +/- 0.5°C or no bonus

RH Sensors															
	Cost	Height	Area	Size	V	I	Power Required	Accuracy	Comp	Exp	Familiarity	Availability	Bonus	WEIGHTED TOTAL	RANK
Honeywell HIH5030	1	2	1	1.5	3	4	3.5	3	5	5	5	5	1	1327.5	
Honeywell HIH7130	1	2	1	1.5	3	2	2.5	3	3	2	2.5	2	1	965	
Honeywell HIHB130	1	1	1	1	3	2	2.5	4	3	2	2.5	1	1	960	
TE MEAS HTU20D	2	4	3	3.5	3	3	3	1	3	1	2	5	3	1235	
TE MEAS HTU21D	1	4	3	3.5	3	3	3	3	3	1	2	5	3	1295	
Silicon Labs Si7034-A10-IM	3	5	4	4.5	4	3	3.5	3	3	2	2.5	1	3	1535	
Silicon Labs Si7006-A20-IM	4	2	3	2.5	3	4	3.5	2	3	2	2.5	5	1	1485	
Silicon Labs Si7013-A20-GM	3	5	3	4	3	4	3.5	4	3	2	2.5	4	3	1670	
Silicon Labs Si7020-A20-GM	3	5	3	4	3	4	3.5	3	3	2	2.5	5	3	1625	
Silicon Labs Si7021-A20-GM	3	5	3	4	3	4	3.5	4	3	2	2.5	5	3	1705	
Sensirion SHTW2	4	5	5	5	4	3	3.5	3	3	1	2	5	2	1787.5	#2
Sensirion SHTC1	4	5	4	4.5	4	3	3.5	3	3	1	2	5	3	1742.5	
Texas Instruments HDC1010	4	5	4	4.5	3	4	3.5	4	3	2	2.5	4	4	1825	#1
Texas Instruments HDC1080	4	5	3	4	3	4	3.5	4	3	2	2.5	4	4	1775	#3
	Cost			Size			Power Required	Accuracy			Familiarity	Availability	Bonus		
WEIGHTS	100			100			95	80			65	35	5		
NOTES	1=expensive 5=cheap			size =avg(height+area) 1=big 5=small			P =avg(V+I) (typ values) 1=high 5=low	(typ values) 1=low 5=high			familiarity =avg(compatibility + experience) 1=low 5=high	1=low 5=high	1=no extra benefit 5=huge extra benefit		

Temperature Sensor Comparison

TEMPERATURE SENSOR CRITERIA		5	4	3	2	1
Cost		≤ $0.10	≤ $0.50	≤ $1	≤ $2	≤ $3+
Size	Height	≤ 0.8 mm	≤ 0.9 mm	≤ 1.0 mm	≤ 1.5 mm	≤ 2mm +
	Area	≤ 1 mm^2	≤ 4 mm^2	≤ 9 mm^2	≤16 mm^2	≤25 mm^2
Power	V (typ)	≤ 1.5V	≤ 2.5V	≤ 3.5V	≤ 4.5V	≤ 5.5V +
	I (typ on)	≤ 1uA	≤ 250uA	≤ 500 uA	≤ 750 uA	≤ 1mA +
Accuracy		≤ +/- 0.1°C	≤ +/- 0.2°C	≤ +/- 0.3°C	≤ +/- 0.4°C	≤ +/- 0.5°C
Familiarity	Compatibility	Output is analog voltage		Output is SPI or I2C		Other
	Experience	Used previously	Manufacturer and product known	Product known	Manufacturer known	Neither known
Availability		No wait time, many available	No wait time, few available	Wait time is < 1 week	Wait time is 1-2 weeks	Wait time is > 2 weeks
Bonus	Relative humidity sensor accuracy	≤ +/- 1%	≤ +/- 2%	≤ +/- 3%	≤ +/- 4%	≤ +/- 5% or no bonus

T Sensors

	Cost	Height	Area	Size	V	I	Power Required	Accuracy	Comp	Exp	Familiarity	Availability	Bonus	WEIGHTED TOTAL	RANK
Murata NCP15XH103D03RC	4	5	5	5	5	1	3	4	5	5	5	5	1	2010	#2
Murata NCP15XH103E03RC	5	5	5	5	5	1	3	2	5	5	5	5	1	1950	#3
Murata NCP15XH103F03RC	5	5	5	5	5	1	3	3	5	5	5	5	1	2030	#1
Murata NCP15XH103J03RC	5	5	5	5	5	1	3	1	5	5	5	5	1	1870	
Maxim MAX6612	4	5	3	4	3	4	3.5	1	5	5	5	5	1	1717.5	
Silicon Labs Si7051-A20-IM	2	5	3	4	3	4	3.5	5	3	2	2.5	5	1	1675	
LMT70YFQT	2	5	5	5	3	4	3.5	4	5	2	3.5	5	1	1760	
Honeywell HIH7130	1	2	1	1.5	3	2	2.5	1	3	2	2.5	2	3	815	
Honeywell HIH8130	1	1	1	1	3	2	2.5	1	3	2	2.5	1	4	735	
TE MEAS HTU20D	1	4	3	3.5	3	3	3	3	3	1	2	5	1	1285	
TE MEAS HTU21D	1	4	3	3.5	3	3	3	3	3	1	2	5	3	1295	
Silicon Labs Si7034-A10-IM	1	5	4	4.5	4	3	3.5	3	3	2	2.5	1	3	1335	
Silicon Labs Si7006-A20-IM	2	2	3	2.5	3	4	3.5	1	3	2	2.5	5	2	1210	
Silicon Labs Si7013-A20-GM	1	5	3	4	3	4	3.5	3	3	2	2.5	4	4	1395	
Silicon Labs Si7020-A20-GM	1	5	3	4	3	4	3.5	3	3	2	2.5	5	3	1425	
Silicon Labs Si7021-A20-GM	1	5	3	4	3	4	3.5	3	3	2	2.5	5	4	1430	
Sensirion SHTW2	2	5	5	5	4	3	3.5	2	3	1	2	5	3	1512.5	
Sensirion SHTC1	2	5	4	4.5	4	3	3.5	3	3	1	2	5	3	1542.5	
Texas Instruments HDC1010	2	5	4	4.5	3	4	3.5	4	3	2	2.5	4	4	1625	
Texas Instruments HDC1080	2	5	3	4	3	4	3.5	4	3	2	2.5	4	4	1575	

	Cost			Size			Power Required	Accuracy			Familiarity	Availability	Bonus		
WEIGHTS	100			100			95	80			65	35	5		
NOTES	1=expensive 5=cheap			size =avg(height+area) 1=big 5=small			P =avg(V+I) (typ values) 1=high 5=low	(typ values) 1=low 5=high			familiarity =avg(compatibility + experience) 1=low 5=high	1=low 5=high	1=no extra benefit 5=huge extra benefit		

Microcontroller and Antenna Comparison

Microcontrollers														
	Cost	Height	Area	Size	V	I	Power Required	Accuracy	Comp	Exp	Familiarity	Availability	Bonus	WEIGHTED TOTAL	RANK
CC430F5137	5	2	1	1.5	4	1	2.5	5	1	5	3	5	1	1662.5	
CC1310	5	3	4	3.5	4	3	3.5	5	1	4	2.5	1	1	1785	
CC2640	5	3	4	3.5	4	4	4	5	1	4	2.5	5	1	1972.5	2
CC2650MODA	4	3	5	4	4	4	4	5	5	4	4.5	3	5	2002.5	1
RFD22301	1	1	4	2.5	2	1	1.5	1	5	3	4	5	1	1012.5	
nRF9E5	5	4	2	3	3	1	2	1	1	2	1.5	1	1	1207.5	
nRF51822	5	4	2	3	5	4	4.5	5	1	2	1.5	1	1	1785	
ATA8743	4	0	0	0	3	2	2.5	0	1	1	1	5	1	882.5	
ATBTLC1000	4	5	5	5	4	5	4.5	3	1	1	1	5	1	1812.5	3
ATSAMB11	4	5	2	3.5	1	5	3	3	1	1	1	5	1	1520	
ADUCRF101	4	0	2	1	2	1	1.5	5	1	1	1	1	1	1147.5	
														0	
	Cost			Size			Power Required	Accuracy			Familiarity	Availability	Bonus		
WEIGHTS	100			100			95	80			65	35	5		
NOTES	1=expensive 5=cheap			size =avg(height+area) e.g. 1=big 5=small			ρ =avg(V+I) (typ values) 1=high 5=low	(typ values) 1=low 5=high			familiarity =avg(compatibility + experience) 1=low 5=high	1=low 5=high	1=no extra benefit 5=huge extra benefit		

Antennas														
	Cost	Height	Area	Size	V	I	Power Required	Accuracy	Comp	Exp	Familiarity	Availability	Bonus	WEIGHTED TOTAL	RANK
2450AT07A0100T	5	5	5	5	0	0	0	5	0	0	0	5	0	1575	1
SRCW0004	5	4	5	4.5	0	0	0	5	0	0	0	3	0	1455	2
2450AT42A100E	5	5	5	5	0	0	0	5	0	0	0	5	0	1575	1
W3008C	4	2	3	2.5	0	0	0	5	0	0	0	5	0	1225	
0915AT43A0026E	5	3	1	2	0	0	0	1	0	0	0	1	0	815	2
W3084	5	1	3	2	0	0	0	5	0	0	0	1	0	1135	1

Power Source Comparison

POWER SOURCE CRITERIA		5	4	3	2	1
Cost		≤ $0.10	≤ $0.50	≤ $1	≤ $2	≤ $3+
Size	Height	≤ 0.8 mm	≤ 0.9 mm	≤ 1.0 mm	≤ 1.5 mm	≤ 2mm +
	Area	≤ 40mm^2	≤ 160mm^2	≤ 650mm^2	≤ 1450mm^2	≤ 2500mm^2
Power	V (nominal)	≥ 3.5V	≥ 3.0V	≥ 2.5V	≥ 2.0V	≥ 1.5V
	I (max drain)	≥ 11 mA	≥ 9 mA	≥ 7 mA	≥ 5 mA	≥ 3 mA
Capacity		≥ 35 mAh	≥ 30 mAh	≥ 25 mAh	≥ 20 mAh	≥ 15 mAh
Availability		No wait time, many available	No wait time, few available	Wait time is < 1 week	Wait time is 1-2 weeks	Wait time is > 2 weeks
Bonus	Minimum number required	1		2		3+ or no bonus
	Flexible	Very		Somewhat		Not at all

Power Options														
Manufacturer	Product	Cost	Height	Area	Size	V	I	Power Output	Capacity	Availability	Flex	Min#	Bonus	WEIGHTED TOTAL	RANK
Enfucell	Reg 1.5V	1	5	1	3	1	4	2.5	5	2	5	2	3.5	1160	
Enfucell	Reg 1.5V Plus	1	5	1	3	1	5	3	5	2	5	2	3.5	1207.5	
Enfucell	Mini 1.5V Plus	1	5	1	3	1	3	2	1	2	5	2	3.5	792.5	
Enfucell	Reg 3.0V Plus	1	5	1	3	4	3	3.5	1	2	5	5	5	957.5	
VARTA Microbattery	Lithium Button CR1616	3	1	3	2	4	3	3.5	5	5	1	5	3	1452.5	3rd
VARTA Microbattery	Lithium Button CR1620	4	1	3	2	4	3	3.5	5	5	1	5	3	1552.5	2nd
VARTA Microbattery	Lithium Button CR2016	4	1	3	2	4	4	4	5	5	1	5	3	1600	1st
SEIZAIKEN	Silver Oxide SR920W UCAR# 370	1	1	4	2.5	1	4	2.5	5	5	1	2	1.5	1185	
SEIZAIKEN	Silver Oxide SR927W UCAR# 399	2	1	4	2.5	1	4	2.5	5	5	1	2	1.5	1285	
SEIZAIKEN	Silver Oxide SR1120W UCAR# 391	2	1	4	2.5	1	5	3	5	5	1	2	1.5	1382.5	
STMicroelectronics	EnFilm	1	5	3	4	5	4	4.5	1	4	5	1	3	1192.5	
PD Battery	Lithium Polymer PDCP044040	1	5	1	3	4	4	4	5	2	5	5	5	1325	
PD Battery	Lithium Polymer PDCP044560	1	5	1	3	4	5	4.5	5	2	5	5	5	1372.5	4th
PD Battery	Lithium Polymer PDCP053050	1	5	1	3	4	5	4.5	5	2	5	5	5	1372.5	4th
PD Battery	Lithium Polymer PDCP073545	1	5	1	3	4	5	4.5	5	2	4	5	4.5	1365	
PD Battery	Lithium Polymer PDCP0101830	1	3	3	3	4	5	4.5	5	2	3	5	4	1357.5	
Bright Volt	Rexion Thin Film Lithium BV-542229-25	1	5	2	3.5	4	1	2.5	3	1	5	5	5	1057.5	
Bright Volt	Rexion Thin Film Lithium BV-454523-25	1	5	2	3.5	4	1	2.5	3	1	5	5	5	1057.5	
Bright Volt	Rexion Thin Film Lithium BV-454523-35	1	5	2	3.5	4	1	2.5	5	1	5	5	5	1197.5	
GMB Power	CP452345	1	5	2	3.5	4	4	4	4	2	3	5	4	1280	
GMB Power	CP142828	1	2	2	2	4	5	4.5	5	2	3	5	4	1257.5	
GMB Power	CP153030	1	2	2	2	4	5	4.5	5	2	3	5	4	1257.5	
		Cost			Size			Power Output	Capacity	Availability			Bonus		
	WEIGHTS	100			100			95	80	35			15		
	NOTES	1=expensive 5=cheap			size =avg(height+area) 1=big 5=small			P=avg(V+I) (typ values) 1=high 5=low	(typ values) 1=low 5=high	1=low 5=high			B=avg(flexibility + min number)		

Appendix B - Interlink FSR-402 Short Pressure Sensor Test Data

Recorded Data

DATE	FORCE	TIME (s)									
		30	60	90	120	150	180	210	240	270	300
11/30/16	190.06 g	1.64 V	1.64 V	1.68 V	1.72 V	1.72 V	1.72 V	1.72 V	1.72 V	1.72 V	1.72 V
	284.12 g	1.92 V	2.00 V	2.00 V	2.00 V	2.00 V	2.00 V	2.00 V	2.00 V	2.00 V	2.00 V
	386.18 g	2.28 V	2.32 V	2.32 V	2.36 V	2.36 V	2.36 V	2.36 V	2.36 V	2.36 V	2.36 V
	488.24 g	2.40 V	2.40 V	2.44 V	2.44 V	2.44 V	2.44 V	2.44 V	2.44 V	2.44 V	2.44 V
	590.30 g	2.56 V	2.56 V	2.56 V	2.56 V	2.56 V	2.56 V	2.56 V	2.56 V	2.56 V	2.56 V
12/01/16	102.06 g	.995 V	1.02 V	1.05 V	1.07 V	1.08 V	1.08 V	1.09 V	1.10 V	1.10 V	1.10 V
	204.12 g	1.44 V	1.47 V	1.48 V	1.48 V	1.48 V	1.49 V	1.49 V	1.49 V	1.49 V	1.49 V
	306.18 g	2.20 V	2.21 V	2.22 V	2.23 V	2.23 V	2.24 V	2.24 V	2.24 V	2.24 V	2.24 V
	408.24 g	2.40 V	2.40 V	2.40 V	2.40 V	2.40 V	2.40 V	2.40 V	2.40 V	2.40 V	2.40 V
12/03/16	51.030 g	.852 V	.862 V	.866 V	.878 V	.882 V	.886 V	.903 V	.904 V	.909 V	.910 V
	53.298 g	.921 V	.943 V	.959 V	.959 V	.959 V	.960 V	.960 V	.960 V	.960 V	.961 V
	56.700 g	.995 V	1.02 V	1.03 V	1.03 V	1.04 V	1.04 V	1.04 V	1.04 V	1.04 V	1.04 V
	58.968 g	.959 V	.960 V	.962 V	.964 V	.968 V	.967 V	.973 V	.987 V	.989 V	.992 V
	62.370 g	.959 V	.962 V	.967 V	.990 V	.992 V	.999 V	1.01 V	1.01 V	1.03 V	1.03 V
	64.630 g	.921 V	.935 V	.958 V	.958 V	.960 V	.961 V	.963 V	.970 V	.977 V	.989 V
	68.040 g	1.01 V	1.04 V	1.04 V	1.05 V	1.07 V	1.08 V	1.08 V	1.08 V	1.08 V	1.08 V
	70.308 g	1.00 V	1.02 V	1.04 V	1.06 V	1.07 V	1.07 V	1.08 V	1.08 V	1.08 V	1.08 V
	72.576 g	1.09 V	1.11 V	1.12 V	1.12 V	1.14 V	1.15 V	1.16 V	1.16 V	1.18 V	1.18 V
	85.050 g	1.09 V	1.13 V	1.15 V	1.15 V	1.16 V	1.16 V	1.16 V	1.16 V	1.17 V	1.17 V
	204.12 g	1.85 V	1.88 V	1.88 V	1.89 V	1.90 V	1.91 V	1.91 V	1.92 V	1.92 V	1.92 V
12/06/16	119.07 g	1.84 V	1.86 V	1.87 V	1.88 V	1.88 V	1.90 V	1.91 V	1.92 V	1.92 V	1.92 V
	158.76 g	1.95 V	1.97 V	1.99 V	2.00 V	2.00 V	2.00 V	2.00 V	2.00 V	2.00 V	2.00 V
	181.44 g	2.15 V	2.16 V	2.16 V	2.17 V	2.17 V	2.18 V	2.18 V	2.18 V	2.18 V	2.19 V
1/25/17	51.030 g	.412V	.424V	.451V	.469V	.476V	.483V	.489V	.495V	.510V	.506V

	53.298 g	.555V	.572V	.586V	.594V	.601V	.602V	.605V	.611V	.612V	.615V
	56.700 g	.677V	.691V	.714V	.729V	.745V	.747V	.770V	.780V	.746V	.759V
	58.968 g	.771V	.780V	.793V	.800V	.805V	.803V	.811V	.809V	.817V	.815V
	62.37 g	.758V	.793V	.814V	.827V	.837V	.844V	.847V	.847V	.846V	.847V
	64.638 g	.886V	.899V	.926V	.948V	.981V	.999V	1.01V	1.03V	1.04V	1.04V
	68.040 g	.883V	.918V	.941V	.959V	.961V	.968V	.980V	.974V	.985V	.984V
	70.308 g	1.08V	1.10V	1.12V	1.13V	1.13V	1.14V	1.14V	1.14V	1.15V	1.17V
	72.576 g	.969V	.981V	.997V	1.02V	1.02V	1.04V	1.05V	1.06V	1.06v	1.06V
1/31/17	19.278 g	.094V	.140V	.147V	.157V	.171V	.144V	.158V	.148V	.166V	.162V
	39.690 g	.385V	.397V	.390V	.404V	.398V	.417V	.407V	.380V	.390V	.386V
	49.896 g	.869V	.871V	.864V	.864V	.876V	.860V	.865V	.867V	.877V	.871V
	52.164 g	.753V	.747V	.769V	.772V	.768V	.764V	.769V	.767V	.769V	.774V
	54.432 g	.859V	.853V	.841V	.851V	.876V	.860V	.865V	.863V	.863V	.866V
	56.700 g	.528V	.540V	.515V	.527V	.534V	.522V	.531V	.532V	.534V	.532V
	58.968 g	.637V	.637V	.643V	.635V	.637V	.630V	.632V	.636V	.640V	.638V
	61.236 g	.564V	.566V	.565V	.578V	.571V	.571V	.571V	.564V	.567V	.572V
	79.380 g	.905V	.905V	.891V	.887V	.877V	.875V	.883V	.886V	.884V	.880V
	119.07 g	1.39V	1.40V	1.42V	1.41V	1.41V	1.42V	1.42V	1.43V	1.43V	1.43V
	161.028g	1.75V	1.74V	1.79V	1.79V	1.79V	1.79V	1.79V	1.80V	1.81V	1.81V

	19.278 g	.132V	.061V	.128V	.037V	.057V	.078V	.086V	.080V	.082V	.077V
	39.690 g	.564V	.551V	.526V	.515V	.508V	.507V	.500V	.506V	.495V	.488V
	49.896 g	.588V	.579V	.563V	.576V	.562V	.576V	.579V	.566V	.567V	.583V
	52.164 g	.766V	.777V	.775V	.771V	.773V	.782V	.777V	.777V	.776V	.779V
	54.432 g	.802V	.796V	.789V	.785V	.790V	.780V	.786V	.786V	.781V	.779V
2/1/17	56.700 g	1.05V	1.04V	1.04V	1.04V	1.04V	1.05V	1.05V	1.04V	1.05V	1.06V
	58.968 g	.945V	.953V	.954V	.945V	.945V	.951V	.950V	.958V	.962V	.965V
	61.236 g	.734V	.745V	.742V	.754V	.742V	.743V	.736V	.776V	.774V	.767V
	79.380 g	1.24V	1.25V	1.25V	1.24V	1.25V	1.24V	1.25V	1.25V	1.25V	1.25V
	119.07 g	1.59V	1.60V	1.62V	1.62V	1.63V	1.64V	1.64V	1.63V	1.64V	1.64V
	161.028g	1.97V	1.99V	1.99V	1.99V	2.00V	2.00V	1.79V	2.01V	2.01V	2.00V

MATLAB Code Used to Process Recorded Data

```
Function File: maphex2resistance.m
function r = maphex2resistance(hex_array,fixed,v_supply)
%converts MCU output in hex to resistance in ohms
%hex_array = array of hex values, each of which represents one ADC voltage
% output value in mV
%fixed = resistance of fixed resistor in voltage divider in ohms
%v_supply = supply voltage to voltage divider in V
r = zeros(1,length(hex_array));
for ii=1:length(hex_array)
%(1)convert hex value to voltage value
v = hex2dec(hex_array(ii,:))/1000;
%(2)converttage value to resistance value
r(ii) = fixed*(v_supply - v)/v;
end
Main File: Interlink_FSR_402_short_calibration.m
close all;
%% Constants
vs = 3.3; % volts
r_fixed = 10e3; %ohms
```

```
grams2newtons = 1/101.97162; %N/g
pressure2mmHg = 1/133.32239; %mmHg / N/m^2
sensing_area = pi*(12.7e-3/2)^2; %m^2
F2P = (grams2newtons/sensing_area)*pressure2mmHg;
%% Actual Weights and Pressures
weights = [0,19.278,39.69,49.896,52.164,54.432,56.7,58.968,61.236,79.38,11
pressures = weights*F2P; %mmHg
%% Recorded Values
time = 0:30:300; %seconds
f00_31Jan17 = ['0004';'0004';'0006']; %hex value -> voltage in mV
f01_31Jan17 = ['005e';'008c';'0093';'009d';'00ab';'0090';'009e';'0094';'00a
f02_31Jan17 = ['0181';'018d';'0186';'0194';'018e';'01a1';'0197';'017c';'018
f03_31Jan17 = ['0365';'0367';'0360';'0360';'036c';'036d';'0367';'0363';'036
f04_31Jan17 = ['02f1';'02eb';'0301';'0304';'0300';'02fc';'0301';'02ff';'030
f05_31Jan17 = ['035b';'0355';'0349';'0353';'036c';'035c';'0361';'035f';'035
f06_31Jan17 = ['0210';'021c';'0203';'020f';'0216';'020a';'0213';'0214';'021
f07_31Jan17 = ['027d';'027d';'0283';'027b';'027d';'0276';'0278';'027c';'028
f08_31Jan17 = ['0234';'0236';'0235';'0242';'023b';'023b';'023b';'0234';'023
f09_31Jan17 = ['0389';'0389';'037b';'0377';'036d';'036b';'0373';'0376';'037
f10_31Jan17 = ['0570';'0573';'0587';'0586';'0585';'0589';'058b';'0597';'059
f11_31Jan17 = ['06d1';'06d0';'0702';'06fd';'06fc';'0702';'0701';'0709';'070
f00_01Feb17 = ['0005';'0002'];
f01_01Feb17 = ['0084';'003d';'0080';'0025';'0039';'004e';'0056';'0050';'005
f02_01Feb17 = ['0234';'0227';'020e';'0203';'01fc';'01fb';'01f4';'01fa';'01e
f03_01Feb17 = ['024c';'0243';'0233';'0240';'0232';'0240';'0243';'0236';'023
f04_01Feb17 = ['02fe';'0309';'0307';'0303';'0305';'030e';'0309';'0309';'030
f05_01Feb17 = ['0322';'031c';'0315';'0311';'0316';'030c';'0312';'0312';'030
f06_01Feb17 = ['041e';'0411';'0413';'0413';'040b';'041b';'0415';'0414';'041
f07_01Feb17 = ['03b1';'03b9';'03ba';'03b1';'03b1';'03b7';'03b6';'03be';'03c
f08_01Feb17 = ['02de';'02e9';'02e6';'02f2';'02e6';'02e7';'02e0';'0308';'030
f09_01Feb17 = ['04d9';'04e1';'04e3';'04dc';'04e0';'04d6';'04dd';'04df';'04e
f10_01Feb17 = ['0634';'063c';'0650';'064f';'065a';'0664';'0665';'0661';'066
f11_01Feb17 = ['07b0';'07c1';'07c4';'07c8';'07d3';'07d1';'0700';'07d5';'07c
f00_01Feb17_redo = ['0005';'0002'];
f01_01Feb17_redo = ['0084';'003d';'0080';'0025';'0039';'004e';'0056';'0050'
f02_01Feb17_redo = ['0234';'0227';'020e';'0203';'01fc';'01fb';'01f4';'01fa'
f03_01Feb17_redo = ['024c';'0243';'0233';'0240';'0232';'0240';'0243';'0236
f04_01Feb17_redo = ['02fe';'0309';'0307';'0303';'0305';'030e';'0309';'0309'
f05_01Feb17_redo = ['0322';'031c';'0315';'0311';'0316';'030c';'0312';'0312'
f06_01Feb17_redo = ['041e';'0411';'0413';'0413';'040b';'041b';'0415';'0414'
f07_01Feb17_redo = ['0303';'030e';'030e';'0313';'0312';'030c';'0313';'0317'
f08_01Feb17_redo = ['038c';'0386';'0386';'037d';'0378';'0390';'0387';'0391'
f09_01Feb17_redo = ['04d9';'04e1';'04e3';'04dc';'04e0';'04d6';'04dd';'04df'
f10_01Feb17_redo = ['0634';'063c';'0650';'064f';'065a';'0664';'0665';'0661
f11_01Feb17_redo = ['07b0';'07c1';'07c4';'07c8';'07d3';'07d1';'0700';'07d5'
%% Resistance Values
R_31Jan17 = [maphex2resistance(f01_31Jan17,r_fixed,vs);...
maphex2resistance(f02_31Jan17,r_fixed,vs);...
```

```
maphex2resistance(f03_31Jan17,r_fixed,vs);...
maphex2resistance(f04_31Jan17,r_fixed,vs);...
maphex2resistance(f05_31Jan17,r_fixed,vs);...
maphex2resistance(f06_31Jan17,r_fixed,vs);...
maphex2resistance(f07_31Jan17,r_fixed,vs);...
maphex2resistance(f08_31Jan17,r_fixed,vs);...
maphex2resistance(f09_31Jan17,r_fixed,vs);...
maphex2resistance(f10_31Jan17,r_fixed,vs);...
maphex2resistance(f11_31Jan17,r_fixed,vs);...
];
R_01Feb17 = [maphex2resistance(f01_01Feb17,r_fixed,vs);...
maphex2resistance(f02_01Feb17,r_fixed,vs);...
maphex2resistance(f03_01Feb17,r_fixed,vs);...
maphex2resistance(f04_01Feb17,r_fixed,vs);...
maphex2resistance(f05_01Feb17,r_fixed,vs);...
maphex2resistance(f06_01Feb17,r_fixed,vs);...
maphex2resistance(f07_01Feb17,r_fixed,vs);...
maphex2resistance(f08_01Feb17,r_fixed,vs);...
maphex2resistance(f09_01Feb17,r_fixed,vs);...
maphex2resistance(f10_01Feb17,r_fixed,vs);...
maphex2resistance(f11_01Feb17,r_fixed,vs);...
];
R_01Feb17_redo = [maphex2resistance(f01_01Feb17_redo,r_fixed,vs);...
maphex2resistance(f02_01Feb17_redo,r_fixed,vs);...
maphex2resistance(f03_01Feb17_redo,r_fixed,vs);...
maphex2resistance(f04_01Feb17_redo,r_fixed,vs);...
maphex2resistance(f05_01Feb17_redo,r_fixed,vs);...
maphex2resistance(f06_01Feb17_redo,r_fixed,vs);...
maphex2resistance(f07_01Feb17_redo,r_fixed,vs);...
maphex2resistance(f08_01Feb17_redo,r_fixed,vs);...
maphex2resistance(f09_01Feb17_redo,r_fixed,vs);...
maphex2resistance(f10_01Feb17_redo,r_fixed,vs);...
maphex2resistance(f11_01Feb17_redo,r_fixed,vs);...
];
%% P_NOM and R_NOM Values
idx_nom = find((pressures > 29) & (pressures < 31));
p_nom = pressures(idx_nom); %about 30 mmHg
r_nom = mean([mean(R_31Jan17(:,idx_nom+1)),mean(R_01Feb17(:,idx_nom+1)),mea
%% x Values
log_R_31Jan17 = log10(R_31Jan17/r_nom);
log_R_01Feb17 = log10(R_01Feb17/r_nom);
log_R_01Feb17_redo = log10(R_01Feb17_redo/r_nom);
x = (mean([mean(log_R_31Jan17(end-1,:)),mean(log_R_01Feb17(end-1,:))]) ...
- mean([mean(log_R_31Jan17(2,:)),mean(log_R_01Feb17(2,:))])) ...
/ (log10(pressures(end-1)/p_nom) - log10(pressures(3)/p_nom));
figure(1); hold on; %normalized log-log plot, resistance versus pressure
for ii = 1:length(time)-1
plot(log10(pressures(2:end)/p_nom),log_R_31Jan17(:,ii),'bo');
```

```
plot(log10(pressures(2:end)/p_nom),log_R_01Feb17(:,ii),'bo');
plot(log10(pressures(2:end)/p_nom),log_R_01Feb17_redo(:,ii),'bo');
end
plot(log10(pressures(end-1)/p_nom),mean([mean(log_R_31Jan17(end-1,:)),mean(
plot(log10(pressures(3)/p_nom),mean([mean(log_R_31Jan17(2,:)),mean(log_R_01
title('Log-Log Plot: Normalized Resistance v. Normalized Pressure');
xlabel('Log Normalized Pressure'); ylabel('Log Normalized Resistance'); hol
%% Resistance to Pressure
P_31Jan17 = p_nom*(R_31Jan17/r_nom).^(1/x);
P_01Feb17 = p_nom*(R_01Feb17/r_nom).^(1/x);
P_01Feb17_redo = p_nom*(R_01Feb17_redo/r_nom).^(1/x);
%% Calibration
%(1)linear regression using all data points
actual = repmat(reshape(pressures(2:end),[11,1]),1,30);
predicted = horzcat(P_01Feb17,P_01Feb17_redo,P_31Jan17);
[r,m,b]=regression(actual,predicted,'one');
%(2)adjust all values and plot
figure(2); hold on; %measured pressure versus actual pressure
for ii = 1:length(time)-1
%plot pressure versus pressure before calibration
plot(pressures(2:end),P_31Jan17(:,ii),'bo');
plot(pressures(2:end),P_01Feb17(:,ii),'bo');
plot(pressures(2:end),P_01Feb17_redo(:,ii),'bo');
%plot pressure versus pressure after calibration
plot(pressures(2:end),P_31Jan17(:,ii)*(1/m)-b,'ro');
plot(pressures(2:end),P_01Feb17(:,ii)*(1/m)-b,'ro');
plot(pressures(2:end),P_01Feb17_redo(:,ii)*(1/m)-b,'ro');
end
%plot line of identity
plot(pressures(2:end),pressures(2:end),'k--');
title('Measured Pressure v. Actual Pressure, Before and After Calibration')
xlabel('Actual Pressure (mmHg)'); ylabel('Output Pressure (mmHg)'); hold o
%(3)plot error
figure(3); hold on; %error
for ii=1:length(time)-1
%plot error versus pressure before calibration
plot(pressures(2:end),P_31Jan17(:,ii)-reshape(pressures(2:end),[11,1]),'bo
plot(pressures(2:end),P_01Feb17(:,ii)-reshape(pressures(2:end),[11,1]),'bo
plot(pressures(2:end),P_01Feb17_redo(:,ii)-reshape(pressures(2:end),[11,1])
%plot error versus pressure after calibration
plot(pressures(2:end),(P_31Jan17(:,ii)*(1/m)-b)-reshape(pressures(2:end),[1
plot(pressures(2:end),(P_01Feb17(:,ii)*(1/m)-b)-reshape(pressures(2:end),[1
plot(pressures(2:end),(P_01Feb17_redo(:,ii)*(1/m)-b)-reshape(pressures(2:en
end
%plot zero
plot(pressures(2:end),zeros(length(pressures(2:end)),1),'k-');
title('Measurement Error, Before and After Calibration');
xlabel('Actual Pressure (mmHg)'); ylabel('Error (mmHg)'); hold off;
```

```
%(4) plot mean values and error at each actual pressure before and after ca
figure(4);
subplot(2,1,1); hold on;
plot(pressures(2:end),mean(predicted,2),'bo');
plot(pressures(2:end),mean(predicted,2)*(1/m)-b,'ro');
%plot line of identity
plot(pressures(2:end),pressures(2:end),'k--');
xlabel('Actual Pressure (mmHg)');ylabel('Measured Pressure (mmHg)');
title('Average Measured Pressure Before and After Calibration');
hold off;
subplot(2,1,2); hold on;
%plot errors of mean values at each actual pressure before and after calibr
plot(pressures(2:end),mean(predicted,2)-reshape(pressures(2:end),[11,1]),'b
plot(pressures(2:end),(mean(predicted,2)*(1/m)-b)-reshape(pressures(2:end)
%plot zero
plot(pressures(2:end),zeros(length(pressures(2:end))),1),'k-');
xlabel('Actual Pressure (mmHg)');ylabel('Measurement Error (mmHg)');
title('Average Measurement Error Before and After Calibration');
hold off;
```

Appendix C - Tangio TPE-502 Pressure Sensor Data Collected 2/17/17

Recorded Data

Time (s)	30	60	90	120	150	180	210	240		
Coins Used	7q									
Weight (g)	39.690								MEAN over TIME	OVERALL MIN
R1 (ohms)	8.48E+04	8.75E+04	8.00E+04	7.93E+04	8.00E+04	8.48E+04	8.46E+04	8.40E+04	8.31E+04	2.36E+04
R2 (ohms)	3.24E+04	2.92E+04	2.68E+04	2.56E+04	2.53E+04	2.46E+04	2.37E+04	2.36E+04	2.64E+04	
R3 (ohms)	8.76E+04	8.44E+04	8.44E+04	8.00E+04	7.46E+04	6.56E+04	5.34E+04	5.46E+04	7.31E+04	OVERALL MAX
R4 (ohms)	8.36E+04	7.32E+04	6.83E+04	6.56E+04	6.54E+04	6.39E+04	6.38E+04	6.27E+04	6.83E+04	8.76E+04
MEAN wrt TIME	7.21E+04	6.86E+04	6.49E+04	6.26E+04	6.13E+04	5.97E+04	5.64E+04	5.62E+04		OVERALL MEAN
										6.27E+04
Coins Used	8q + 2d									
Weight (g)	49.896								MEAN over TIME	OVERALL MIN
R1 (ohms)	3.46E+04	3.42E+04	3.40E+04	3.42E+04	3.39E+04	3.38E+04	3.37E+04	3.31E+04	3.39E+04	1.16E+04
R2 (ohms)	1.48E+04	1.40E+04	1.38E+04	1.37E+04	1.17E+04	1.19E+04	1.21E+04	1.16E+04	1.30E+04	
R3 (ohms)	1.89E+04	1.86E+04	1.81E+04	1.77E+04	1.75E+04	1.84E+04	1.78E+04	1.78E+04	1.81E+04	OVERALL MAX
R4 (ohms)	1.47E+04	1.42E+04	1.42E+04	1.42E+04	1.39E+04	1.40E+04	1.40E+04	1.39E+04	1.41E+04	3.46E+04
MEAN wrt TIME	2.08E+04	2.03E+04	2.00E+04	2.00E+04	1.93E+04	1.95E+04	1.94E+04	1.91E+04		OVERALL MEAN
										1.98E+04
Coins Used	8q + 3d									
Weight (g)	52.164								MEAN over TIME	OVERALL MIN
R1 (ohms)	2.36E+04	2.36E+04	2.31E+04	2.29E+04	2.28E+04	2.18E+04	2.17E+04	2.17E+04	2.27E+04	1.01E+04
R2 (ohms)	1.64E+04	1.58E+04	1.53E+04	1.50E+04	1.47E+04	1.46E+04	1.46E+04	1.44E+04	1.51E+04	
R3 (ohms)	1.08E+04	1.07E+04	1.05E+04	1.02E+04	1.01E+04	1.01E+04	1.01E+04	1.01E+04	1.03E+04	OVERALL MAX
R4 (ohms)	1.91E+04	1.86E+04	1.83E+04	1.81E+04	1.80E+04	1.79E+04	1.79E+04	1.78E+04	1.82E+04	2.36E+04
MEAN wrt TIME	1.75E+04	1.72E+04	1.68E+04	1.66E+04	1.64E+04	1.61E+04	1.61E+04	1.60E+04		OVERALL MEAN
										1.66E+04

Coins Used	8q + 4d									
Weight (g)	54.432								MEAN over TIME	OVERALL MIN
R1 (ohms)	2.48E+04	2.36E+04	2.27E+04	2.14E+04	2.14E+04	2.11E+04	2.09E+04	2.10E+04	2.21E+04	1.15E+04
R2 (ohms)	1.43E+04	1.39E+04	1.36E+04	1.35E+04	1.35E+04	1.33E+04	1.31E+04	1.31E+04	1.35E+04	
R3 (ohms)	1.26E+04	1.22E+04	1.22E+04	1.21E+04	1.21E+04	1.19E+04	1.18E+04	1.15E+04	1.21E+04	OVERALL MAX
R4 (ohms)	1.45E+04	1.40E+04	1.39E+04	1.37E+04	1.36E+04	1.36E+04	1.36E+04	1.35E+04	1.38E+04	2.48E+04
MEAN wrt TIME	1.66E+04	1.59E+04	1.56E+04	1.52E+04	1.52E+04	1.50E+04	1.49E+04	1.48E+04		OVERALL MEAN
										1.54E+04
Coins Used	10q									
Weight (g)	56.7								MEAN over TIME	OVERALL MIN
R1 (ohms)	1.03E+04	1.01E+04	9.60E+03	9.46E+03	9.46E+03	9.40E+03	9.37E+03	9.34E+03	9.63E+03	7.91E+03
R2 (ohms)	1.65E+04	1.68E+04	1.69E+04	1.67E+04	1.70E+04	1.66E+04	1.65E+04	1.64E+04	1.67E+04	
R3 (ohms)	8.02E+03	8.06E+03	8.07E+03	8.05E+03	7.99E+03	7.97E+03	7.91E+03	7.95E+03	8.00E+03	OVERALL MAX
R4 (ohms)	1.49E+04	1.45E+04	1.45E+04	1.42E+04	1.33E+04	1.29E+04	1.30E+04	1.29E+04	1.38E+04	1.70E+04
MEAN wrt TIME	1.24E+04	1.24E+04	1.23E+04	1.21E+04	1.19E+04	1.17E+04	1.17E+04	1.16E+04		OVERALL MEAN
										1.20E+04
Coins Used	10q + 1d									
Weight (g)	58.968								MEAN over TIME	OVERALL MIN
R1 (ohms)	9.03E+03	8.48E+03	8.28E+03	7.94E+03	7.87E+03	7.81E+03	7.78E+03	7.71E+03	8.11E+03	7.71E+03
R2 (ohms)	1.47E+04	1.45E+04	1.44E+04	1.43E+04	1.43E+04	1.43E+04	1.43E+04	1.42E+04	1.44E+04	
R3 (ohms)	1.33E+04	1.29E+04	1.29E+04	1.27E+04	1.26E+04	1.22E+04	1.22E+04	1.20E+04	1.26E+04	OVERALL MAX
R4 (ohms)	3.48E+04	3.51E+04	3.45E+04	3.50E+04	3.25E+04	3.29E+04	3.16E+04	3.19E+04	3.35E+04	3.51E+04
MEAN wrt TIME	1.80E+04	1.77E+04	1.75E+04	1.75E+04	1.68E+04	1.68E+04	1.65E+04	1.65E+04		OVERALL MEAN
										1.72E+04
Coins Used	10q + 2d									
Weight (g)	61.236								MEAN over TIME	OVERALL MIN
R1 (ohms)	7.60E+03	7.47E+03	7.41E+03	7.34E+03	7.30E+03	7.25E+03	7.23E+03	7.19E+03	7.35E+03	7.19E+03
R2 (ohms)	2.89E+04	2.88E+04	2.85E+04	2.76E+04	2.75E+04	2.76E+04	2.74E+04	2.72E+04	2.79E+04	

R3 (ohms)	5.14E+04	5.20E+04	5.13E+04	5.03E+04	4.98E+04	4.84E+04	4.69E+04	4.66E+04	4.96E+04	OVERALL MAX
R4 (ohms)	4.97E+04	4.79E+04	4.65E+04	4.52E+04	4.28E+04	4.26E+04	4.34E+04	4.27E+04	4.51E+04	5.20E+04
MEAN wrt TIME	3.44E+04	3.40E+04	3.34E+04	3.26E+04	3.19E+04	3.15E+04	3.12E+04	3.09E+04		OVERALL MEAN
										3.25E+04
Coins Used	14q									
Weight (g)	79.38								MEAN over TIME	OVERALL MIN
R1 (ohms)	4.71E+03	4.63E+03	4.63E+03	4.60E+03	4.59E+03	4.60E+03	4.61E+03	4.60E+03	4.62E+03	4.59E+03
R2 (ohms)	9.20E+03	8.50E+03	8.40E+03	8.30E+03	8.20E+03	8.10E+03	8.10E+03	8.00E+03	8.35E+03	
R3 (ohms)	1.19E+04	1.18E+04	1.18E+04	1.17E+04	1.16E+04	1.17E+04	1.17E+04	1.15E+04	1.17E+04	OVERALL MAX
R4 (ohms)	9.00E+03	8.90E+03	8.80E+03	8.80E+03	8.70E+03	8.70E+03	8.60E+03	8.60E+03	8.76E+03	1.19E+04
MEAN wrt TIME	8.70E+03	8.46E+03	8.41E+03	8.35E+03	8.27E+03	8.28E+03	8.25E+03	8.18E+03		OVERALL MEAN
										8.36E+03
Coins Used	21q									
Weight (g)	119.07								MEAN over TIME	OVERALL MIN
R1 (ohms)	2.95E+03	2.93E+03	2.90E+03	2.89E+03	2.88E+03	2.88E+03	2.87E+03	2.86E+03	2.90E+03	2.86E+03
R2 (ohms)	4.00E+03	3.90E+03	3.80E+03	3.80E+03	3.70E+03	3.70E+03	3.70E+03	3.70E+03	3.79E+03	
R3 (ohms)	3.20E+03	3.10E+03	3.10E+03	3.10E+03	3.10E+03	3.00E+03	3.00E+03	2.90E+03	3.06E+03	OVERALL MAX
R4 (ohms)	3.12E+03	3.00E+03	3.00E+03	3.00E+03	3.00E+03	2.90E+03	2.90E+03	3.00E+03	2.99E+03	4.00E+03
MEAN wrt TIME	3.32E+03	3.23E+03	3.20E+03	3.20E+03	3.17E+03	3.12E+03	3.12E+03	3.12E+03		OVERALL MEAN
										3.18E+03
Coins Used	28q									
Weight (g)	158.76								MEAN over TIME	OVERALL MIN
R1 (ohms)	2.12E+03	2.10E+03	2.08E+03	2.02E+03	2.02E+03	2.02E+03	2.02E+03	2.01E+03	2.05E+03	2.01E+03
R2 (ohms)	2.70E+03	2.70E+03	2.60E+03	2.60E+03	2.60E+03	2.60E+03	2.50E+03	2.50E+03	2.60E+03	
R3 (ohms)	2.30E+03	2.30E+03	2.30E+03	2.30E+03	2.30E+03	2.30E+03	2.30E+03	2.30E+03	2.30E+03	OVERALL MAX
R4 (ohms)	2.30E+03	2.20E+03	2.20E+03	2.20E+03	2.20E+03	2.20E+03	2.20E+03	2.20E+03	2.21E+03	2.70E+03
MEAN wrt TIME	2.36E+03	2.33E+03	2.30E+03	2.28E+03	2.28E+03	2.28E+03	2.26E+03	2.25E+03		OVERALL MEAN
										2.29E+03

MATLAB Code Used to Process Recorded Data

```
Main File: Tangio_FSR_TPE_502_calibration.m
close all;
%% Constants
grams2newtons = 1/101.97162; %N/g
pressure2mmHg = 1/133.32239; %mmHg / N/m^2
sensing_area = pi*(12.7e-3/2)^2; %m^2
F2P = (grams2newtons/sensing_area)*pressure2mmHg;
%% Actual Weights and Pressures
weights = [39.69,49.896,52.164,54.432,56.7,58.968,61.236,79.38,119.07,158.
pressures = weights*F2P; %mmHg
%% Recorded Values
time = 30:30:240; %seconds
%resistance readings on DMM in ohms
%Rxx corresponds to weight at index xx in weights
%e.g. R01 values were recorded with weights(1)
%columns correspond to time, rows correspond to sample
R01 = [8.48E+04,8.75E+04,8.00E+04,7.93E+04,8.00E+04,8.48E+04,8.46E+04,8.40E
3.24E+04,2.92E+04,2.68E+04,2.56E+04,2.53E+04,2.46E+04,2.37E+04,2.36E+04; ..
8.76E+04,8.44E+04,8.44E+04,8.00E+04,7.46E+04,6.56E+04,5.34E+04,5.46E+04; ..
8.36E+04,7.32E+04,6.83E+04,6.56E+04,6.54E+04,6.39E+04,6.38E+04,6.27E+04];
R02 = [3.46E+04,3.42E+04,3.40E+04,3.42E+04,3.39E+04,3.38E+04,3.37E+04,3.31E
1.48E+04,1.40E+04,1.38E+04,1.37E+04,1.17E+04,1.19E+04,1.21E+04,1.16E+04; ..
1.89E+04,1.86E+04,1.81E+04,1.77E+04,1.75E+04,1.84E+04,1.78E+04,1.78E+04; ..
1.47E+04,1.42E+04,1.42E+04,1.42E+04,1.39E+04,1.40E+04,1.40E+04,1.39E+04];
R03 = [2.36E+04,2.36E+04,2.31E+04,2.29E+04,2.28E+04,2.18E+04,2.17E+04,2.17E
1.64E+04,1.58E+04,1.53E+04,1.50E+04,1.47E+04,1.46E+04,1.46E+04,1.44E+04; ..
1.08E+04,1.07E+04,1.05E+04,1.02E+04,1.01E+04,1.01E+04,1.01E+04,1.01E+04; ..
1.91E+04,1.86E+04,1.83E+04,1.81E+04,1.80E+04,1.79E+04,1.79E+04,1.78E+04];
R04 = [2.48E+04,2.36E+04,2.27E+04,2.14E+04,2.14E+04,2.11E+04,2.09E+04,2.10E
1.43E+04,1.39E+04,1.36E+04,1.35E+04,1.35E+04,1.33E+04,1.31E+04,1.31E+04; ..
1.26E+04,1.22E+04,1.22E+04,1.21E+04,1.21E+04,1.19E+04,1.18E+04,1.15E+04; ..
1.45E+04,1.40E+04,1.39E+04,1.37E+04,1.36E+04,1.36E+04,1.36E+04,1.35E+04];
R05 = [1.03E+04,1.01E+04,9.60E+03,9.46E+03,9.46E+03,9.40E+03,9.37E+03,9.34E
1.65E+04,1.68E+04,1.69E+04,1.67E+04,1.70E+04,1.66E+04,1.65E+04,1.64E+04; ..
8.02E+03,8.06E+03,8.07E+03,8.05E+03,7.99E+03,7.97E+03,7.91E+03,7.95E+03; ..
1.49E+04,1.45E+04,1.45E+04,1.42E+04,1.33E+04,1.29E+04,1.30E+04,1.29E+04];
R06 = [9.03E+03,8.48E+03,8.28E+03,7.94E+03,7.87E+03,7.81E+03,7.78E+03,7.71E
1.47E+04,1.45E+04,1.44E+04,1.43E+04,1.43E+04,1.43E+04,1.43E+04,1.42E+04; ..
1.33E+04,1.29E+04,1.29E+04,1.27E+04,1.26E+04,1.22E+04,1.22E+04,1.20E+04; ..
3.48E+04,3.51E+04,3.45E+04,3.50E+04,3.25E+04,3.29E+04,3.16E+04,3.19E+04];
R07 = [7.60E+03,7.47E+03,7.41E+03,7.34E+03,7.30E+03,7.25E+03,7.23E+03,7.19E
2.89E+04,2.88E+04,2.85E+04,2.76E+04,2.75E+04,2.76E+04,2.74E+04,2.72E+04; ..
5.14E+04,5.20E+04,5.13E+04,5.03E+04,4.98E+04,4.84E+04,4.69E+04,4.66E+04; ..
4.97E+04,4.79E+04,4.65E+04,4.52E+04,4.28E+04,4.26E+04,4.34E+04,4.27E+04];
R08 = [4.71E+03,4.63E+03,4.63E+03,4.60E+03,4.59E+03,4.60E+03,4.61E+03,4.60E
9.20E+03,8.50E+03,8.40E+03,8.30E+03,8.20E+03,8.10E+03,8.10E+03,8.00E+03; ..
```

```
1.19E+04,1.18E+04,1.18E+04,1.17E+04,1.16E+04,1.17E+04,1.17E+04,1.15E+04; ..
9.00E+03,8.90E+03,8.80E+03,8.80E+03,8.70E+03,8.70E+03,8.60E+03,8.60E+03];
R09 = [2.95E+03,2.93E+03,2.90E+03,2.89E+03,2.88E+03,2.88E+03,2.87E+03,2.86E
4.00E+03,3.90E+03,3.80E+03,3.80E+03,3.70E+03,3.70E+03,3.70E+03,3.70E+03; ..
3.20E+03,3.10E+03,3.10E+03,3.10E+03,3.10E+03,3.00E+03,3.00E+03,2.90E+03; ..
3.12E+03,3.00E+03,3.00E+03,3.00E+03,3.00E+03,2.90E+03,2.90E+03,3.00E+03];
R10 = [2.12E+03,2.10E+03,2.08E+03,2.02E+03,2.02E+03,2.02E+03,2.02E+03,2.01E
2.70E+03,2.70E+03,2.60E+03,2.60E+03,2.60E+03,2.60E+03,2.50E+03,2.50E+03; ..
2.30E+03,2.30E+03,2.30E+03,2.30E+03,2.30E+03,2.30E+03,2.30E+03,2.30E+03; ..
2.30E+03,2.20E+03,2.20E+03,2.20E+03,2.20E+03,2.20E+03,2.20E+03,2.20E+03];
%% P_NOM and R_NOM Values
idx_nom = find((pressures > 29) & (pressures < 31));
p_nom = pressures(idx_nom); %about 30 mmHg
r_nom = mean(mean(R03));
%% x Values
R_sample1 = vertcat(R01(1,:),R02(1,:),R03(1,:),R04(1,:),R05(1,:),...
R06(1,:),R07(1,:),R08(1,:),R09(1,:),R10(1,:));
R_sample2 = vertcat(R01(2,:),R02(2,:),R03(2,:),R04(2,:),R05(2,:),...
R06(2,:),R07(2,:),R08(2,:),R09(2,:),R10(2,:));
R_sample3 = vertcat(R01(3,:),R02(3,:),R03(3,:),R04(3,:),R05(3,:),...
R06(3,:),R07(3,:),R08(3,:),R09(3,:),R10(3,:));
R_sample4 = vertcat(R01(4,:),R02(4,:),R03(4,:),R04(4,:),R05(4,:),...
R06(4,:),R07(4,:),R08(4,:),R09(4,:),R10(4,:));
log_R_sample1 = log10(R_sample1/r_nom);
log_R_sample2 = log10(R_sample2/r_nom);
log_R_sample3 = log10(R_sample3/r_nom);
log_R_sample4 = log10(R_sample4/r_nom);
x = (mean([mean(log_R_sample1(end-1,:)),mean(log_R_sample2(end-1,:)),mean(l
- mean([mean(log_R_sample1(2,:)),mean(log_R_sample2(2,:)),mean(log_R_sample
/ (log10(pressures(end-1)/p_nom) - log10(pressures(2)/p_nom));
figure(1); hold on; %normalized log-log plot, resistance versus pressure
for ii = 1:length(time)
plot(log10(pressures/p_nom),log_R_sample1(:,ii),'bo');
plot(log10(pressures/p_nom),log_R_sample2(:,ii),'bo');
plot(log10(pressures/p_nom),log_R_sample3(:,ii),'bo');
plot(log10(pressures/p_nom),log_R_sample4(:,ii),'bo');
end
plot(log10(pressures(end-1)/p_nom),...
mean([mean(log_R_sample1(end-1,:)),mean(log_R_sample2(end-1,:)),mean(log_R_
'r.','MarkerSize',20);
plot(log10(pressures(2)/p_nom),...
mean([mean(log_R_sample1(2,:)),mean(log_R_sample2(2,:)),mean(log_R_sample3(
'r.','MarkerSize',20);
title('Log-Log Plot: Normalized Resistance v. Normalized Pressure');
xlabel('Log Normalized Pressure'); ylabel('Log Normalized Resistance'); hol
%% Resistance to Pressure
P_sample1 = p_nom*(R_sample1/r_nom).^(1/x);
P_sample2 = p_nom*(R_sample2/r_nom).^(1/x);
```

```
P_sample3 = p_nom*(R_sample3/r_nom).^(1/x);
P_sample4 = p_nom*(R_sample4/r_nom).^(1/x);
%% Calibration
%(1)linear regression using all data points
actual = repmat(reshape(pressures,[10,1]),1,32);
predicted = horzcat(P_sample1,P_sample2,P_sample3,P_sample4);
[r,m,b]=regression(actual,predicted,'one');
%(2)adjust all values and plot
figure(2); hold on; %measured pressure versus actual pressure
for ii = 1:length(time)
%plot pressure versus pressure before calibration
plot(pressures,P_sample1(:,ii),'bo');
plot(pressures,P_sample2(:,ii),'bo');
plot(pressures,P_sample3(:,ii),'bo');
plot(pressures,P_sample4(:,ii),'bo');
%plot pressure versus pressure after calibration
plot(pressures,P_sample1(:,ii)*(1/m)-b,'ro');
plot(pressures,P_sample2(:,ii)*(1/m)-b,'ro');
plot(pressures,P_sample3(:,ii)*(1/m)-b,'ro');
plot(pressures,P_sample4(:,ii)*(1/m)-b,'ro');
end
%plot line of identity
plot(pressures,pressures,'k--');
title('Measured Pressure v. Actual Pressure, Before and After Calibration')
xlabel('Actual Pressure (mmHg)'); ylabel('Output Pressure (mmHg)'); hold o
%(3)plot error
figure(3); hold on; %error
for ii=1:length(time)
%plot error versus pressure before calibration
plot(pressures,P_sample1(:,ii)-reshape(pressures,[10,1]),'bo');
plot(pressures,P_sample2(:,ii)-reshape(pressures,[10,1]),'bo');
plot(pressures,P_sample3(:,ii)-reshape(pressures,[10,1]),'bo');
plot(pressures,P_sample4(:,ii)-reshape(pressures,[10,1]),'bo');
%plot error versus pressure after calibration
plot(pressures,(P_sample1(:,ii)*(1/m)-b)-reshape(pressures,[10,1]),'ro');
plot(pressures,(P_sample2(:,ii)*(1/m)-b)-reshape(pressures,[10,1]),'ro');
plot(pressures,(P_sample3(:,ii)*(1/m)-b)-reshape(pressures,[10,1]),'ro');
plot(pressures,(P_sample4(:,ii)*(1/m)-b)-reshape(pressures,[10,1]),'ro');
end
%plot zero
plot(pressures,zeros(length(pressures),1),'k-');
title('Measurement Error, Before and After Calibration');
xlabel('Actual Pressure (mmHg)'); ylabel('Error (mmHg)'); hold off;
%(4)plot mean values at each actual pressure before and after calibration
figure(4);
subplot(2,1,1); hold on;
plot(pressures,mean(predicted,2),'bo');
plot(pressures,mean(predicted,2)*(1/m)-b,'ro');
```

```
%plot line of identity
plot(pressures,pressures,'k--');
xlabel('Actual Pressure (mmHg)');ylabel('Measured Pressure (mmHg)');
title('Average Measured Pressure Before and After Calibration');
hold off;
subplot(2,1,2); hold on;
%plot errors of mean values at each actual pressure before and after calibr
plot(pressures,mean(predicted,2)-reshape(pressures,[10,1]),'bo');
plot(pressures,(mean(predicted,2)*(1/m)-b)-reshape(pressures,[10,1]),'ro');
%plot zero
plot(pressures,zeros(length(pressures),1),'k-');
xlabel('Actual Pressure (mmHg)');ylabel('Measurement Error (mmHg)');
title('Average Measurement Error Before and After Calibration');
hold off;
```

Appendix D - Temperature Sensor Testing Data 2/15/17

Target Temperature (◦C)	Incubator Temperature (◦C)	MCU Reading	Time (s)
35	35.2	5B0	30
	35.3	5B3	60
	35.5	5B8	90
	35.6	5BB	120
	35.7	5BA	150
	35.7	5BC	180
	35.7	5BD	210
	35.7	5BD	240
	35.7	5BB	270
	35.7	5BC	300
36	36.0	5C1	30
	36.1	5C2	60
	36.2	5C2	90
	36.3	5C7	120
	36.3	5C4	150
	36.3	5C5	180
	36.4	5C8	210
	36.4	5C6	240
	36.4	5C8	270

	36.4	5C8	300
37	37.0	5D1	30
	37.1	5CE	60
	37.1	5D2	90
	37.1	5D3	120
	37.1	5D1	150
	37.2	5D3	180
	37.2	5D4	210
	37.2	5D1	240
	37.1	5D1	270
	37.1	5D2	300
40	39.9	5F9	30
	39.9	5F8	60
	39.9	5F7	90
	39.9	5F9	120
	39.9	5F9	150
	39.9	5FA	180
	39.9	5F9	210
	39.9	5F9	240
	39.9	5F8	270
	39.9	5F8	300

MATLAB Code Used to Process Recorded Data

```
%vt = hex2dec('6d5');
%temp = -66.875 + (218.75*(vt/3300))
%temp = -45 - (17.5/0.8) + ((175/0.8)*(vt/3300))
t = [30 60 90 120 150 180 210 240 270 300];
mcu = 100/95;
%% sensor vs. cc oven 35 degrees

vt35 = [hex2dec('5b0') hex2dec('5b3') hex2dec('5b8') hex2dec('5bb') hex2dec
        hex2dec('5bc') hex2dec('5bd') hex2dec('5bd') hex2dec('5bb') hex2dec


sense_temp35 = -66.875 + (218.75*(vt35/3300));

cctemp35 = [35.2 35.3 35.5 35.6 35.7 35.7 35.7 35.7 35.7 35.7];

figure1 = figure;
plot(t, sense_temp35, 'b-o');
hold on
plot(t, cctemp35, 'r-o');
xlabel('Time (s)')
ylabel('Temperature ( C )');
title('Target Temperature of 35 C vs. Time');
%saveas(figure1,'35.jpeg')

%% sensor vs. cc oven 36 degrees

vt36 = [hex2dec('5c1') hex2dec('5c2') hex2dec('5c2') hex2dec('5c7') hex2dec
        hex2dec('5c5') hex2dec('5c8') hex2dec('5c6') hex2dec('5c8') hex2dec

sense_temp36 = -66.875 + (218.75*(vt36/3300));

cctemp36 = [36 36.1 36.2 36.3 36.3 36.3 36.4 36.4 36.4 36.4];

figure2 = figure;
plot(t, sense_temp36, 'b-o');
hold on
plot(t, cctemp36, 'r-o');
xlabel('Time (s)')
ylabel('Temperature ( C )');
title('Target Temperature of 36 C vs. Time');
%saveas(figure2,'36.jpeg')
%% sensor vs. cc oven 37 degrees

vt37 = [hex2dec('5d1') hex2dec('5ce') hex2dec('5d2') hex2dec('5d3') hex2dec
        hex2dec('5d3') hex2dec('5d4') hex2dec('5d1') hex2dec('5d1') hex2dec
```

```
sense_temp37 = -66.875 + (218.75*(vt37/3300));

cctemp37 = [37 37.1 37.1 37.1 37.1 37.2 37.2 37.2 37.1 37.1];

figure3 = figure;
plot(t, sense_temp37, 'b-o');
hold on
plot(t, cctemp37, 'r-o');
xlabel('Time (s)')
ylabel('Temperature ( C)');
title('Target Temperature of 37 C vs. Time');
%saveas(figure3,'37.jpeg')
%% sensor vs. cc oven 40 deg

vt40 = [hex2dec('5f9') hex2dec('5f8') hex2dec('5f7') hex2dec('5f9') hex2dec
        hex2dec('5fa') hex2dec('5f9') hex2dec('5f9') hex2dec('5f8') hex2d

sense_temp40 = -66.875 + (218.75*(vt40/3300));

cctemp40 = [39.9 39.9 39.9 39.9 39.9 39.9 39.9 39.9 39.9 39.9];

figure4 = figure;
plot(t, sense_temp40, 'b-o');
hold on
plot(t, cctemp40, 'r-o');
xlabel('Time (s)')
ylabel('Temperature ( C)');
title('Target Temperature of 40 C vs. Time');
%saveas(figure4,'40.jpeg')
%% Error (difference in temp) 35

error35 = sense_temp35 - cctemp35;

figure5 = figure;
plot(t, error35, 'ro')
xlabel('Time (s)')
ylabel('Difference ( C)');
title('Difference in Temperature Between MCU and Cell Culture Oven (35 C)
%saveas(figure5,'35error.jpeg')
%% Error 36

error36 =  sense_temp35 - cctemp36;
baseline = [0 0 0 0 0 0 0 0 0 0];

figure6 = figure;
plot(t, error36, 'ro')
%hold on
%plot(t, baseline, 'b-')
```

```
xlabel('Time (s)')
ylabel('Difference ( C)');
title('Difference in Temperature Between MCU and Cell Culture Oven (36 C)
%saveas(figure6,'36error.jpeg')
%% Error 37

error37 =  sense_temp36 - cctemp37;

figure7 = figure;
plot(t, error37, 'ro')
xlabel('Time (s)')
ylabel('Difference ( C)');
title('Difference in Temperature Between MCU and Cell Culture Oven (37 C)
%saveas(figure7,'37error.jpeg')
%% Error 40

error40 = sense_temp40 - cctemp40;

figure8 = figure;
plot(t, error40, 'ro')
xlabel('Time (s)')
ylabel('Difference ( C)');
title('Difference in Temperature Between MCU and Cell Culture Oven (40 C)
saveas(figure8,'40error.jpeg')

%% Error over range

% vt38 = [hex2dec('5e4') hex2dec('5e6')];
%
% sense_temp38 = -66.875 + (218.75*(vt38/3300));
%
% cctemp38 = [38.2 38.5];
%
% error38 = cctemp38 - sense_temp38;
%
% vt39 = [hex2dec('5ef') hex2dec('5f4')];
%
% sense_temp39 = -66.875 + (218.75*(vt39/3300));
%
% cctemp39 = [39 39.5];
%
% error39 = cctemp39 - sense_temp39;
%
%
% temp = [;
% mintemp = [min(error35) min(error36) min(error37) min(error38) min(error3
% meantemp = [mean(error35) mean(error36) mean(error37) mean(error38) mean(
% maxtemp = [max(error35) max(error36) max(error37) max(error38) max(error3
```

```
%
%
% plot(temp, mintemp, 'b-o')
% hold on
% plot(temp, meantemp, 'g-o')
% hold on
% plot(temp, maxtemp, 'r-o')
%
allerror = [error35 error36 error36 error40];
allcc = [cctemp35 cctemp36 cctemp37 cctemp40];

figure30 = figure;
plot(allcc, allerror, 'bo');
hold on
plot(allcc, baseline, 'k-');
axis([allcc(1) allcc(end) -8 8])
xlabel('Time (s)')
ylabel('Difference Between MCU Reading and Oven( C )');
title('Error of MCU Reading Before Calibration');
saveas(figure30,'enoc.jpeg')
%% Error Over Range pt. 2
vt35_7 = [hex2dec('5ba') hex2dec('5bc') hex2dec('5bd') hex2dec('5bd') hex2c
sense_temp35_7 = -66.875 + (218.75*(vt35_7/3300));
cctemp35_7 = [35.7 35.7 35.7 35.7 35.7 35.7];
error35_7 = cctemp35_7 - sense_temp35_7;

vt36_4 = [hex2dec('5c7') hex2dec('5c4') hex2dec('5c5') hex2dec('5c8') hex2c
sense_temp36_4 = -66.875 + (218.75*(vt36_4/3300));
cctemp36_4 = [36.4 36.4 36.4 36.4 36.4 36.4 36.4];
error36_4 = cctemp36_4 - sense_temp36_4;

vt37_1 = [hex2dec('5ce') hex2dec('5d2') hex2dec('5d3') hex2dec('5d1') hex2c
sense_temp37_1 = -66.875 + (218.75*(vt37_1/3300));
cctemp37_1 = [37.1 37.1 37.1 37.1 37.1 37.1];
error37_1 = cctemp37_1 - sense_temp37_1;

mintemp = [min(error35_7) min(error36_4) min(error37_1) min(error40)];
meantemp = [mean(error35_7) mean(error36_4) mean(error37_1) mean(error40)];
maxtemp = [max(error35_7) max(error36_4) max(error37_1) max(error40)];

temp = [35.7 36.4 37.1 39.9];

figure
plot(temp, mintemp, 'b-o')
hold on
plot(temp, meantemp, 'g-o')
hold on
plot(temp, maxtemp, 'r-o')
```

```
%% MCU vs. CCoven

figure11 = figure;
plot(cctemp35, sense_temp35, 'bo')
hold on
plot(cctemp36, sense_temp36, 'bo')
hold on
plot(cctemp37, sense_temp37, 'bo')
hold on
plot(cctemp40, sense_temp40, 'bo')
hold on
plot(linspace(35, 40, 5), linspace(35, 40, 5), 'k-');
xlabel('Temperature of Cell Culture Oven ( C )');
ylabel('Temperature from MCU ( C )');
title('Temperature from MCU vs. Cell Culture Oven');
saveas(figure11,'mcuvscc.jpeg')

cc = [cctemp35 cctemp36 cctemp37 cctemp40];
sense = [sense_temp35 sense_temp36 sense_temp37 sense_temp40];

%minpoint =

[r, m, b] = regression(cc, sense, 'one');
figure12 = figure;
plotregression(cc, sense)
b_fit = mean(sense - cc);
leboundx = [35.2 39.9];
leboundy = [34.99 39.66];
saveas(figure12,'regression.jpeg')

calibsense = sense + abs(b_fit);
figure13 = figure;
plot(cc, calibsense, 'bo');
hold on
plot(linspace(35, 40, 5), linspace(35, 40, 5), 'k-')
xlabel('Temperature of Cell Culture Oven ( C )');
ylabel('Temperature from MCU ( C )');
title('Temperature from MCU vs. Cell Culture Oven After Calibration');
saveas(figure13,'calib.jpeg')
%hold on
%plot(leboundx, leboundy, 'r-')

%% Percent error

pe = ((abs(calibsense - cc)/cc)*100);
e = calibsense - cc;
```

```
baseline = linspace(0, 0, 40);
%pe = ((abs(calibsense(1) - cc(1))/cc(1))*100);
lerror = (pe*calibsense) + calibsense;
herror = calibsense - (pe*calibsense);
lboundx = [lerror(1) lerror(40)];
lboundy = [35.2 39.9];
hboundx = [herror(1) herror(40)];
hboundy = [35.2 39.9];

%
% figure
% plot(cc, calibsense, 'bo')
% hold on
% plot(lboundx, lboundy, 'r-o')
% hold on
% plot(hboundx, hboundy, 'r-o')
% hold on
% plot(linspace(35, 40, 5), linspace(35, 40, 5), 'k-')


% figure
% plot(cc, RMSE, 'bo')
% hold on
% plot(cc, 0, 'k-')
%
figure14 = figure;
plot(cc, pe, 'bo')
hold on
plot(cc, baseline, 'k-')
axis([cc(1) cc(40) -0.5 0.5])
xlabel('Temperature ( C )')
ylabel('Percent Error (%)')
title('Percent Error of MCU Reading After Calibration')
saveas(figure14,'pe.jpeg')

figure15 = figure;
plot(cc, e, 'bo')
hold on
plot(cc, baseline, 'k-')
xlabel('Temperature ( C )')
ylabel('Difference in Temperature ( C )')
title('Error of MCU Reading After Calibration')
saveas(figure15,'e.jpeg')

figure
plot(cc, calibsense, 'bo')
hold on
plot(cc, lerror, 'r-o')
```

```
hold on
plot(cc, herror, 'r-o')
hold on
plot(linspace(35, 40, 5), linspace(35, 40, 5), 'k-')


bline = linspace(0, 0, 10);
figure16 = figure;
plot(cctemp35, error35, 'bo')
hold on
plot(cctemp36, error36, 'bo')
hold on
plot(cctemp37, error37, 'bo')
hold on
plot(cctemp40, error40, 'bo')
hold on
plot(t, bline, 'k-')
axis([t(1) t(end) -8 8])
xlabel('Time (s)')
ylabel('Difference Between MCU Reading and Oven( C )');
title('Error of MCU Reading Before Calibration');
saveas(figure16,'overalle.jpeg')

pe_i = ((abs(sense - cc)/cc)*100);
figure17 = figure;
plot(cc, pe_i, 'bo')
hold on
plot(cc, baseline, 'k-')
%axis([cc(1) cc(40) - 0.5])
xlabel('Temperature ( C )')
ylabel('Percent Error (%)')
title('Percent Error of MCU Reading Before Calibration')
%saveas(figure17,'pei.jpeg')


%% Last Five Average

mcuavg35 = mean(sense_temp35(5:end));
mcuavg36 = mean(sense_temp36(5:end));
mcuavg37 = mean(sense_temp37(5:end));
mcuavg40 = mean(sense_temp40(5:end));
allavgmcu = [mcuavg35 mcuavg36 mcuavg37 mcuavg40];

ccavg35 = mean(cctemp35(5:end));
ccavg36 = mean(cctemp36(5:end));
ccavg37 = mean(cctemp37(5:end));
ccavg40 = mean(cctemp40(5:end));
allavgcc = [ccavg35 ccavg36 ccavg37 ccavg40];
```

```
figure
plot(allavgmcu, allavgcc, 'bo')
hold on
plot(allavgcc, allavgcc, 'k-')

% calibavg = allavgmcu + abs(b_fit);
%
% figure21 = figure;
% plot(calibavg, allavgcc, 'bo')
% hold on
% plot(allavgcc, allavgcc, 'k-')
% xlabel('Temperature from Cell Culture Oven ( C)')
% ylabel('Temperature from MCU ( C)')
% title('Average MCU Temperature v. Cell Culture Oven After Calibration')
% saveas(figure21,'avg.jpeg')
% avgerror = allavgcc - calibavg;
%
% avgbase = linspace(0, 0, 4);
% figure22 = figure;
% plot(allavgcc, avgerror, 'bo');
% hold on
% plot(allavgcc, avgbase, 'k-');
% axis([allavgcc(1) allavgcc(end) -0.2 0.2])
% xlabel('Temperature ( C)')
% ylabel('Difference in Temperature ( C)')
% title('Error After Averaging and Calibration')
% saveas(figure22, 'eavg.jpeg')
%%
[r1, m1, b1] = regression(allavgcc, allavgmcu, 'one');

b1_fit = mean(allavgmcu - allavgcc);
calibavg = allavgmcu + abs(b1_fit);

figure21 = figure;
plot(calibavg, allavgcc, 'bo')
hold on
plot(allavgcc, allavgcc, 'k-')
xlabel('Temperature from Cell Culture Oven ( C)')
ylabel('Temperature from MCU ( C)')
title('Average MCU Temperature v. Cell Culture Oven After Calibration')
saveas(figure21,'avg.jpeg')

avgerror = allavgcc - calibavg;

avgbase = linspace(0, 0, 4);
figure22 = figure;
plot(allavgcc, avgerror, 'bo');
```

```
hold on
plot(allavgcc, avgbase, 'k-');
axis([allavgcc(1) allavgcc(end) -0.15 0.15])
xlabel('Temperature ( C )')
ylabel('Difference in Temperature ( C )')
title('Error After Averaging and Calibration')
saveas(figure22, 'eavg.jpeg')
```

Appendix E - Relative Humidity Sensor Testing Data 1/25/17

Recorded Data

Test	Time (s)	Vernier RH-BTA Probe (%RH)	SHT31-ARP-B Output (V)	SHT31-ARP-B Output (%RH)
Baseline	0	23.4571999722000	0.954000000000000	23.6363636363636
	10	23.3225457350000	0.950000000000000	23.4848484848485
	20	23.2528969917000	0.948000000000000	23.4090909090909
	30	23.1530671262000	0.948000000000000	23.4090909090909
	40	23.0694886341000	0.943000000000000	23.2196969696970
	50	23.0300210129000	0.942000000000000	23.1818181818182
	60	22.9069748996000	0.938000000000000	23.0303030303030
	70	22.8001801597000	0.937000000000000	22.9924242424242
	80	22.7026719190000	0.933000000000000	22.8409090909091
	90	22.6492745491000	0.933000000000000	22.8409090909091
	100	22.6167718022000	0.929000000000000	22.6893939393939
	110	22.5656960570000	0.928000000000000	22.6515151515152
	120	22.5703393066000	0.930000000000000	22.7272727272727
	130	22.5355149349000	0.929000000000000	22.6893939393939
	140	22.5540879332000	0.929000000000000	22.6893939393939
	150	22.5656960570000	0.931000000000000	22.7651515151515
	160	22.5122986871000	0.934000000000000	22.8787878787879
	170	22.5053338128000	0.932000000000000	22.8030303030303
	180	22.5053338128000	0.933000000000000	22.8409090909091
	190	22.4821175650000	0.931000000000000	22.7651515151515
	200	22.4821175650000	0.930000000000000	22.7272727272727
	210	22.4728310659000	0.933000000000000	22.8409090909091
Increasing RH	0	24.9616128291000	1.67700000000000	51.0227272727273
	10	74.1266607770000	2.67400000000000	88.7878787878788
	20	90.0994392575000	2.74300000000000	91.4015151515152
	30	94.9307404229000	2.76100000000000	92.0833333333333
	40	95.9336823275000	2.78000000000000	92.8030303030303
	50	96.0590500656000	2.79100000000000	93.2196969696970
	60	95.6458008549000	2.80600000000000	93.7878787878788
	70	95.4763222460000	2.80400000000000	93.7121212121212
	80	95.1814758991000	2.80400000000000	93.7121212121212
	90	95.0607514106000	2.80400000000000	93.7121212121212
	100	94.8494835556000	2.80400000000000	93.7121212121212
	110	94.8518051804000	2.80500000000000	93.7500000000000
	120	94.5708885822000	2.80300000000000	93.6742424242424
	130	94.7612618140000	2.80300000000000	93.6742424242424
	140	94.8634133043000	2.80200000000000	93.6363636363636
	150	94.8100159344000	2.80500000000000	93.7500000000000
	160	94.6033913291000	2.80700000000000	93.8257575757576
	170	94.5105263379000	2.80700000000000	93.8257575757576
	180	94.3642639768000	2.80500000000000	93.7500000000000
	190	93.0804054739000	2.80600000000000	93.7878787878788
	200	92.2260475552000	2.80400000000000	93.7121212121212
	210	92.8366348721000	2.80500000000000	93.7500000000000
	220	93.5447304298000	2.80700000000000	93.8257575757576
	230	94.1854988688000	2.80700000000000	93.8257575757576

	240	94.3015801078000	2.80700000000000	93.8257575757576
	250	94.4710587166000	2.80500000000000	93.7500000000000
	260	94.2690773609000	2.80500000000000	93.7500000000000
	270	93.8883308971000	2.80500000000000	93.7500000000000
	280	93.9811958882000	2.80600000000000	93.7878787878788
	290	94.2388962387000	2.80400000000000	93.7121212121212
	300	94.6010697043000	2.80200000000000	93.6363636363636
	310	92.8343132474000	2.80500000000000	93.7500000000000
	320	91.0977379126000	2.80300000000000	93.6742424242424
	330	89.3936653247000	2.80500000000000	93.7500000000000
	340	90.7309211974000	2.80500000000000	93.7500000000000
	350	91.8104767198000	2.80400000000000	93.7121212121212
	360	93.0989784722000	2.80600000000000	93.7878787878788
	370	93.8604713997000	2.80500000000000	93.7500000000000
	380	93.9092255201000	2.80400000000000	93.7121212121212
	390	94.3247963556000	2.80400000000000	93.7121212121212
	400	93.9347633927000	2.80400000000000	93.7121212121212
	410	94.5337425857000	2.80300000000000	93.6742424242424
	420	94.9423485468000	2.80600000000000	93.7878787878788
Decreasing RH	0	65.2394811225000	1.85200000000000	57.6515151515152
	10	62.6996236141000	1.89000000000000	59.0909090909091
	20	59.9276036278000	1.93700000000000	60.8712121212121
	30	54.8269939880000	1.95800000000000	61.6666666666667
	40	51.5976139202000	1.90100000000000	59.5075757575758
	50	47.7599681603000	1.82500000000000	56.6287878787879
	60	46.0419658237000	1.80100000000000	55.7196969696970
	70	45.1574267829000	1.75000000000000	53.7878787878788
	80	44.4771907226000	1.72500000000000	52.8409090909091
	90	43.8294574092000	1.70300000000000	52.0075757575758
	100	43.6019381809000	1.79600000000000	55.5303030303030
	110	43.0447482339000	1.80900000000000	56.0227272727273
	120	42.8265155046000	1.69900000000000	51.8560606060606
	130	42.2995066798000	1.64700000000000	49.8863636363636
	140	42.0116252071000	1.62200000000000	48.9393939393939
	150	41.9187602160000	1.58300000000000	47.4621212121212
	160	41.8119654761000	1.59900000000000	48.0681818181818
	170	41.6215922442000	1.57100000000000	47.0075757575758
	180	41.4474703858000	1.57400000000000	47.1212121212121
	190	41.2338809061000	1.56000000000000	46.5909090909091
	200	41.0017184282000	1.56100000000000	46.6287878787879
	210	40.6674044600000	1.57600000000000	47.1969696969697
	220	40.4793528529000	1.54100000000000	45.8712121212121
	230	40.1752200068000	1.52900000000000	45.4166666666667
	240	40.0846766405000	1.52900000000000	45.4166666666667
	250	39.9059115325000	1.49300000000000	44.0530303030303
	260	39.8246546652000	1.48300000000000	43.6742424242424
	270	39.9128764068000	1.50400000000000	44.4696969696970
	280	39.3997973306000	1.50700000000000	44.5833333333333
	290	39.2396052208000	1.51200000000000	44.7727272727273
	300	39.2071024739000	1.49000000000000	43.9393939393939
	310	39.0260157412000	1.49400000000000	44.0909090909091
	320	38.9563669978000	1.47800000000000	43.4848484848485

	330	38.3806040526000	1.43100000000000	41.7045454545455
	340	38.3666743039000	1.44700000000000	42.3106060606061
	350	38.5988367818000	1.46900000000000	43.1439393939394
	360	38.3713175535000	1.46300000000000	42.9166666666667

MATLAB Code Used to Process Recorded Data

```
Main File: RH_sensor_data_25_Jan_17.m
close all;
%% RH test results
%% RH baseline (in %RH)
VDD = 3.3; %supply voltage
time_RH = [0;10;20;30;40;50;60;70;80;90;100;110;120;130;140;150;160;170;180
probe_RH = [23.4571999722;23.322545735;23.2528969917;23.1530671262;23.06948
MCU_out_base = hex2dec({'3ba','3b6','3b4','3b4','3af','3ae','3aa','3a9','3a
%Convert MCU output to RH in %
MCU_RH_base = -12.5+125*MCU_out_base/VDD;
%Plot MCU ouput and probe output over time
figure(1);
plot(time_RH,MCU_RH_base,'bo'); hold on;
plot(time_RH,probe_RH,'ro'); hold off;
title('RH Sensor: Baseline')
xlabel('Time (s)'); ylabel('Relative Humidity Reading (%RH)');
legend('MCU','Probe','Location','southeast');
figure(2)
plot(time_RH,MCU_RH_base-probe_RH,'bo');
title('RH Sensor: Baseline Error')
xlabel('Time (s)'); ylabel('Error (%RH)');
%% RH with 100mL boiling water in box (in %RH)
time_100mL = [0;10;20;30;40;50;60;70;80;90;100;110;120;130;140;150;160;170;
probe_RH1 = [24.9616128291;74.126660777;90.0994392575;94.9307404229;95.9336
MCU_out1 = hex2dec({'68d','a72','ab7','ac9','adc','ae7','af6','af4','af4','
%Convert MCU output to RH in %
MCU_RH1 = -12.5+125*MCU_out1/VDD;
%Plot MCU output and probe output over time
figure(3);
plot(time_100mL,MCU_RH1,'bo'); hold on;
plot(time_100mL,probe_RH1,'ro'); hold off;
title('RH Sensor: Increasing RH Test')
xlabel('Time (s)'); ylabel('Relative Humidity Reading (%RH)');
legend('MCU','Probe','Location','southeast');
figure(4)
plot(time_100mL,MCU_RH1-probe_RH1,'bo');
title('RH Sensor: Increasing RH Test Error')
xlabel('Time (s)'); ylabel('Error (%RH)');
%% RH after 100mL boiling water removed from box (in %RH)
time_post100mL = [0;10;20;30;40;50;60;70;80;90;100;110;120;130;140;150;160;
probe_RH2 = [65.2394811225;62.6996236141;59.9276036278;54.826993988;51.5976
MCU_out2 = hex2dec({'73c','762','791','7a6','76d','721','709','6d6','6bd','
```

```
%Convert MCU output to RH in %
MCU_RH2 = -12.5+125*MCU_out2/VDD;
%Plot MCU output and probe output over time
figure(5);
plot(time_post100mL,MCU_RH2,'bo'); hold on;
plot(time_post100mL,probe_RH2,'ro'); hold off;
title('RH Sensor: Decreasing RH Test')
xlabel('Time (s)'); ylabel('Relative Humidity Reading (%RH)');
legend('MCU','Probe','Location','southeast');
figure(6)
plot(time_post100mL,MCU_RH2-probe_RH2,'bo'); hold on;
title('RH Sensor: Decreasing RH Test Error')
xlabel('Time (s)'); ylabel('Error (%RH)');
%% %RH versus %RH Plots
figure(7); %MCU output versus probe output versus line of identity
subplot(3,1,1);
plot(probe_RH,MCU_RH_base,'bo'); hold on;
plot(probe_RH,probe_RH,'--k'); hold off;
xlabel('Probe Output (%RH)'); ylabel('MCU Output (%RH)');
title('Baseline Test');
subplot(3,1,2);
plot(probe_RH1, MCU_RH1,'bo'); hold on;
plot(probe_RH1,probe_RH1,'-k'); hold off;
xlabel('Probe Output (%RH)'); ylabel('MCU Output (%RH)');
title('Increasing RH Test');
subplot(3,1,3);
plot(probe_RH2,MCU_RH2,'bo'); hold on;
plot(probe_RH2,probe_RH2,'--k'); hold off;
xlabel('Probe Output (%RH)'); ylabel('MCU Output (%RH)');
title('Decreasing RH Test');
figure(8); %error
subplot(3,1,1);
plot(probe_RH,MCU_RH_base-probe_RH,'bo'); hold on;
plot(probe_RH,zeros(size(probe_RH)),'--k'); hold off;
xlabel('Probe Output (%RH)'); ylabel('Error in MCU Output (%RH)');
title('Baseline Test');
subplot(3,1,2);
plot(probe_RH1, MCU_RH1-probe_RH1,'bo'); hold on;
plot(probe_RH1,zeros(size(probe_RH1)),'-k'); hold off;
xlabel('Probe Output (%RH)'); ylabel('Error in MCU Output (%RH)');
title('Increasing RH Test');
subplot(3,1,3);
plot(probe_RH2,MCU_RH2-probe_RH2,'bo'); hold on;
plot(probe_RH2,zeros(size(probe_RH2)),'--k'); hold off;
xlabel('Probe Output (%RH)'); ylabel('Error in MCU Output (%RH)');
title('Decreasing RH Test');
```

Appendix F - Original Length of Stay Data and Average Length of Stay Calculation

	Data Collection Time Period	Mean	Median	Min	Max
Acute long-term care hospital in Southern Florida, sample size 100, split into experimental group (50) and matched control group (50), patients 60+ years with pressure ulcers either upon admission or acquired at hospital (Allen, 2012)	10 January 2008 - 31 September 2009 and 10 January 2009 - 31 August 2010	43.2		10	165
Healthcare Cost and Utilization Project Nationwide Inpatient Sample data from various hospitals across 38 states (Russo & Elixhauser, 2006)	2003	13			
Healthcare Cost and Utilization Project Nationwide Inpatient Sample data from various hospitals across 40 states (primary diagnosis) (Russo et al., 2008)	2006	14.1			
Healthcare Cost and Utilization Project Nationwide Inpatient Sample data from various hospitals across 40 states (secondary diagnosis) (Russo et al., 2008)	2006	12.7			
German university hospital, sample size 3198, split into pressure ulcer on admission group (119), hospital acquired pressure ulcer group (109), and matched control group (2970), patients 75+ years (primary diagnosis) (Theisen et al., 2011)	2008 - 2009	13.8	9	0	86
German university hospital, sample size 3198, split into pressure ulcer on admission group (119), hospital acquired pressure ulcer group (109), and matched control group (2970), patients 75+ years (secondary diagnosis) (Theisen et al., 2011)	2008 - 2009	24.5	20	2	114
Teaching hospital in Nashville, Tennessee, sample size 32963, divided into hospital acquired pressure ulcer group (931) and matched control group (3721) (Hayes et al., 2015)	01 July 2010 - 31 March 2013		17		
Healthcare Cost and Utilization Project Nationwide Inpatient Sample data, sample size 504094, split into hospital acquired pressure ulcer group (148) and matched control group, patients 1 to 17 years (Goudie et al., 2015)	2009 - 2011	11.8			

MEAN (secondary diagnosis)		15.5			

Appendix G - Original Excess Cost Per Stay and Excess Length of Stay Data

	Data Collection Time Period	Average Stay	Excess Stay	Excess Charge
Healthcare Cost and Utilization Project Nationwide Inpatient Sample data from 994 acute-care general hospitals across 28 states (Zhan & Miller, 2003)	2000	9.98*	3.98	$10,845
Healthcare Cost and Utilization Project Nationwide Inpatient Sample data from various hospitals across 38 states (Russo & Elixhauser, 2006)	2003	13	8.4	
Healthcare Cost and Utilization Project Nationwide Inpatient Sample data from various hospitals across 40 states (primary diagnosis) (Russo et al., 2008)	2006	14.1	9.1	$6,900
Healthcare Cost and Utilization Project Nationwide Inpatient Sample data from various hospitals across 40 states (secondary diagnosis) (Russo et al., 2008)	2006	12.7	7.7	$10,500
German university hospital, sample size 3198, split into pressure ulcer on admission group (119), hospital acquired pressure ulcer group (109), and matched control group (2970), patients 75+ years (Theisen et al., 2011)	2008 - 2009	PD: 13.8 SD: 24.5	PD: 3.9 SD: 14.6	
Teaching hospital in Nashville, Tennessee, sample size 32963, divided into hospital acquired pressure ulcer group (931) and matched control group (3721) (Hayes et al., 2015)	01 July 2010 - 31 March 2013	17	5.2	
Healthcare Cost and Utilization Project Nationwide Inpatient Sample data, sample size 504094, split into hospital acquired pressure ulcer group (148) and matched control group, patients 1 to 17 years (Goudie et al., 2015)	2009 - 2011	11.8	4.9	$19,740

Appendix H - Python Code

```
#!/usr/bin/python

## include relevant libraries
from bluepy.btle import Peripheral, Scanner, DefaultDelegate
import matplotlib.pyplot as plt
import numpy as np

## create plot handle given specifications
def createPlot(fig, subplot, xlabel, ylabel, ylim, title, grid):
    myPlot = fig.add_subplot(subplot)
    if subplot % 10 == 0:
        myPlot.set_xlabel(xlabel)
    myPlot.set_ylabel(ylabel)
    myPlot.set_ylim(ylim)
    myPlot.set_title(title, verticalalignment = 'bottom')
    myPlot.grid(grid)
    return myPlot

## convert hex string into dec int
def hex2int(hex_data):
    inter_data = hex_data[3] + hex_data[4] + hex_data[1] + hex_data[0]
    int_data = int(inter_data, 16)
    return int_data

## no idea. do NOT touch
class ScanDelegate(DefaultDelegate):
    def __init__(self):
        DefaultDelegate.__init__(self)

    def handleDiscovery(self, dev, isNewDev, isNewData):
        if isNewDev:
            print "Discovered device", dev.addr
        elif isNewData:
            print "Received new data from", dev.addr

## main function
def main():
    ## initialization
    keyword = "Patch" ## search for this string when scanning for BLE devices
    data_types = ['pressure', 'humidity', 'tempture']
    dict_chars = {'f0001131-0451-4000-b000-000000000000': 'pressure',
                  'f0001132-0451-4000-b000-000000000000': 'humidity',
                  'f0001133-0451-4000-b000-000000000000': 'tempture'}
    num_devices = 1
    num_datapts = 100 ## number of datapoints

    ## pressure conversion variables
    Fnom = 58.968
```

```
Rnom = 2.0242e4
area = 0.00012667 ## area of pressure sensor
conv = 133.322 ## pascal to mmHg
m = -1.0313
g2N = 0.00980665 ## gram-force to Newtons conversion
Vdd = 3300 ## supply voltage

## search for devices
scanner = Scanner().withDelegate(ScanDelegate())
scan_duration = 0
list_devices = []
print "Scanning."
while len(list_devices) < num_devices: ## loops indefinitely if not enough d
    list_devices = []
    scan_duration = scan_duration + 5.0
    devices = scanner.scan(scan_duration)
    for dev in devices:
        print "Device %s (%s), RSSI=%d dB" % (dev.addr, dev.addrType, dev.rs
        for (adtype, desc, value) in dev.getScanData():
            print "  %s = %s" % (desc, value)
            if keyword in value:
                list_devices.append([str(dev.addr), dev.addrType, value])
        if len(list_devices) >= num_devices:
            break

## initialize data structure to zeros
dict_data = {}
dict_plots = {}
dict_lines = {}
for i in list_devices:
    dict_data[i[2]] = {}
    dict_plots[i[2]] = {}
    dict_lines[i[2]] = {}
    for j in data_types:
        dict_data[i[2]][j] = 0
        dict_plots[i[2]][j] = 0
        dict_lines[i[2]][j] = 0

## create subplots
n = np.arange(0, num_datapts, 1)
plt.ion()
fig = plt.figure(figsize = (20, 12))
subplot_axes = 100*len(data_types)+ 10*num_devices + 1
for i in dict_data:
    for j in data_types: ## initialize x axis
        dict_data[i][j] = [0]*num_datapts
        if j == "pressure":
            dict_plots[i][j] = createPlot(fig, subplot_axes, "sample", "pres
        else:
            dict_plots[i][j] = createPlot(fig, subplot_axes, "sample", "volt
        dict_lines[i][j], = dict_plots[i][j].plot(n, dict_data[i][j])
```

```
            subplot_axes = subplot_axes + 1

    ## application main loop. runs indefinitely
    while True:
        for i in list_devices:
            while True: ## loops indefinitely if failed to connect
                try:
                    per = Peripheral(i[0], i[1], 0) ## connect to device
                    break
                except:
                    print "Retrying"
            for charac in per.getCharacteristics():
                uuid  = str(charac.uuid) ## define data type
                if uuid in dict_chars:
                    name_data = dict_chars[uuid] ## retrieve data name
                    if name_data == "pressure": ## convert voltage to mmHg
                        Vp = hex2int(charac.read())
                        if Vp == 0:
                            Vp = 1
                        Rfsr = 10000*(Vdd - Vp)/Vp
                        val_data = Fnom*pow(Rfsr/Rnom, 1/m)*g2N/area/conv
                    else: ## leave other types as voltage
                        val_data = hex2int(charac.read())
                    dict_data[i[2]][name_data].append(val_data)
                    if len(dict_data[i[2]][name_data]) > num_datapts: ## lose ol
                        dict_data[i[2]][name_data].pop(0)
                    dict_lines[i[2]][name_data].set_ydata(dict_data[i[2]][name_d
            per.disconnect()
        fig.canvas.draw()

if __name__ == "__main__":
    main()
```

References

Ackroyd-Stolarz, S. (2014). Improving the prevention of pressure ulcers as a way to reduce health care expenditures. *Canadian Medical Association Journal, 186*(10), E370-E371. doi: 10.1503/cmaj.131620

Agency for Healthcare Research and Quality. (2016, December). *National scorecard on rates of hospital-acquired conditions 2010 to 2015: Interim data from national efforts to make health care safer.* Rockville, MD: Author. Retrieved from http://www.ahrq.gov/professionals/quality-patient-safety/pfp/2015-interim.html

Agency for Healthcare Research and Quality. (2015, December). *Saving lives and saving money: Hospital-acquired conditions update.* Rockville, MD: Author. Retrieved from http://www.ahrq.gov/professionals/quality-patient-safety/pfp/interimhacrate2014.html

Agency for Healthcare Research and Quality. (2015, October). *2013 annual hospital-acquired condition rate and estimates of cost savings and deaths averted from 2010 to 2013.* Rockville, MD: Author. Retrieved from http://www.ahrq.gov/professionals/quality-patient- safety/pfp/hacrate2013.html

Agency for Healthcare Research and Quality. (2014, October). Are we ready for this change? Rockville, MD: Author. Retrieved from http://www.ahrq.gov/professionals/systems/hospital/pressureulcertoolkit/putool1.html

Agency for Healthcare Research and Quality. (2014, October). Preventing Pressure Ulcers in Hospitals. Rockville, MD: Author. Retrieved from http://www.ahrq.gov/professionals/systems/hospital/pressureulcertoolkit/index.html

Agency for Healthcare Research and Quality. (2014, September). *Updated information on the annual hospital-acquired condition rate: 2011 and 2012.* Rockville, MD: Author. Retrieved from http://www.ahrq.gov/professionals/quality-patient-safety/pfp/hacrate2011-12.html

Allen, B. (2012). Effects of a comprehensive nutritional program on pressure ulcer healing, length of hospital stay, and charges to patients. *Clinical Nursing Research, 22*(2), 186-205. doi: 10.1177/1054773812457673

ALLEVYN Life. (n.d.). Retrieved September 22, 2016, from http://www.smith-nephew.com/key-products/advanced-wound-management/allevyn/allevyn-life/

Averill, R. F., Hughes, J. S., Fuller, R. L., & Goldfield, N. I. (2016). Quality improvement initiatives need rigorous evaluation: The case of pressure ulcers. *American Journal of Medical Quality,* 1-4. doi: 10.1177/1062860616666672

Berlowitz, D., Lukas, C. V., Niederhauser, A., Silver, J., Logan, C., Ayello, E., & Zulkowski, K. (2012). *Preventing pressure ulcers in hospitals: a toolkit for improving quality of care*. Rockville, MD: Agency for Healthcare Research and Quality. Retrieved from https://www.ahrq.gov/sites/default/files/publications/files/putoolkit.pdf

Boyte-White, C. (2016, November 7). What is the formula for calculating net present value (NPV) in Excel? Retrieved from http://www.investopedia.com/ask/answers/021115/what-formula-calculating-net-present-value-npv-excel.asp

Brem, H., Maggi, J., Nierman, D., Rolnitzky, L., Bell, D., Rennert, R., … Vladeck, B. (2010). High cost of stage IV pressure ulcers. *American Journal of Surgery*, *200*(4), 473–477. http://doi.org/10.1016/j.amjsurg.2009.12.021

Brown, C. (2013a, July 16). *ICAD 2013 keynote with Nam Suh*. Retrieved from https://www.youtube.com/watch?v=xSI8UxSi5eM

Brown, C. (2013b, September 10). *MFE 594 an introduction to axiomatic design part 1*. Retrieved from https://www.youtube.com/watch?v=xCcysLQ0dGk.

Brown, C. (2013c, September 10). *MFE 594 an introduction to axiomatic design part 2*. Retrieved from https://www.youtube.com/watch?v=gFGZz3QtVJ8.

Brown, C. (2013d, September 10). *MFE 594 an introduction to axiomatic design part 3*. Retrieved from https://www.youtube.com/watch?v=0mm7x_gJyK8.

Brown, C. (2013e, September 10). *MFE 594 an introduction to axiomatic design part 4*. Retrieved from https://www.youtube.com/watch?v=qURM1A1BZJw.

Brown, C. (2013f, September 18). *Teaching axiomatic design: Part 1 - Introduction (rough cut)*. Retrieved from https://www.youtube.com/watch?v=bFIMaHrJ8No

Brown, C. (2013g, September 18). *Teaching axiomatic design: Part 2 - Building solutions (rough cut)*. Retrieved from https://www.youtube.com/watch?v=hN1S1baQyo0

Brown, C. (2013h, September 19). *Teaching axiomatic design: Part 3 - Axiomatic design (rough cut)*. Retrieved from https://www.youtube.com/watch?v=eAGOGjpoQRI

Brown, C. (2013i, September 19). *Teaching axiomatic design: Part 4 - Addressing limitations (rough cut)*. Retrieved from https://www.youtube.com/watch?v=ZeCeDadBqvs

Brown, C. (2013j, September 19). *Teaching axiomatic design: Part 5 - Customer needs (rough cut)*. Retrieved from https://www.youtube.com/watch?v=pdIr5xJNKdc

Brown, C. (2013k, September 19). *Teaching axiomatic design: Part 6 - Creating value (rough cut)*. Retrieved from https://www.youtube.com/watch?v=_UoWQBg-38o

Brown, C. (2013l, September 19). *Teaching axiomatic design: Part 7 - The axioms (rough cut)*. Retrieved from https://www.youtube.com/watch?v=PwHULkomAU0

Brown, C. (2013m, September 19). *Teaching axiomatic design: Part 8 - Decomposition (rough cut)*. Retrieved from https://www.youtube.com/watch?v=rOLSIWFj54c

Consumer Technology Association. (n.d.). Average selling price of smartphones worldwide from 2010 to 2016 (in U.S. dollars). In *Statista - The Statistics Portal*. Retrieved February 21, 2017, from https://www.statista.com/statistics/510668/smartphone-average-selling-price-worldwide/.

Crivello, M., Sen, D., McNeill, J., Mendelson, Y., Dunn, R., & Hickle, K. (2016a). Modeling of force sensor nonlinearity for time-domain-based pressure measurement in biomedical sensors. In

Proceedings of NEBEC 2016: *The 42nd Annual Northeast Biomedical Engineering Conference*. Binghamton, NY: IEEE.

Crivello, M., Sen, D., McNeill, J., Mendelson, Y., Dunn, R., & Hickle, K. (2016b). Flexible sensor for measurement of skin pressure and temperature in a clinical setting. In Proceedings of SENSORS 2016: *IEEE SENSORS*. Orlando, FL: IEEE.

Domingo, J. S., & Murray, M. (2017, February 6). The best laptops of 2017. *PC Mag*. Retrieved February 21, 2017, from http://www.pcmag.com/article2/0,2817,2369981,00.asp

Donovan, B. J. (2012, August 11). Selecting Antennas for Embedded Designs. Retrieved October 10, 2016, from http://www.digikey.com/en/articles/techzone/2012/nov/selecting-antennas-for-embeddeddesigns

Enokibori, Y., Shimakami, Y., Suzuki, A., Mase, K., & Mizuno, H. (2013). E-Textile pressure sensor based on conductive fiber and its structure. *UbiComp'13 Adjunct*, (pp. 207-210). Zurich, Switzerland. doi: 10.1145/2494091.2494158

Goudie, A., Dynan, L., Brady, P. W., Fieldston, E., Brilli, R. J., & Walsh, K. E. (2015, September). Costs of venous thromboembolism, catheter-associated urinary tract infection, and pressure ulcer. *Pediatrics, 136*(3), 432-439. doi: 10.1542/peds.2015-1386

Gutierrez, B. M., Jones, S. K., & Morianos, M. M. (2011). *Pressure Ulcer Prevention Device* (Major qualifying project). Worcester Polytechnic Institute, Worcester, MA. Retrieved from https://web.wpi.edu/Pubs/E-project/Available/E-project-042811-094326/

Hause, A. R., Truhanovitch, A., & Williams, M. D. (2012). *Wireless Pressure Ulcer Prevention Device* (Major qualifying project). Worcester Polytechnic Institute, Worcester, MA. Retrieved from https://web.wpi.edu/Pubs/E-project/Available/E-project-042612-040907/

Hayes, R. M., Spear, M. E., Lee, S. I., Krauser Lupear, B. E., Benoit, R. A., Valerio, R., & Dmochowski, R. R. (2015). Relationship between time in the operating room and incident pressure ulcers: A matched case-control study. *American Journal of Medical Quality, 30*(6), 591-597. doi: 10.1177/1062860614545125

Hearing Aid Battery Shop. (2017). Hearing aid battery technical specifications. Retrieved March 2, 2017, from http://www.hearingaidbatteryshop.com/specifications/

Hopeman, M. W. (2016). *Cross disciplinary project management* (Major qualifying project). Worcester Polytechnic Institute, Worcester, MA. Retrieved from https://web.wpi.edu/Pubs/E-project/Available/E-project-022616-141153/

Imani, S., Bandodkar, A. J., Vinu-Mohan, A. N., Kumar, R., Yu, S., Wang, J., & Mercier, P. (2016, May 23). A wearable chemical–electrophysiological hybrid biosensing system for real-time health and fitness monitoring. *Nature Communications, 7*.

Inoue, K. C., & Matsude, L. M. (2016). Cost of dressings for prevention of sacral pressure ulcers. *Revista Brasileira de Enfermagem, 69*(4), 598-602. http://dx.doi.org/10.1590/0034-7167.2016690404i

International Review. (2010, September 2). Pressure ulcer prevention: Pressure, shear, friction, and microclimate in context -- a consensus document. London, England: Wounds International. http://www.woundsinternational.com/media/issues/300/files/content_8925.pdf

Investopedia. (n.d.). Net present value - NPV. Retrieved February 21, 2017, from http://www.investopedia.com/terms/n/npv.asp

Investopedia. (n.d.). Profit margin. Retrieved March 2, 2017, from http://www.investopedia.com/terms/p/profitmargin.asp

Investopedia. (n.d.). Return on investment - ROI. Retrieved March 2, 2017, from http://www.investopedia.com/terms/r/returnoninvestment.asp

Kokate, J. Y., Leland, K. J., Held, A. M., Hansen, G. L., Kveen, G. L., Johnson, B. A., . . . Iaizzo, P. A. (1995). Temperature-modulated pressure ulcers: A porcine model. Archives of Physical Medicine and Rehabilitation, 76(7), 666-673. doi: 10.1016/s0003-9993(95)80637-7

Leaf Healthcare, Inc. (2016). *The Financial Impact of Pressure Ulcers.* Retrieved from http://www.leafhealthcare.com/pdfs/LH_WP_FinancialOverview_1563AB_013117.pdf

Leaf Healthcare, Inc. (2014, August 11). *Technical Overview of the Leaf Patient Monitoring System.* Retrieved from Leaf Healthcare: http://leafhealthcare.com/pdfs/LH_WP_TechOverview_1564AA_PDF_081114.pdf

McNeill, J., Sen, D., Mendelson, Y., Crivello, M., Mazumder, S., Agdeppa, A., Hussain, S. A., Kim, H., Loehle, V., Dunn, R., & Hickle, K. (2017). Wearable wireless sensor patch for continuous monitoring of skin temperature, pressure, and relative humidity. Proceedings from ISCAS 2017: *2017 IEEE International Symposium on Circuits & Systems*. Baltimore, MD: IEEE.

Medical Price Online. (2017). Average ICU CCU monitors price quotes and cost information. Retrieved January 21, 2017, from https://www.medicalpriceonline.com/medical-equipment/icu-ccu-monitors/

Michalson, W. (2016). *Return on investment* [ECE2799 lecture slides]. Retrieved March 2, 2017, from http://users.wpi.edu/~sjbitar/ece2799/lectures/Topic21%20-%20ROI/Return%20On%20Investment.pdf

Moore, Z., Cowman, S., 7 Posnett, J. (2012). An economic analysis of repositioning for the prevention of pressure ulcers. *Journal of Clinical Nursing, 22*, 2354-2360. doi: 10.1111/j.1365-2702.2012.04310.x

National Guideline Clearinghouse. (2012, January 1). *Guideline summary: Pressure ulcer prevention and treatment protocol. Health care protocol*. In: National Guideline Clearinghouse (NGC) [Web site]. Rockville (MD): Agency for Healthcare Research and Quality (AHRQ). Retrieved September 25, 2016, from https://www.guideline.gov/summaries/summary/36059/Pressure-ulcer-prevention-and-treatment-protocol-Health-care-protocol

National Pressure Ulcer Advisory Panel, European Pressure Ulcer Advisory Panel and Pan Pacific Pressure Injury Alliance. (2014). *Prevention and treatment of pressure ulcers: Quick reference guide*. Emily Haesler (Ed.). Cambridge Media: Osborne Park, Australia.

Newnan, D. G., Lavelle, J. P., & Eschenbach, T. G. (2014). *Engineering economic analysis* (12th ed.). New York, NY: Oxford University Press.

OPSITE◊ Film Dressings. (n.d.). Retrieved September 22, 2016, from http://www.smith-nephew.com/key-products/advanced-wound-management/opsite-films/

Pantelopoulos, A., & Bourbakis, N. (2010). A survey on wearable sensor-based systems for health monitoring and prognosis. *IEEE Transactions on Systems, Man, and Cybernetics - Part C: Applications and Reviews*, *40(1)*, 1094-6977. doi: 10.1109/TSMCC.2009.2032660

Pantelopoulos, A., & Bourbakis, N. (2008). A Survey on Wearable Biosensor Systems for Health Monitoring. *30th Annual International Conference of the IEEE Engineering in Medicine and Biology Society* (pp. 4887 - 4890). Vancouver, British Columbia, Canada: IEEE.

Pappas, S. H. (2008, May). The cost of nurse-sensitive adverse events. *Journal of Nursing Administration, 38*(5), 230 - 236. doi: 10.1097/01.NNA.0000312770.19481.ce

Patient Safety Network. (2016, July). Never events. San Francisco, CA: University of California and Agency for Healthcare Research and Quality. Retrieved from https://psnet.ahrq.gov/primers/

Pressure Ulcer and Skin Care. (n.d.). Retrieved October 1, 2016, from https://www.rnoh.nhs.uk/our-services/spinal-cord-injury-centre/medical-management-advice/pressure-ulcer-and-skin-care

REPLICARE◊ Thin. (n.d.). Retrieved October 13, 2016, from http://www.smith-nephew.com/professional/products/advanced-wound-management/replicare/replicare-thin/primer/3/never-events

Russo, C. A., & Elixhauser, A. (2006, April). Hospitalizations related to pressure sores, 2003. HCUP Statistical Brief #3. Agency for Healthcare Research and Quality, Rockville, MD. http://www.hcup-us.ahrq.gov/ reports/statbriefs/sb3.pdf

Russo, C. A., Steiner, C., & Spector, W. (2008, December). Hospitalizations related to pressure ulcers, 2006. HCUP Statistical Brief #64. Agency for Healthcare Research and Quality, Rockville, MD. http://www.hcup-us.ahrq.gov/reports/statbriefs/sb64.pdf

Srivastava, R. N., Dwivedi, M. K., Bhagat, A., Raj, S., Agarwal, R., & Chandra, A. (2016). A non-randomised, controlled clinical trial of an innovative device for negative pressure wound therapy of pressure ulcers in traumatic paraplegia patients. *International Wound Journal, 13*, 343-348. doi: 10.1111/iwj.12309

Suh, N. P. (1990). *The principles of design*. New York, NY: Oxford University Press.

Tabletmonkeys. (2017, February 10). List of tablets: Tablet comparison chart 2017. Retrieved February 21, 2017, from http://tabletmonkeys.com/tablet-comparison/

Texas Instruments. (2016, August). *CC2650MODA Datasheet*. Retrieved from Texas Instruments: http://www.ti.com/lit/ds/symlink/cc2650moda.pdf

Theisen, S., Drabik, A., & Stock, S. (2011). Pressure ulcers in older hospitalised patients and its impact on length of stay: a retrospective observational study. *Journal of Clinical Nursing, 21*, 380-387. doi: 10.1111/j.1365-2702.2011.03915.x

Thompson, M. K. (2013). A classification of procedural errors in the definition of functional requirements in axiomatic design theory. In Proceedings of ICAD2013: *The Seventh International Conference on Axiomatic Design*. Worcester, MA: Functional Specs, Inc.

Towner, Jr., W. T. (2013a). *The design of engineering education as a manufacturing system* (Doctoral dissertation). Worcester Polytechnic Institute, Worcester, MA. Retrieved from https://web.wpi.edu/Pubs/ETD/Available/etd-042313-125039/

Towner, Jr., W. T. (2013b). *Session 01D Axiomatic Design Introduction*. [PowerPoint slides]. Retrieved from Axiomatic Design Materials - Professor Walter Towner's MQP Site: https://my.wpi.edu/webapps/blackboard/content/listContent.jsp?course_id=_41843_1&content_id=_139920_1&mode=reset

Towner, Jr., W. T. (2013c). *Session 01F Decomposition in Axiomatic Design*. [PowerPoint slides]. Retrieved from Axiomatic Design Materials - Professor Walter Towner's MQP Site: https://my.wpi.edu/webapps/blackboard/content/listContent.jsp?course_id=_41843_1&content_id=_139920_1&mode=reset

Towner, Jr., W. T. (2013d). *Session 01H Axiomatic Design Tip-Sheet*. [PowerPoint slides]. Retrieved from Axiomatic Design Materials - Professor Walter Towner's MQP Site: https://my.wpi.edu/webapps/blackboard/content/listContent.jsp?course_id=_41843_1&content_id=_139920_1&mode=reset

Towner, Jr., W. T. (2013e, December 3). *WPI Industrial Engineering Club Introduction to Axiomatic Design*. [PowerPoint slides]. Retrieved from Axiomatic Design Materials - Professor Walter Towner's MQP Site: https://my.wpi.edu/webapps/blackboard/content/listContent.jsp?course_id=_41843_1&content_id=_139920_1&mode=reset

UMass Memorial Health Care. (2017). Statistics - UMass Memorial Medical Center. Retrieved January 21, 2017, from https://www.umassmemorialhealthcare.org/umass-memorial-medical-center/about-us/statistics

Voland, G. (2004). *Engineering by design* (2nd ed.). Upper Saddle River, NJ: Pearson/Prentice Hall.

Wellsense. (n.d.). Retrieved October 10, 2016, from http://themapsystem.com/

Whalen, D., Houchens, R., Elixhauser, A. (2003). Final 2000 NIS Comparison Report. HCUP Methods Series Report #2003-1. ONLINE. February 28, 2003. U.S. Agency for Healthcare Research and Quality. http://www.hcup-us.ahrq.gov/db/nation/nis/reports/NIS_Comparison_Report_2000.pdf

World Intellectual Property Organization. (2015). Successful technology licensing. In *IP assets management series*. Retrieved March 2, 2017, from http://www.wipo.int/edocs/pubdocs/en/licensing/903/wipo_pub_903.pdf

Zaharoff, H. G. (2012, June 18). Setting values and royalty rates for medical and life science businesses. Retrieved March 2, 2017, from http://www.mbbp.com/news/setting-values-and-royalty-rates

Zhan, C., & Miller, M. R. (2003). Excess length of stay, charges, and mortality attributable to medical injuries during hospitalization. *Journal of the American Medical Association, 290*(14), 1868-1874.

Zipkin, N. (2014, July 22). Your one-stop guide to royalty rates (info-graphic). Retrieved March 2, 2017, from https://www.entrepreneur.com/article/235851